Chem Soc Rev

REVIEW ARTICLE

View Article Online
View Journal

Cite this: DOI: 10.1039/d0cs00908c

Phenolic-enabled nanotechnology: versatile particle engineering for biomedicine

Di Wu, †[a] Jiajing Zhou, †[b] Matthew N. Creyer,[b] Wonjun Yim,[c] Zhong Chen,*[ad] Phillip B. Messersmith[ef] and Jesse V. Jokerst*[bcg]

Received 2nd December 2020

DOI: 10.1039/d0cs00908c

rsc.li/chem-soc-rev

Phenolics are ubiquitous in nature and have gained immense research attention because of their unique physiochemical properties and widespread industrial use. In recent decades, their accessibility, versatile reactivity, and relative biocompatibility have catalysed research in phenolic-enabled nanotechnology (PEN) particularly for biomedical applications which have been a major benefactor of this emergence, as largely demonstrated by polydopamine and polyphenols. Therefore, it is imperative to overveiw the fundamental mechanisms and synthetic strategies of PEN for state-of-the-art biomedical applications and provide a timely and comprehensive summary. In this review, we will focus on the principles and strategies involved in PEN and summarize the use of the PEN synthetic toolkit for particle engineering and the bottom-up synthesis of nanohybrid materials. Specifically, we will discuss the attractive forces between phenolics and complementary structural motifs in confined particle systems to synthesize high-quality products with controllable size, shape, composition, as well as surface chemistry and function. Additionally, phenolic's numerous applications in biosensing, bioimaging, and disease treatment will be highlighted. This review aims to provide guidelines for new scientists in the field and serve as an up-to-date compilation of what has been achieved in this area, while offering expert perspectives on PEN's use in translational research.

[a] College of Pharmaceutical Sciences, Zhejiang University, Hangzhou 310058, China. E-mail: chenzhong@zju.edu.cn
[b] Department of NanoEngineering, University of California San Diego, 9500 Gilman Dr, La Jolla, CA, 92093, USA. E-mail: jjokerst@eng.ucsd.edu
[c] Materials Science and Engineering Program, University of California San Diego, 9500 Gilman Dr, La Jolla, CA, 92093, USA
[d] Key Laboratory of Neuropharmacology and Translational Medicine of Zhejiang Province, College of Pharmaceutical Science, Zhejiang Chinese Medical University, Hangzhou 311402, China
[e] Department of Bioengineering and Department of Materials Science and Engineering, University of California, Berkeley, Berkeley, California 94720-1760, USA
[f] Materials Sciences Division, Lawrence Berkeley National Laboratory, Berkeley, California 94720, USA
[g] Department of Radiology, University of California San Diego, 9500 Gilman Dr, La Jolla, CA, 92093, USA
† These authors contributed equally.

Di Wu

Di Wu received his PhD degree from Department of Chemistry, Zhejiang University under the supervision of Prof. Wenjun Fang in 2019. He then joined Prof. Zhong Chen's group as a postdoctoral fellow in College of Pharmaceutic Sciences, Zhejiang University. His research interests focus on the development of multifunctional materials for biosensing and disease therapy.

Jiajing Zhou

Jiajing Zhou completed his PhD in bioengineering in 2016 at Nanyang Technological University under the supervision of Prof. Hongwei Duan. He worked with Prof. Frank Caruso as a post-doctoral fellow at The University of Melbourne from 2018 to 2020. More recently, he joined Prof. Jesse V. Jokerst's group. His research focuses on the synthesis of functional nanohybrids for biomedical applications.

1. Introduction

Phenolic compounds are a large family of naturally occurring molecules present in a wide range of organisms. From fungi to bacterium and from plants to animals, these ubiquitous compounds have gained immense research attention because of their unique physiochemical properties.[1–3] Phenolics have many uses—one of the earliest examples being leather manufacturing.[4] In the late twentieth century, Waite and Tanzer piqued the interest of chemical researchers by discovering the presence of phenolic-containing proteins (*i.e.*, mussel adhesive protein, MAP) in the adhesive pads of marine mussels.[5] Subsequent discoveries made by several groups over a period of many years have gradually revealed details of the adhesive mechanism of mussels,[6–11] inspiring biomimetic systems such as synthetic polymers and peptides that carry catechols.[12] In 2007, Messersmith and co-workers were similarly successful in mimicking the adhesive properties of mussels by using the mussel-inspired simple molecule, dopamine, which can undergo oxidation in a basic environment and self-polymerize into polydopamine (PDA).[13] Of particular importance is the universal processing method that can be used to emulate the underwater adhesive properties of mussels on virtually any natural substrate.[14] These two discoveries lead to the development of synthetic polymers containing phenolic (*e.g.*, catechols) and amine (*e.g.*, PDA) groups and have now been extensively explored for material-independent surface engineering applications.[15] In 2013, Caruso and co-workers reported a simple and rapid conformal coating method for various films and particles using assembly *via* coordination between tannic acid (TA), a natural polyphenol, and Fe^{3+}.[16] This stimulated interest in phenolic-based coatings by using natural polyphenols and metal ions. These seminal examples show the robustness of both covalent and non-covalent chemistries of phenolic compounds and demonstrate their great potential for engineering materials with targeted applications.

The ever-increasing attention of phenolic compounds in materials engineering is mainly due to their unique structural and chemical features.[17] In particular, the presence of versatile phenolic moieties (*e.g.*, catechol and gallol groups) in the structures can form diverse non-covalent and covalent interactions with various materials including inorganic materials (*e.g.*, metal ion, metal, metal oxide, semiconductor, carbon, silica), organic materials (*e.g.*, small molecule, synthetic polymers), and even bioactive biomacromolecules and living microorganisms. In such scenarios, phenolic compounds exert multiple physicochemical interactions with one or two being dominant (*e.g.*, metal coordination, hydrogen bonds, hydrophobic interactions, π interactions, covalent bonds, and electrostatic interactions) with the complementary building blocks (Fig. 1).[18] Moreover, adding phenolics can potentially endow the hybrid materials with a variety of excellent phenolic-based properties including adhesiveness,

Zhong Chen

Zhong Chen is currently the president of Zhejiang Chinese Medical University and the Qiushi Distinguished Professor of Zhejiang University. He is the winner of National Natural Science Fund for Distinguished Young Scholars and Cheung Kong Scholar & Professor of Ministry of Education. Dr Chen received his PhD degree from Okayama University of Japan in 1999 and was promoted to professor and PhD supervisor at Zhejiang University in 2002. His research interests include molecular mechanisms of neurological disorder and new therapeutic strategies in neuropharmacology.

Phillip B. Messersmith

Phillip B. Messersmith is the Class of 1941 Professor in the Departments of Bioengineering and Materials Science and Engineering at UC-Berkeley. He earned his BS degree in life sciences from the University of Illinois at Urbana, MS degree in bioengineering from Clemson University, and his PhD degree in materials science and engineering from the University of Illinois at Urbana. Previously, he was a faculty member at the University of Illinois-Chicago and Northwestern University. His current research interests are in understanding structure–processing–property relationships in biological and bioinspired materials, studying molecular phenomena in biological adhesion, and developing novel materials for regenerative medicine.

Jesse V. Jokerst

Jesse V. Jokerst is an Associate Professor in the Department of NanoEngineering at UC San Diego. Dr Jokerst completed a PhD in Chemistry at The University of Texas at Austin in 2009. Jesse was a postdoc at Stanford Radiology from 2009–2013 and was an Instructor in that same department from 2013–2015. Jesse started at UCSD in July of 2015, and he has received the NIH K99/R00 Pathway to Independence Award, the NIH New Innovator Award, the NSF CAREER Award, and Stanford Radiology Alumni of the Year Award.

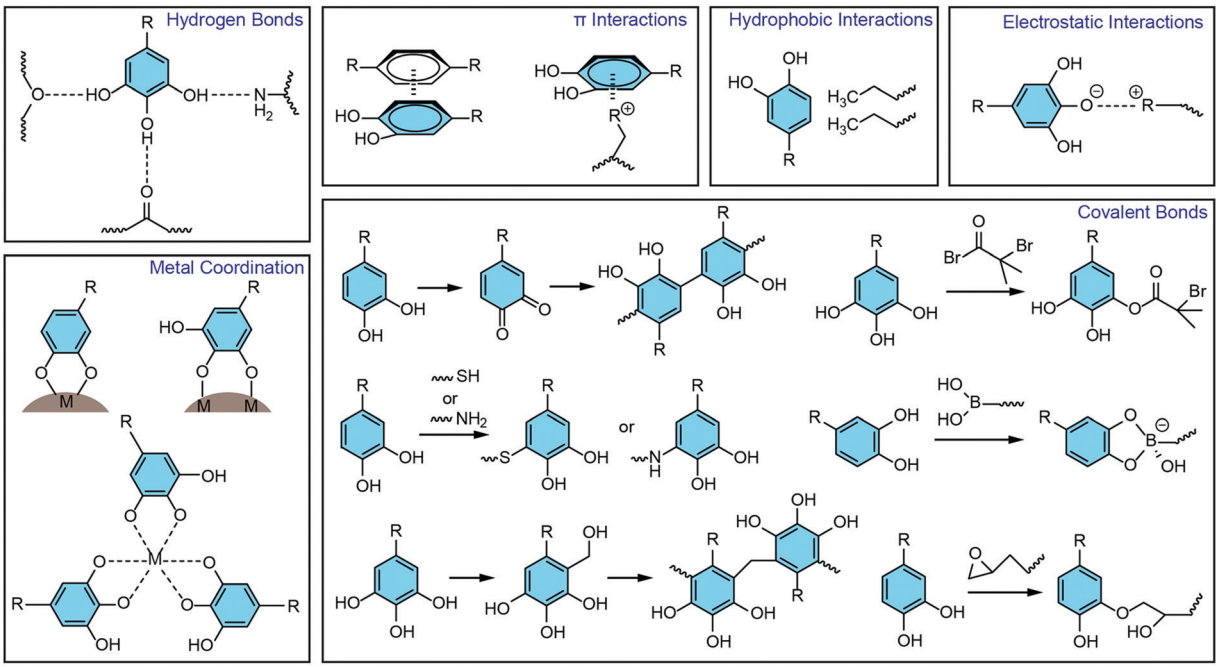

Fig. 1 Phenolic-mediated interactions with different materials in PENs.

antioxidation, antibacterial properties, *etc.*, which in turn make the products multifunctional towards diverse applications.

Over the past decades, we have witnessed rapid advances in exploiting nanotechnology in biomedical applications including biosensing, imaging, drug delivery, and many other disease theranostic modalities.[19,20] The accessibility, versatile reactivity, and relative biocompatibility of phenolics have catalysed the broad research in nanotechnology. As an emerging field, phenolic-enabled nanotechnology (PEN) provides simple yet versatile approaches for assembling nanostructures with unique properties and high flexibility in biomedical applications. Consequently, a number of engineered nanostructures have been developed with controllable size, shape, composition, surface chemistry, as well as degradability and function underscoring the immense potential of PEN for nanomedicine.

Efforts to create various phenolic-based materials have been accompanied by reviews of the latest progress but most of the literature emphasizes either PDA- or polyphenol-based materials for applications in surface coatings and hydrogels, respectively.[21,22] PDA-based platforms have been reviewed recently with a focus on surface modification for nanomedicine.[23] An even more recently published review covers plant polyphenols where the six different fundamental interactions between polyphenols and other materials are discussed but the strategies for making these nanostructures were not discussed.[18] Biomedical applications that utilize PEN have been a major benefactor of this emergence, yet a timely and comprehensive review is lacking. Based on the increasing interest in phenolic-based materials, a comprehensive review summarizing the fundamental mechanisms and synthetic strategies of PEN for state-of-the-art biomedical applications is in demand. Therefore, it is critical to consolidate this information into a single piece of literature to provide a complete picture of phenolic-based materials. This review aims to provide guidelines for new scientists in the field while offering expert perspectives on PEN's use in translational research.

In light of the exceptional advantages of PEN for synthesizing functional materials for biomedical applications—as well as the extensive interest and the high level of activity of this area—we will overview the development of phenolic-based nanosystems and reveal how PEN can be utilized for biomedical applications, not only for surface modification but also for delicate material design (Fig. 2). Specifically, the physicochemical interactions of phenolics with organic, inorganic, and biogenic substrates in confined nanosystems will be discussed from the molecular to nano scale to paint a comprehensive picture. Three main strategies for particle engineering are highlighted with relevant fundamental mechanisms and representative nanostructures. Their potential in biomedicine will be discussed starting from their bio-nano interactions, pharmacokinetics, and toxicology profiles before moving onto their specific applications in biosensing, bioimaging, and disease treatment. This review will be of great value to those working in phenolic-based materials, supramolecular chemistry, bio-inspired self-assembly, functional nanohybrid synthesis, and especially for those in biomedicine and translational medicine. We hope that this review will not only become a resource for what has been achieved in this field but also provide a go-to reference that facilitates the rational design of nanosystems with customized properties.

2. The physicochemical interaction of phenolics from molecular level in PEN

The physicochemical interactions of phenolics with other chemical building blocks play a mediating role in the design

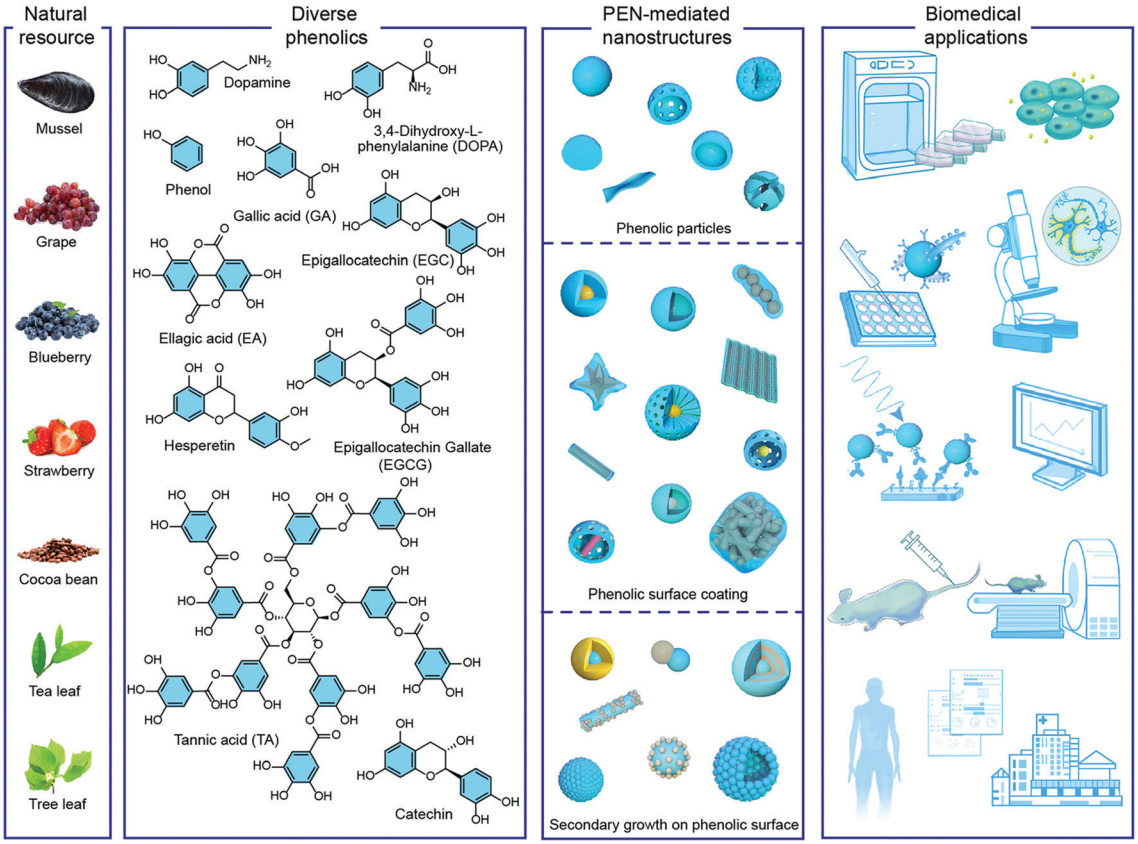

Fig. 2 The development of PEN for biomedical applications. From left to right: Representative natural resource of phenolics, chemical structure of representative phenolic molecules, schematic illustration of some typical PEN-mediated particles, and the potential applications in biomedical field, including study of bio–nano interactions, biosensing, imaging and disease treatment, from single molecular and cellular level to animal and clinical trials.

of nanostructures. Inorganic, organic, and biological substances have all been reported to interact with phenolics, and it is important to point out the fundamental interactions prior to the discussion of the use of PEN for engineering diverse nanostructures. Due to the versatile physical properties of phenolics, their presence in one nanosystem may have multiple roles. To better understand this complexity, the next section discusses the interactions between phenolics and other types of materials by considering each discrete component. We hope that this will clarify the interactions between phenolics and other materials and will enable the reader to design functional materials more intelligently using PEN.

2.1 Inorganic materials with phenolics

Inorganic nanoparticles exhibit novel electronic and optical properties at the nanometer length scales due to quantum effects.[24,25] Therefore, using PEN to create functional phenolic–inorganic hybrid nanoparticles with physicochemical properties arising from both the inorganic and phenolic components is attractive in biomedical applications.

2.1.1 Metal ions. The coordination between phenolics and metal ions is one of the most well-studied topics. It is well-known that catechol or gallol groups can coordinate to various metal ions such as Fe^{3+}, Zn^{2+}, Cu^{2+}, Al^{3+}, and Zr^{4+} forming a class of metal–organic materials: metal–phenolic networks (MPNs) (Fig. 3).[16] MPNs are a rapid, robust, and universal method for coating various substrates by using the coordination of polyphenols and metal ions.[26,27] Since the chelation between the catechol and/or gallol groups of polyphenol and metal ions is pH-dependent, MPN materials have interesting assembly–disassembly properties. When the catechol and gallol groups are protonated at low pH, the MPNs disassemble due to the breakdown of coordination bonds.[28] The tuneable disassembly profiles in acidic environments using different or mixed metal ions allowed for customizable degradation kinetics and permeability.

Metal ions not only contribute to the final function of hybrid MPNs but also modulate the assembly of phenolic compounds thermodynamically.[29] For example, the polymerization of dopamine and the deposition rate of PDA was greatly accelerated using $CuSO_4/H_2O_2$ as a trigger.[30] The Cu^{2+} and H_2O_2 produce reactive oxygen species (ROS) in an alkaline medium that aids in the polymerization of dopamine. Substitution of Fe^{3+} with Fe^{2+}, as formulated in the iron gall ink, can produce a thickness-controllable (*i.e.*, from 120 nm to 2.5 μm) MPN film at the interface without the assistance of stabilizers. The steady O_2 oxidation of Fe^{2+} to Fe^{3+} in a Fe^{2+}–TA complex generates Fe^{3+}–TA species *in situ* leading to the formation of micrometer-thick Fe^{3+}–TA films that are transferable and self-healable.[31]

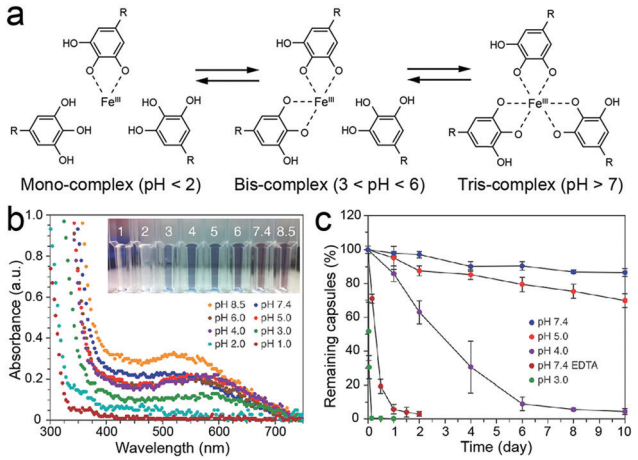

Fig. 3 (a) pH-Dependent transition of dominant TA–Fe coordination interaction. (b) UV absorption spectra and photo of spherical TA–Fe capsule dispersions at different pH. (c) Stability profiles of capsules at different pH. Reproduced with permission. Copyright 2013, American Association for the Advancement of Science.

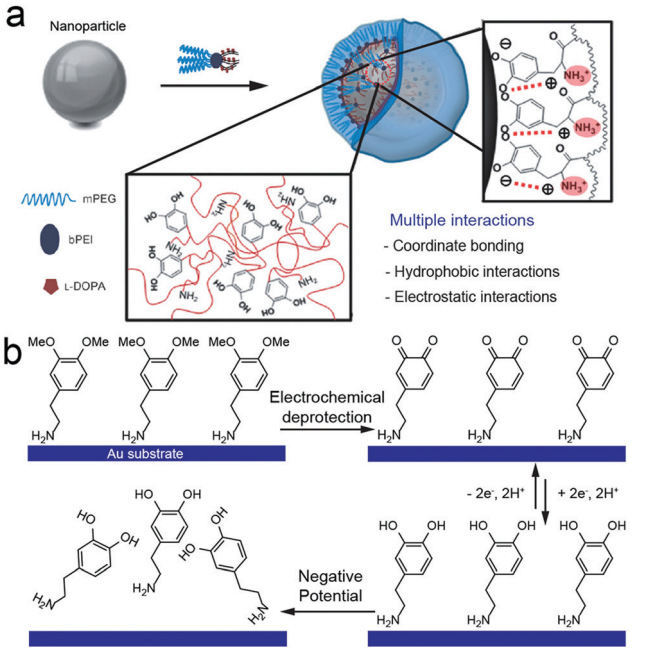

Fig. 4 (a) Schematic illustration of the synthesis of water-dispersible nanoparticles using a ligand with multiple interactions. Reproduced with permission. Copyright 2011, Wiley-VCH. (b) Construction and release process of dopamine self-assembled monolayers on the Au surface under electrochemical modulation. Reproduced with permission. Copyright 2019, American Chemical Society.

2.1.2 Metal and metal oxides. The coordination chemistry of phenolics has also been used for coating and stabilizing metal and metal oxide nanoparticles.[32] A representative example is the use of dopamine derivative ligands for iron oxide nanoparticles: a spectroscopic study showed that the bidentate catechol can convert the under-coordinated Fe on the surface to oxygen-coordinated Fe with an octahedral geometry resulting in tight binding of dopamine to iron oxide.[33] Hyeon and co-workers developed a multivalent ligand that contains a MAP-mimicking poly(L-3,4-dihydroxyphenylalanine) (polyDOPA) domain with catechol and primary amine groups.[34] This ligand can stabilize various nanoparticles (*e.g.*, Fe_3O_4, MnO, and Au) through a combinational binding effect including directional interactions arising from catechol and amine groups, micelle formation, and electrostatic interactions between positively charged ligands and negatively charged nanoparticle surfaces (Fig. 4a). Similarly, multivalent peptide dendrons containing a surface-binding catechol domain exhibit binding affinity for a wide range of metal oxides (hydroxyapatite, TiO_2, ZrO_2, CeO_2, Fe_3O_4).[35]

Aside from the native functional groups, other moieties on phenolic compounds can offer chelation properties. The amino group in dopamine is one such group and can interact with Au. To better understand the binding mechanism, Jiang and co-workers protected the two hydroxyl groups on dopamine with methyl groups leaving the amino groups free to bind to Au substrates (Fig. 4b). They further confirmed and investigated the binding using X-ray photoelectric spectroscopy.[36]

Phenolic compounds usually exhibit a typical redox behaviour due to the presence of alcohol groups. While the electrochemical oxidation is affected by the chemical substituents on the aromatic rings (*e.g.*, amine, sugar, *etc.*), environmental pH is a key factor because it directly determines phenolics' antioxidant capacity, radical scavenging activity, and oxidative product formation. Differential pulse voltammograms showed that phenol oxidation to a phenoxy radical on the first scan is pH-dependent corresponding to an irreversible electron-proton exchange.[37] On the second scan, the oxidation peaks of the adsorbed phenol oxidation products, *i.e.*, *ortho*-quinone (catechol) and *para*-quinone (hydroquinone), also showed a reversible two-electron and two-proton transfer. As is typical for the electrochemical oxidation of organic species, a higher pH triggers easier electron loss. Furthermore, as a general rule, *para*-benzenediol and *ortho*-benzenediol (+0.15 V and 0.20 V *vs.* Ag/AgCl at pH 7) oxidize at a lower potential than *meta*-benzenediol and mono-phenols (>0.70 V, *vs.* normal hydrogen electrode (NHE)) at neutral pH.

Therefore, phenolic compounds have been directly used to reduce noble metal ions such as Ag^+, Au^{3+}, Pt^{4+}, *etc.*, which represents a "green" method to synthesize nanoparticles. For example, dopamine has been used as a reductant for synthesizing Au nanoparticles from Au^{3+} by taking advantage of the two-electron oxidation of dopamine.[38] Moreover, diverse plant polyphenols such as TA and epigallocatechin gallate (EGCG) have been used to synthesize noble metal nanoparticles.[39]

With this reductive property in mind, phenolic groups were also conjugated to polymers to create multivalent polymers that act as strong reductants. For example, Duan and co-workers developed a block copolymer where the hydrophilic block of 4-vinylphenol (VPh) and di(ethylene glycol)methyl ether methacrylate (EGM) copolymer (PVPhEGM) contains a number of pendant phenolic group.[40] Au nanoparticles were produced upon addition of $KAuCl_4$ into the solution of PVPhEGM emphasizing its strong reducing activity. Micelles made from this

polymer enabled Au precursor reduction on the micelle surface producing a complete nanoshell. In addition to the formation of monodisperse metallic nanoparticles in solution, the phenolic-containing peptide coating can efficiently reduce Ag^{+} into a seamless Ag layer and form a remarkable seamless metallic coating on the surface.[41]

2.1.3 Semiconductor materials and upconversion materials. In addition to coordination, hydrogen bonding is also present in the interactions with semiconductor and upconversion materials. Waite and co-workers investigated the interactions of catechol-containing peptides on TiO_2 (anatase).[42] The results revealed that bidentate coordinative bonds on TiO_2 were formed at the initial stage of absorption. Hydrogen bonding later became dominant; long-range electrostatic and van der Waals interactions would emerge later (Fig. 5a). Hydrophobic interactions between the aromatic structures in phenolic and semiconductor materials are also notable. For instance, several polyphenols have been used to exfoliate various transition metal dichalcogenide (TMDs) into monolayer nanosheets *via* ultrasonication. The hydrophobic aromatic structures in polyphenols can interact with the TMD monolayer *via* hydrophobic interactions while the hydrophilic hydroxyl of polyphenols can improve the colloidal stability of exfoliated nanosheets.[43] In the example of PDA-mediated $MoSe_2$ nanosheets, the interactions involved not only hydrophobic interactions but also electrostatic interactions between the negatively charged phenolic group and the positively charged $MoSe_2$.[44]

The surface effects on catechol–semiconductor (SiC, GaN, InN, CdS, CdSe) interfaces have been simulated and investigated.[45] One interesting result is that catechol is located in the proximity of two Cd surface cations while the produced Cd–O coupling is weak as suggested by the absence of the surface dimer relaxation and the lower adsorption energy. Moreover, catechol maintains its original geometry without protonating or rotating the lateral hydroxyl groups.

In one example, ZnS was modified with catechol-functionalized polyethylene glycol (PEG) *via* a bidentate and/or a bridging bidentate interaction.[46] The directly chelated catechol-containing molecules efficiently quenched the fluorescence of the nanoparticles due to their fast and reversible oxidation processes. Specifically, it was hypothesized that when an electron of quantum dot (QD) is excited to the conduction band, an electron from the catechol ligand can immediately refill the valence band hole to quench the fluorescence. Moreover, linear assembly of QDs can be obtained *via* catechol-conjugated hyaluronic acid (HA) as a soft template by taking advantage of the affinity between catechol and QDs.[47]

Besides direct conjugation with semiconductor materials, it is also notable that the redox-active phenolic moiety can conjugate with QD *via* other groups (*e.g.*, Histag) to modulate the photophysics of the complex (Fig. 5b and c).[48] For example, the oxidation of dopamine to quinone by O_2 readily occurs at basic pH, and this quinone can act as an electron acceptor to quench the photoluminescence of QD in a pH-dependent manner due to electron transfer. In another work, two typical phenol derivatives with electron-donating (*i.e.*, 4-methoxy) and electron-withdrawing (*i.e.*, 4-nitro) moieties were investigated to reveal the charge transfer dynamics of QD-phenolic molecules.[49] The results showed that both 4-nitrophenol (4NP) and 4-methoxyphenol (4MP) can quench the photoluminescence of CdSe QD; cyclic voltametric analysis suggested that the excited CdSe transferred electrons to 4NP and holes to 4MP.

Similarly, phenolic shells on the surface of sodium citrate-capped upconversion nanoparticles (UCNPs) can also serve as efficient quenchers for the upconversion fluorescence. Of particular interest, the fluorescence of the UCNP can be retained after phenolic coating by using a water-in-oil microemulsion method where hydrophobic oleic-acid-capped UCNPs ($NaGdF_4$:Yb,Er@$NaGdF_4$) were directly coated with PDA.[50,51] Moreover, the upconversion fluorescence intensity of UCNP@PDA–PEG is similar to that of UCNP@SiO_2. This is likely due to the presence of oleic acids which serve as an insulator to reduce the electron transfer between the PDA and UCNP. It is notable that the PDA shell can also significantly inhibit the leaking of Gd^{3+} from UCNP over time.

2.1.4 Carbon materials. Polyphenols can also conjugate to various carbon materials such as graphene oxide, carbon nanotubes (CNTs), and carbon QDs.[52,53] For example, reduced graphene oxide (rGO) with good colloidal stability was prepared *via* an environmentally-friendly method where TA serves as the reductant for graphene oxide (GO) as well as a stabilizing ligand for rGO.[54] Compared with traditional chemical reducing agents such as hydrazine or dimethylhydrazine, polyphenols are safe and economical. The reduction of GO was proposed to involve two steps: first, the phenolic hydroxyl groups of TA attacks the epoxy group on graphene oxide simultaneously generating a new hydroxyl nearby; second, this new hydroxyl is attacked by

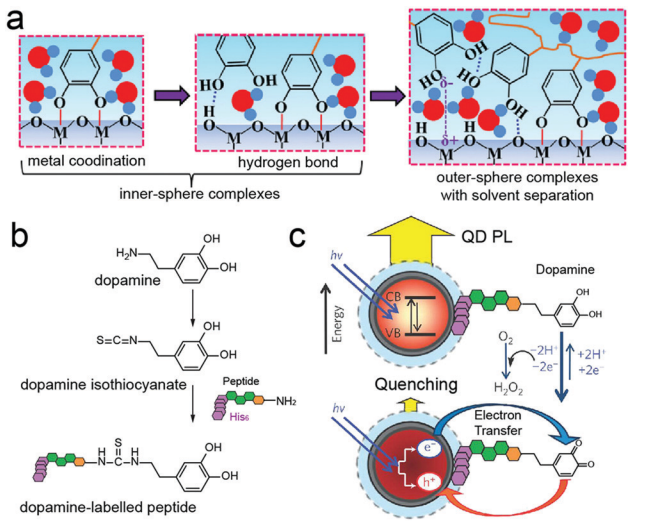

Fig. 5 (a) Proposed adsorption mechanism of catechol groups on metal oxide (*e.g.*, TiO_2) surface. Reproduced with permission. Copyright 2016, Wiley-VCH. (b) Synthesis of a dopamine–peptide *via* amine-reactive isothiocyanate. The His6 sequence in dopamine–peptide can self-assemble onto DHLA–PEG QDs. (c) Proposed energy-transfer mechanism between dopamine–peptide and QD. (b and c) Reproduced with permission. Copyright 2010, Nature Publishing Group.

another phenolic hydroxyl of TA. The resulting intermediate undergoes an elimination reaction resulting in a conjugate bond at the original epoxy site while the gallol groups convert into diquinone (Fig. 6). The successful reduction of graphene oxide was proved by XPS in which the sp^2 fraction of rGO was as high as 71%—close to the reduction by hydrazine and thermal annealing at 1000 °C (80%). Due to the π–π stacking with TA, the rGO sheet had a thickness of ~1.5 nm compared to pristine GO (1.1 nm). The electrostatic repulsion and sterics of TA facilitated the good dispersion of rGO in diverse solvents such as ethanol, dimethylformamide, and dimethylsulfoxide, which allowed for the preparation of high-performance polymer composites by direct blending.[55]

To understand how TA can stabilize CNTs, Xing and co-workers proposed a two-step adsorption model to explain their interaction.[56] First, the aromatic rings of TA molecules interact with the surface carbon rings of CNTs through π–π interactions to form a monolayer of TA molecules; the TA monolayer then further interacts with the dissolved TA by hydrogen bonding and other polar interactions. The adsorbed TA increases the steric repulsion between individual CNTs to produce relatively monodisperse CNT and stabilize them. Furthermore, the authors showed that the adsorption of phenolic compounds on CNTs increased when aromatic rings with a higher number of hydroxyl substituents were emploited.[57] This suggests that electron-donating substituents on phenolics can facilitate the π–π electron donor–acceptor interaction. In another study, Wang and co-workers investigated the absorption mechanism of three aromatic compounds (*i.e.*, salicylic acid, phthalic acid, and catechol) by using CNT and activated carbon.[58] Their results indicated that hydrophobic interactions, π–π interactions, electrostatic interactions, and hydrogen bonding collectively contribute to the interaction between carbon materials; the magnitude of each type of interaction varies with the specific chemical structure of different aromatic compounds. In addition, activated carbon exhibited higher adsorption capacities compared to MWCNTs suggesting a pore-filling effect.

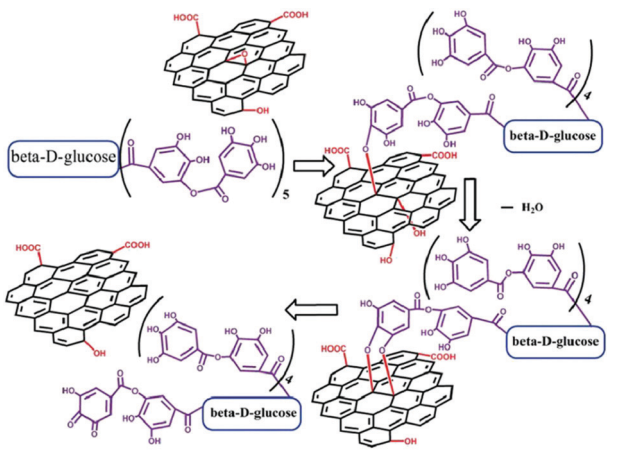

Fig. 6 Proposed mechanism of reduction of GO by TA. Reproduced with permission. Copyright 2011, Royal Society of Chemistry.

2.1.5 Silica materials. Simulation results show that the underwater adhesion mechanism of catechol molecules on hydrophilic silica is hydrogen bonding. Catechol can displace the pre-adsorbed water molecules on silica to bond directly on the surface silanol.[59] The calculated binding energy is 23 kcal mol^{-1}, and the bond can be destroyed by a force of 0.5 nN. Encouraged by this, phenolic compounds have been used to modify silica nanoparticles, mesoporous silica nanoparticles (MSN), *etc.*[60–62]

However, recent studies with dopamine indicate that the interaction is less favourable due to the surface charge repulsion between silica and dopamine molecules.[63] To address this challenge, amino groups modified with silica particles by a co-condensation approach were used to improve the deposition of phenolics (*e.g.*, dopamine) through Schiff base formation and/or Michael type addition.[64]

In addition to post-synthesis methods to modify silica materials, phenolic compounds can also interact with silica precursors to fabricate hybrid silica materials.[65,66] To understand the roles of polyphenol in the synthesis of silica nanoparticles, gallic acid, ethyl gallate, eudesmic acid, quercetin, and TA were used to investigate the effect of chemical structure on their templating ability.[67] The results revealed the mechanism of TA-templated MSN where the silica precursors can attach to the irregular TA supramolecular framework *via* hydrogen bonding, which subsequently acts as the skeleton for porous silica. If dopamine was used instead of TA, PDA would be introduced into the silica framework. This result suggests the important role of amines in PDA towards stable hybridization in the particles.[68]

2.1.6 Other materials. Due to the multifaceted physicochemical properties of the phenolic group, phenolic compounds have been used to design inorganic hybrids with components of different material species although some of the mechanistic details are lacking. For example, Liu and co-workers investigated the formation of $CaCO_3$–PDA hybrid nanoparticles and found that the coordination between Ca^{2+} and PDA could facilitate their biomineralization.[69] Similarly, PDA coatings have been also applied on other carbonates such as $Gd_2(CO_3)_3$ nanoparticles.[70]

Phenolic compounds also interact with nanoclays. As discussed in the previous section, the chemisorption of phenolics to metal oxide surfaces was the monodentate and/or bidentate bond while that of catechol to silica was hydrogen bonding (typically regarded as a weaker bond). Considering these properties, Takahara and co-workers demonstrated that the dopamine derivative can also be firmly linked to alumina on the innermost surface of a halloysite tube instead of to the silica on the outermost surface of halloysite.[71] This selective modification by immobilization of phenolic groups *via* robust coordination bonds could lead to more opportunities for anisotropic surface engineering. In another example, Lu and co-workers found that the catechol moieties can chelate with ions such as Mg and Si and therefore facilitate the conjugation of dopamine molecules to the nanoclay surface. Furthermore, the amino groups of dopamine can provide additional electrostatic interactions in the clay nanosheets similar to the role of common intercalation reagents (*e.g.*, quaternary ammonium halides).[72]

Two-dimensional (2D) MXene materials, such as transition metal carbides, nitrides, and carbonitrides, have demonstrated immense potentials such as photothermal properties. However, MXene-based materials often suffer from mechanical fragility and vulnerability to oxidation. To remedy this, PDA has been used to improve interflake interactions and ordering in MXene-assembled films. The XPS data confirmed that the catechol groups have strong affinities to the multivalent metal ions *via* coordination bonding especially a catechol–titanium oxide complex. In addition, the primary and secondary amine peaks in the PDA-treated MXene films have obvious binding energy downshifts by 0.4–0.6 eV *versus* pure PDA possibly due to the formation of hydrogen bonding with –O and –F terminates of MXene.[73] The facile PEN-mediated Mxene has been widely investigated to address its intrinsic limitation and improve its potentials for a variety of applications.[74]

Phenolics can also be used to modify black phosphorous.[75] The amine group of dopamine can interact with the negatively charged BP.[76] Moreover, redox-active PDA was reported to not only isolate the interior BP nanosheets from oxygen and water to improve its stability but also to enhance its photothermal performance.[77]

Of course, it is impossible to highlight all of the emerging materials that have been integrated with phenolic compounds much less offer a comprehensive discussion of the interactions between the phenolics and diverse materials. For example, phenolic compounds have been also used to design hybrid cobalt phosphides nanoparticle,[78] FeC,[79] and so on. But we hope what the summary here will inspire readers to not only design diverse functional hybrid nanoparticles but also look into the detailed formation mechanisms to underpin the future development of PEN.

2.2 Organic materials with phenolics

The interaction of organic materials with phenolics involve both supramolecular chemistry and covalent bonds. The intermolecular forces in phenolic compounds include hydrogen bonding, π–π interactions, hydrophobic effects, coordination and electrostatic attractions, and common covalent bonds formed by oxidative coupling or base-catalysed reactions. Synthetic details have been discussed in several reviews elsewhere.[21,80] Here, we focus on the types of materials used to design functional hybrids. The interaction between organic materials and phenolics usually involves multiple attractive forces, and thus it is worthwhile to highlight these key interactions to simplify these complex processes.

2.2.1 Small molecules. Phenolics are typical aromatic compounds with hydroxyl moieties, which indicates a suitable electron-rich π system for aromatic π–π stacking.[81] One typical example is the interaction of phenols with organic dyes. Methylene blue was used as a model to investigate the adsorption processes of organic dyes by PDA. The results showed that the adsorption was dependent on several interactions such as π–π stacking and electrostatics.[82] In addition, the catechol groups can react with many organic compounds (*e.g.*, amine and thiol groups) *via* Michael addition or Schiff-base formation.[80] Based on the versatile

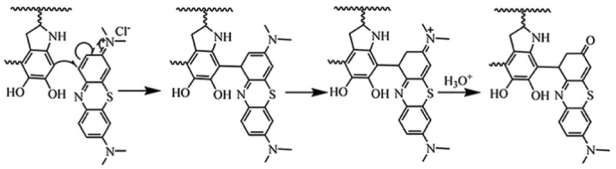

Fig. 7 The proposed adsorption mechanism between PDA and MB. Reproduced with permission. Copyright 2014, Royal Society of Chemistry.

properties of phenolics, a series of organic dyes were used to study the absorbance mechanism on PDA. The results indicate that the PDA-based hydrogel could selectively adsorb the dyes with an Eschenmoser structure (*i.e.*, dimethyl(methylidene)ammonium salts) because the *ortho* position of catechol group can undergo a Michael addition with Eschenmoser groups in the dyes (Fig. 7).[83]

In addition to decontamination of dye pollutants from wastewater, functional dyes such as indocyanine green (ICG), can also complex with PDA as imaging probes. At a pH of 2–3, negatively charged ICG was absorbed on the surface of PDA nanoparticles (isoelectric point ~4.6) by electrostatic and hydrophobic interactions.[84] The anti-cancer drug doxorubicin (DOX) can also strongly interact with PDA *via* π–π stacking and hydrophobic interactions due to its aromatic structure. For example, a high loading efficiency (99%) was achieved with a weight ratio of PDA to DOX of 2.[85] Therapeutic chlorin e6 (Ce6) was also conjugated to the amino groups of PDA through a conventional carbodiimide reaction.[86]

Another commonly used phenolic chemistry is the facile conjugation with small molecules containing amine or thiol moieties. One representative example is the use of 3-aminopropyltriethoxysilane (APTES) and TA to fabricate a hierarchical layer-nanosphere structure on diverse substrate. Here, the TA has two key roles: it is an adhesive layer on the surface of substrates, and it subsequently conjugates with APTES to form a rough layer.[87] Dopamine also contains amines in its structure. Lee and co-workers demonstrated that cation–π interactions are the primary intermolecular interactions during the formation of PDA coating rather than the hydrogen bonding and π–π interactions that are conventionally considered to be responsible for supramolecular assembly of PDA. Moreover, the quaternary ammonium ion has the strongest cation–π interactions with the aromatic rings among different cations including Li^+, Na^+, K^+, R–NH^{3+}, and NR^{4+}.[88]

Phenolic compounds can serve as surfactants and interaction with oil-in-water emulsion to prepare capsules. For example, the ultrasonication of oleic acid mixtures in water generated nanoemulsions of 100–250 nm in diameter, and amphiphilic phenolic compounds self-assembled at the oil/water interface. A phenolic capsule will be produced after crosslinking the phenolic coating.[89]

2.2.2 Synthetic polymers. Phenolic compounds can also form multidentate interactions with synthetic polymers such as PEG, poly(allylamine) (PAH), and poly(vinyl alcohol) (PVA) through multiple hydrogen bonding sites to produce hydrogels used for adhesive purpose.[90] Lee and co-workers reported a class of medical adhesives that were obtained *via* the intermolecular hydrogen bonding between TA and PEG. The TAPE system had

an adhesion strength 2.5 times higher than that of fibrin glue, and the good adhesion was retained in aqueous environments.[91] The strong hydrogen bonding formed between PVA and TA can also give the PVA–TA hydrogels excellent mechanical properties as confirmed by the high tensile strengths (up to 2.88 MPa) and high elongations (up to 1100%).[92] More recently, a similar attempt was tried by mixing PVA and TA to produce a reusable underwater adhesive. In contrast to previously reported PVA–TA systems, increasing the amount of TA (10–50 folds) and molecular weight of PVA led to a sticky sol-state glue with the unique underwater adhesive features of TA due to the formation of hydrogen bonding networks.[93]

Phenolic compounds have shown strong affinities with amine-containing polymers *via* abundant hydrogen bonding and electrostatic interactions. A range of neutral polymers including poly(*N*-vinylpyrrolidone) (PVPON), poly(*N*-vinylcaprolactam) (PVCL), poly(*N*-isopropylacrylamide) (PNIPAM), or poly(*N*-vinylamide) and TA have been assembled to make multi-layer coatings by layer-by-layer (LbL) technique.[94,95] For example, Caruso and co-workers exploited the ability of TA to serve as an efficient hydrogen bond donor to design multicomponent LbL capsules with PVPON at physiological pH.[96]

Another issue that should be considered is hydrolysis of tannin molecules that may occur under basic conditions (*e.g.*, the pK_a of phenolic groups in TA is 8.5) and at elevated temperatures. The deprotonation states make them negatively charged and can interact with positively charged polymers.[97,98] For example, the alternated deposition of PAH and TA can produce multi-layered films (PAH–TA) *via* electrostatic interactions.[99] The deprotonation of TA can also be exploited to form electrostatic interaction with zwitterionic polymers such as poly(sulfobetaine methacrylate) (PSBMA).[100] More specifically, electrostatic interactions between the deprotonated phenolic groups of TA and the quaternary ammoniums of PSBMA comprised the driving force for the TA/PSBMA LbL films. Moreover, the (TA/PSBMA) multilayer film had an improved stability compared to (PAA/PSBMA)—the authors attribute this to the high pK_a of phenolic groups and the dendritic structure of TA, which is in contrast to carboxyl moieties and the linear structure of PAA.

In addition to non-covalent interactions, the amino groups in polymers also formed covalent interactions with the oxidized catechol of TA.[101,102] Inspired by insect cuticle sclerotization, Lee and co-workers demonstrated a biocompatible and waterborne adhesive.[103] The results showed the mixture of phenol (*i.e.*, PG), polyamine (*i.e.*, polyethylenimine, PEI), and silica agglomerates in aqueous environment produced strong adhesion strength (>6 MPa). A two-step reaction was proposed: the oxidation of phenol into phenolquinone by air and the subsequent cross-linking between phenolquinone and PEI. Despite the simple synthesis and strong adhesion, the adhesive had no volatile organic compounds and good biocompatibility suggesting potential as a medical adhesive.

The presence of aromatic group in phenolic compounds further allows the interaction with hydrophobic polymers containing aromatic moieties. For example, PDA and TA have been widely used to surface modify PS nanoparticles for diverse biomedical applications.[104] Recently, Caruso and co-workers used phenolic compounds to mediate the assembly of benzene-1,4-dithiol (BDT) into monodisperse supramolecular nanoparticles *via* π–π interaction, revealing the general formation mechanism for such systems.[105] Co-precipitation is the main driving force for this assembly. The molecular dynamics (MD) simulations also highlighted that the phenolic molecules can interact with BDT through π–π stacking without compromising their ability to form hydrogen bonds (Fig. 8). This further explains the excellent colloidal stability of the nanoparticles in aqueous environment where the phenolics can provide bridging interactions between pBDT and water. Additionally, the π–π interactions in the nanoparticles can be easily destroyed in organic solvents (*e.g.*, dimethylformamide, DMF) triggering the disassembly of the supramolecular nanoparticles.

2.3 Biomacromolecules with phenolics

Phenolic compounds also interact with virtually all biomacromolecules including proteins, polysaccharides, DNA, RNA, *etc.* People have long consumed phenolics as a food and medicine. One notable example is the astringent sensations of wine due to their interactions with salivary proteins in mouth.[106] Tannins have been used in leather-making because phenolics bind to animal skin collagen *via* hydrogen bonding and hydrophobic interactions to give leather improved thermal and enzymatic stability. TA also exhibits strong antioxidant and α-amylase inhibitory activity, which is useful for obese people and type II diabetes patients.[107]

Although the combination of polyphenol and proteins has been explored for a wide range of functional materials, the

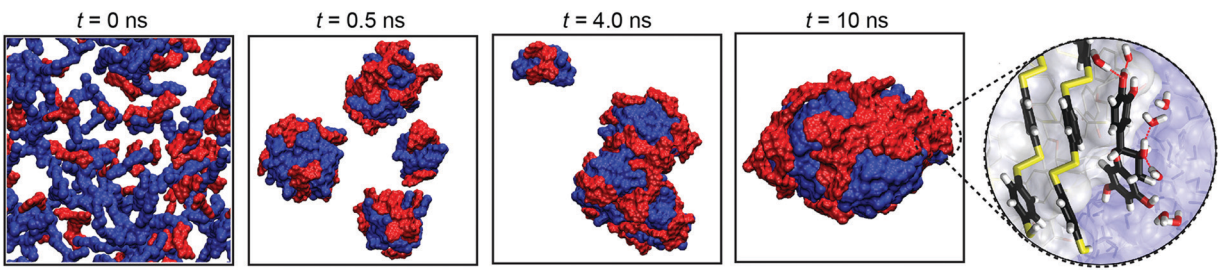

Fig. 8 All-atom MD simulation of the assembly of pBDT (blue) and catechin (red) at 0, 0.5, 4.0, and 10 ns in water. Magnified interface section illustrating the aromatic stacking of BDT and CAT and hydrogen bonding between CAT and water (red lines); carbon, oxygen, hydrogen, and sulphur are coloured black, red, white, and yellow, respectively. Reproduced with permission. Copyright 2020, Nature Publishing Group.

underlying interaction between phenolics and proteins are unclear.[108,109] Phenolics have shown strong yet reversible interactions with various proteins especially for proline-rich and histidine-rich proteins such as gelatin,[109] thrombin,[110] and elastin.[111] Recently, supramolecular interactions (*i.e.*, hydrogen bonding, hydrophobic interactions, and ionic interactions) between TA and a number of proteins with different pI, molecular weight, and aliphatic index were investigated to reveal the roles of proteins on the properties of the protein–polyphenol assemblies (Fig. 9).[112] The three key findings are summarized as follows. (1) The contribution of hydrogen bonding in the assembly mainly relies on the molecular weight of the proteins because the peptide backbone and most of the exposed protein surface is hydrophilic (*i.e.*, polar amino acids). (2) Proteins with high aliphatic indexes (*i.e.*, those containing hydrophobic side chains such as alanine, valine, and isoleucine) often form more hydrophobic interactions with the aromatic groups of phenolics compared to proteins with low aliphatic indexes. (3) The strength of ionic interactions between proteins and phenolics largely relies on the charge of the protein. This work offers a streamlined way to evaluate the stabilizing force in the assembly of polyphenols and diverse proteins; it can serve as a guideline for future systemic investigations of the complex nature of molecular interactions between polyphenols and proteins.

Messersmith and co-workers reported the use of random copolymers containing catechol and amine groups to immobilize DNA and then used this platform for DNA microarrays.[113] They proposed that the DNA probes interact with the polymer in both covalent and noncovalent ways. Specifically, catechols in the polymers that were not bound to the substrate may be oxidized into quinones and react with the amines and thiols of the captured DNA sequence;[114,115] Supramolecular interactions, such as hydrogen bonding, π–electron interactions, and electrostatic interactions between the amines of the copolymer and the DNA phosphate backbone were also likely to play an important role in DNA binding.[116,117]

The temperature-dependent rheological change of a TA–DNA gel suggested that the key driving force for the TA–DNA gels is the formation of reversible hydrogen bonds.[118] Upon mixing with TA, the wavenumber corresponding to antisymmetric vibration of phosphate groups in DNA was significantly shifted from 1238.22 cm^{-1} to 1199.64 cm^{-1}. Meanwhile, the ribose vibrational mode (C–C sugar) was shifted from 1095.49 cm^{-1} to 1085.85 cm^{-1}. Moreover, there is an overall shift in the peaks to lower wavenumbers indicating increased TA–DNA interactions. Therefore, the stabilizing interaction between TA and DNA was proposed to the hydrogen bonding between the gallol group of TA and DNA phosphate backbone. The complexed DNA was released from the assembly due to the degradation of TA through cleavable ester bonds.

More recently, Weil and co-workers used PDA as ''supramolecular glue'' for modulating DNA origami conformations. Specifically, PDA nanostructures have been fabricated based on the DNA origami templates in acidic medium, where a G-quadruplex (G4)/hemin-based DNAzyme can accelerate the oxidation of dopamine into PDA. The negatively charged DNA domains with multiple DNAzyme molecules can accumulate positively charged dopaminochrome/dopamine in a high local concentration thus leading to their preferential polymerization at the DNAzyme domain.[119]

Phenolic compounds can also interact with polysaccharides. TA was used as cross-linkers to improve the hydrogel strength of carboxymethyl chitosan (CMC) as proven by rheological measurements.[120] Under mild conditions, many intermolecular hydrogen bonds formed physical cross-linking on the surface of the microemulsion droplets for rapid hemostasis. In another work, catechol-carrying hyaluronic acid prepared by carbodiimide chemistry can form multilayer films with chitosan *via* electrostatic interactions to produce a bioadhesive film.[121] Phenolic groups can also conjugate to cellulose nanofibers (CNF) *via* covalent bonds. For example, a *N*-(3-(dimethylamino)-propyl)-*N*′-ethylcarbodiimide (EDC)/*N*-hydroxysuccinimide (NHS) catalysed amidation reaction can proceed *via* the amine group of dopamine.[122] The free catechol group can be therefore used for a secondary reaction such as chelation.

The various chemical groups in biomacromolecules offer tremendous opportunities to convert the existing groups into phenolic groups. Lignin can exhibit some tannin-like properties. However, such tannin-like properties of lignin are typically poor due to the limited free phenolic groups in lignin *versus* tannin. Lignin has many phenolic oxygens, and most of them are in the form of aromatic methoxy groups and inter-monomeric ether linkages. Therefore, using chemical or biochemical methods to increase the number of free phenolic groups in lignin can definitely give it a tannin-like functionality. To this end, lignin was functionalized with chemical demethylation to obtain demethylated guaiacyl-type synthetic lignins with tannin-like properties.[123] Meanwhile, tyrosinase led to a biofriendly enzyme-mediated process that can convert the monophenols into catechols *in situ*. This can create catechol groups in a target of interest (*e.g.*, peptides and proteins) that has native monophenol moieties while preserving its inherent function. The modified proteins can thus be used for surface coating while offering additional benefits such as biomineralization and metal ion chelation.[124]

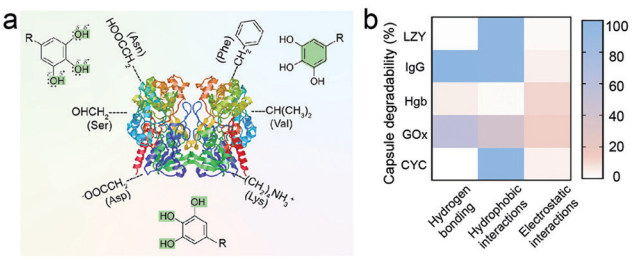

Fig. 9 (a) Schematic illustration of the proposed interactions between the functional moieties of phenolics and different amino acid of proteins. Asn = asparagine, Val = valine, Asp = aspartic acid. (b) Stability of protein–polyphenol capsules (LYZ, IgG, Hgb, GOx, and CYC) after 1 h of incubation with 100 mM of urea, Tween 20, or NaCl, corresponding to the dominant interactions between the different proteins and TA. Reproduced with permission. Copyright 2020, Wiley-VCH.

2.4 Other biomaterials with phenolics

Cell engineering is an important topic for the biomedical applications, but it often involves complicated methods such as the introduction of non-biogenic functional groups by metabolic or genetic engineering. Recently, adsorption of bioactive macromolecules onto cell surfaces or their intracellular delivery into the cytosol has been attempted to manipulate chemical and biological functionalities into living cells. The biogenic nature of phenolics thus provides opportunities to interact with biological substances for functional biomaterials.

Choi and co-workers reported the use of covalently cross-linked dopamine to coat the surface of *Saccharomyces cerevisiae* (*i.e.*, yeast).[125] The PDA encapsulation on yeast cells can control cell division, which is an essential characteristic for artificial spore structures. However, the robust PDA shell was a physical barrier to the biological activity of the encapsulated cells especially if the shell did not disassemble in response to external environmental stimuli. To this end, a cytoprotective shell that can be degraded on-demand was developed *via* MPN (Fig. 10).[126] The TA–Fe(III) shell (~40 nm) was clearly observed on the yeast@MPN biohybrid and suppressed cell division in plate cultures. Interestingly, the growth of yeast dramatically increased after the MPN shell disassembled under mild conditions; the reproduction of coated yeast was similar to native yeast. Besides the cyto-compatible degradability of the MPN shell, the shell can also act as a protective layer against multiple stressors such as UV radiation and silver (Ag) nanoparticles.

PEN can also mediate the interaction of diverse materials and the microorganism. Guo and co-workers developed a bioinorganic hybrid system that consists of TA-modified indium phosphide nanoparticles and genetically engineered *Saccharomyces cerevisiae*.[127] The polyphenol facilitated the immobilization of functional nanoparticles on the surface of yeast, where light-harvesting indium phosphide nanoparticles produces photogenerated electrons for cytosolic regeneration of redox cofactors. Similar biosynthesis-control strategies have been used for TA-capped Au nanoparticles for functionalizing microalgae.[128]

PEN-engineered biomaterials can also be developed from mammalian cells. For example, "cell-particle hybrids" consisting of pancreatic islets and PDA-coated FK506 (a potent calcineurin inhibitor)-loaded biodegradable microspheres (PD-FK506-MS) were fabricated to locally control the immune response at the transplantation site. The results demonstrated that the coating of FK506-MS with PDA allowed for the rapid assembly of stable islet-particle hybrids without significant changes in islet viability and functionality.[129]

Some phenolic compounds have specific affinity to certain cell lines or tissue.[130] The modification of protein and peptide therapeutics with TA can facilitate their adherence to extracellular matrices, elastins, and collagens, which improve heart tissue targeting.[131] Specifically, TA-modified (TANNylated) proteins preferably penetrated the endothelium to bind to myocardium extracellular matrix rather than being captured on endothelial glycocalyx layers in blood vessels. In another example, polyphenols such as TA were found to be mucoadhesive molecules. Therefore, a nanoparticle system assembled from F-68, TA, and anti-inflammation corticosteroid dexamethasone (DEX) was designed for inflammatory bowel disease therapy.[132] The inflamed colon epithelium is positively charged due to accumulation of positively charged proteins (*e.g.*, transferrin) and bactericidal/permeability-increasing proteins. Therefore, negatively charged phenolic nanoparticles can preferentially adhere to the inflamed mucosa in mice with colitis providing both anti-inflammatory and colon-targeting ability.

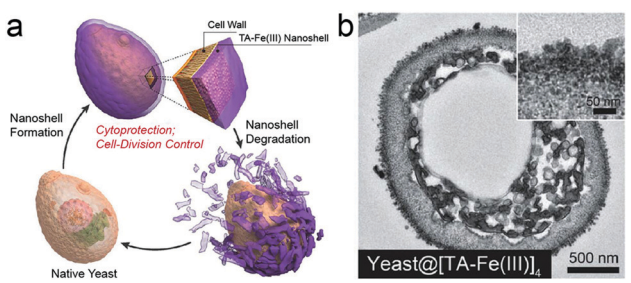

Fig. 10 (a) Schematic illustration of the controlled formation and degradation of the TA–Fe(III) shell on individual *S. cerevisiae*. (b) TEM image of yeast@MPN. Reproduced with permission. Copyright 2014, Wiley-VCH.

3. PEN for functional particle systems

The versatile phenolic chemistry underpinning PEN allows for engineering particle systems with customized structures and properties. However, phenolics were not popular particle building blocks in the beginning, as most phenolic compounds were used in the leathering, wine and food industry.[133] The investigation of PEN-based particles underwent a quick and large expansion after mussel-inspired materials were developed for surface coatings.[13,134]

For materials engineering, phenolics may play different roles either during the synthesis or in post-modification processes. By controlling the physicochemical interactions with stabilizing molecules, phenolics can self-assemble into particles in a confined space, form coating shells on the surface of preformed particles, or serve as templates for secondary growth of other functional materials. In addition to self-assembled particles, phenolics with specific monomers including metal ions, polymers, proteins, nucleic acids, and other functional molecules can co-assemble into particles.[17] Depending on the molecular interactions between each building block, particles with multiple components can be obtained in a simple "one-pot" or "one-step" synthesis. This co-assembly strategy by PEN increases the synthetic library of multifunctional particle systems. Intensive efforts have been made to construct functional particle systems by PEN, and one of the key rules in PEN is that the attractive force between phenolics and complementary structural motifs be balanced with a repulsive force among confined hybrid particles. In this section, we will introduce PEN-derived particle systems with unique architectures, particle surface coatings using

PEN, and engineered secondary nanostructures derived from phenolic-based templates.

3.1 Particle systems with engineered composition and structure

3.1.1 Particles. Phenolic particle systems can be formed by a variety of building blocks through covalent and/or non-covalent interactions. The phenol groups of these building blocks such as catechol and gallol groups can be turned into quinones in oxidative conditions and lead to self-polymerization to form final particles.[22,135] For instance, mussel-inspired dopamine is a famous phenolic compound for particle engineering. In weak alkaline solutions or when treated by oxidants, dopamine molecules easily undergo oxidative self-assembly into PDA.[136] The colloidal PDA particles exhibited excellent physicochemical properties and great potential in biomedical applications.[3] However, along with the investigation of fundamental chemistry of phenolics, a series of multi-component particulate structures have been synthesized by co-assembly of phenolic compounds and other functional motifs including metal ions, small molecule drugs, polymers, peptides, proteins, and nucleic acids. This synthetic strategy provides a new and facile route to integrate different modalities in a single particle system.

Phenolic groups show strong coordination toward metal ions, which enable co-assembly of each component, leading to the formation of metal-contained phenolic particles. For example, Gianneschi and co-workers prepared Fe^{3+}-doped PDA nanoparticles through self-polymerization of dopamine monomers in the presence of Fe^{3+}.[137] This was achieved through the use of a pre-polymerization doping strategy, which employs tris-Fe^{3+}–dopamine complexes and free dopamine as the precursors for the formation of Fe^{3+}-doped PDA. The Fe^{3+} can be continuously incorporated into the particles allowing for tuneable doping levels. The chelating molar ratio of dopamine and Fe^{3+} varied in response to the pH change. Excessive addition of free dopamine could result in the formation of mono- or bis-Fe^{3+}–dopamine precursors. Due to the strong chelating ability of the catechol groups, they further applied this method for the co-assembly of other transition metal ions including Mn^{3+}, Ga^{3+}, Co^{2+}, Ni^{2+}, Cu^{2+}, and Zn^{2+}.[138] PDA nanoparticles of various sizes, shapes, and morphologies could be obtained in the presence of different metal ions. Though the precise mechanism for metal ion-polymerization still needs to be explored, the authors prepared specific metal ion-loaded PDA nanoparticles for on-demand applications such as magnetic resonance imaging.[139] Dopamine can co-assemble into particles with metal ions. Other phenolic compounds including TA and EGCG can also chelate metal ions to fabricate hybrid phenolic particles. Metal–polyphenol coordination crystals were synthesized through oxidative self-polymerization of TA and metal salts under hydrothermal treatment.[140] The coordination interactions between Co^{2+} and TA could be enhanced in alkaline conditions resulting in deprotonation of trihydroxyphenyl groups. Further, the radical generation and oxidative process for self-assembly were driven by dissolved oxygen. Metal/tannic particles (>2 μm) are normally larger than the hybrid PDA particles (20–500 nm), which could be attributed to the different polymerization mechanisms of the two phenolics.

Moreover, the self-assembly of phenolic compounds could also incorporate small molecule drugs in the metal-doped particle system leading to a hybrid particle system for drug delivery. Cheng and co-workers conjugated Bortezomib, a proteasome inhibitor, with four kinds of polyphenols (catechin, EGCG, TA, procyanidin) *via* borate ester bounds.[141] Fe^{3+} was used to form interchain Fe^{3+}–catecholate coordination, and the hybrid conjugates could co-assemble into a highly stable supramolecule. The authors claimed that this strategy could reduce the adverse effects and retain the anticancer activity of the drugs. Similar strategies have also been utilized for hybrid phenolic particle synthesis *via* EGCG, platinum(IV) prodrug, Fe^{3+}, and block copolymers as building blocks (Fig. 11a).[142] The as-prepared particles exhibited a size distribution of 60 nm to 110 nm and showed high stability during *in vivo* circulation (Fig. 11b). In this case, EGCG was a natural nanoplatform consisting of different functional modalities including drug delivery and bioimaging by simple processes—this offers a new avenue for multifunctional nanomedicine. Other metal ions, such as molybdenum (Mo),[143] gadolinium (Gd),[144] and lanthanide (La)[145] have also been successfully imparted into phenolic particles by co-assembly of metal ions and phenolic monomers suggesting the wide applicability of the strategy. The presence of metal ions did not disrupt the polymerization process, and they could even serve as oxidative agents further facilitating the self-assembly. Therefore, PEN offers a simple method for

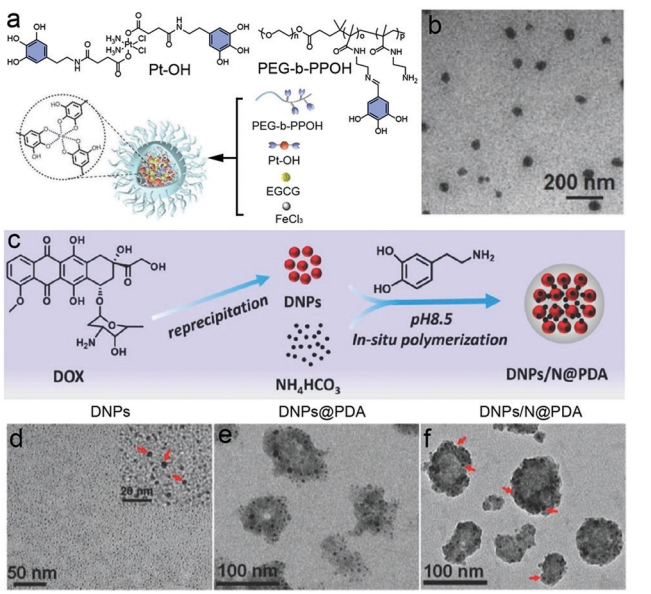

Fig. 11 Co-assembled phenolic particles with metal ions and small molecule drugs. (a) The chemical structures of building blocks (Pt–OH, PEG-*b*-PPOH) and schematic illustration of a phenolic particle prepared by co-polymerization. (b) TEM image of the as-prepared phenolic particles. (a and b) Reproduced with permission. Copyright 2020, Wiley-VCH. (c) Schematic illustration of synthesis of PDA-coated and NIR-responsive carrier-free "nanobomb" (DNPs/N@PDA). (d) TEM images of the DOX nanoparticles (DNPs), PDA-coated DNPs (DNPs@PDA), and NH_4HCO_3-loaded DNPs@PDA (DNPs/N@PDA). (c–f) Reproduced with permission. Copyright 2018, Wiley-VCH.

incorporation of functional metal ions within phenolic particulate substrates.

Phenolic molecules can co-polymerize with peptides/proteins into bioavailable particles. Peptides/proteins are easily degraded over long rounds of blood circulation. They may fail to function in the absence of protective delivery. Therefore, co-assembly with phenolics into particles could be an ideal strategy for protective delivery of peptides/proteins due to the protection from biocompatible phenolics. Kurisawa and co-workers demonstrated that EGCG derivatives could complex with an anticancer protein (Herceptin) to form micellar nanoparticles.[108] The micellar nanocomplex is obtained by complexation of oligomerized EGCG with Herceptin to form a core followed by complexation of PEG–EGCG to form the shell. The protein-contained particles with a monodispersed hydrodynamic size (*ca.* 90 nm) featured a longer blood half-life time *in vivo* than free proteins. Importantly, the particles displayed stabilized protein activity during complexation and dissociation, and this largely improved the therapeutic index. Cheng and co-workers developed a series of polyphenolic-based nanocarriers for cytosolic protein delivery.[146] Four kinds of polyphenols (EGCG, catechin hydrate, procyanidin, ellagic acid) were used for direct co-assembly of protein-contained particles. The authors indicated that both hydrogen bonding and hydrophobic interactions directed the particle assembly. Isothermal titration calorimetry results indicated that the binding of EGCG with bovine serum albumin is an exothermic reaction and the hydrogen bonding dominates the phenol–protein formation. Zhang and co-workers introduced PDA in particle engineering for hemoglobin delivery, which also takes advantage of PEN for protein encapsulation. The abundant catechol groups in PDA permitted non-covalent bonding with hemoglobin forming protein-contained PDA particles.[147]

Phenolic compounds can also be used for high loading of small molecular drugs in self-assembled particles instead of traditional polymeric micelles with low drug loading capacity. The strong binding of phenolic compounds to small molecule drugs formed through hydrophobic interactions, hydrogen bonding, and π–π stacking contributes to the encapsulation of a wide range of drug molecules. Kurisawa and co-workers developed a highly stable and large drug loading micellar nanocomplex based on the self-assembly of DOX and PEG–EGCG.[148] Favourable intermolecular interactions between the DOX and EGCG molecules improved the drug loading capability by 88%. This PEN-based strategy of particle engineering is particularly applicable to small molecule compounds with multiple-ringed structures with structural similarity to phenols. A PDA-coated carrier-free particle was developed for protective delivery of DOX and NH_4HCO_3 (Fig. 11c–f).[149] The biocompatibility and hydrophilicity of PDA prolonged the blood circulation time and prevented the leakage of drug molecules. Meanwhile, NH_4HCO_3 here served as "remote bomb" to facilitate DOX release, which could be triggered by non-invasive NIR irradiation. By taking advantages of PEN for particle fabrication, multifunctional modalities including drug loading, prolonged blood circulation, photothermal conversion, and secondary modification of targeting/imaging were achieved by this "all-in-one" phenolic particle.

3.1.2 Porous particles. Porous particles have been widely used in biomedicine due to their high loading capacity, large surface area, and structural advantages.[150,151] PEN has been considered a powerful toolkit to develop porous particles for specific applications. The intrinsic chemistry of phenolics further endows porous particles with tuneable pore size and shape, potential for second modifications, and stable bonding sites for cargo loading. The combined physical and chemical features of porous phenolic materials enable their widespread use in biomedical applications including drug delivery, biocatalysis, biosensing, and bioimaging.

Phenolic-based porous particles can be synthesized *via* self-assembly on "soft templates". Direct coating of phenolic compounds on pre-formed porous particles is another choice for preparation of porous phenolic-based materials.[152] This coating strategy for porous particle synthesis will be introduced in Section 3.2.1. "Soft templates" such as amphiphilic block copolymers interact with phenolics though hydrogen bonding, electrostatic interactions, and other non-covalent interactions. Yamauchi and co-workers prepared mesoporous PDA nanoparticles (particle size: *ca.* 200 nm; pore size: *ca.* 16 nm) through self-polymerization of dopamine and spontaneous co-assembly of diblock copolymers. The authors found that dopamine molecules could form stable composite micelles with high-molecular-weight block polymer (PS-*b*-PEO). The PS-*b*-PEO micelles herein acted as a sacrificial pore-forming agent that could be removed after particle synthesis. The results indicated that the particle size and pore size of PDA nanoparticles were largely dependent on the ratio of hydrophobic to hydrophilic chains in PS-*b*-PEO.[153]

A similar strategy of copolymer templating was used to prepare bowl-like mesoporous PDA by Lou and co-workers.[154] The dopamine molecules were first dissolved in a quaternary nanoemulsion system consisting of F127 block copolymer/1,3,5-trimethylbenzene/ethanol/water to form stable dopamine micelles. After the addition of an ammonia trigger, continuous cooperative assembly drove the oriented growth of PDA mesochannels. In this case, the F127 block copolymer served as sacrificial surfactant whereas 1,3,5-trimethylbenzene acted as pore swelling agent. By increasing 1,3,5-trimethylbenzene, the resulting product could be continuously tuned from symmetric nanoparticles to asymmetric bowl-like particles. Moreover, in order to increase the pore size, they introduced another block copolymer (P123) with shorter hydrophilic chains.[155] After the same assembly process, walnut-shaped macro-/mesoporous PDA particles with wide pore size distributions from 20 nm to 95 nm could be fabricated (Fig. 12a–e).

In porous particle engineering, the swelling agent is a crucial factor that determines the pore size and shape of particles. Zhao and co-workers provided a deep study of the micelle formation mechanism to give a clear description of mesoporous PDA self-assembly.[156] The authors proposed that 1,3,5-trimethylbenzene can interact with the hydrophobic PPO segment of block polymers and dopamine molecules through van der Waals forces and π–π stacking. This interfacial mediation

promotes the formation of a dopamine nanoemulsion with a size distribution from 8 nm to 52 nm, which in turn self-assembles into mesoporous PDA nanoparticles with pore sizes up to 37 nm. By increasing the amount of swelling agent, the nanoparticles varied from non-mesoporous particles to golf-ball-like nanospheres, multichambered mesoporous spheres, and dendritic-structured porous particles. In all, nanoemulsions are a facile route to prepare porous PDA particles. The results show that solvent, swelling agents, and surfactants are key factors for the fabrication of porous particles.

Unlike dopamine, natural polyphenols like TA, EGCG, and ellagic acid are usually used together with metal ions to prepare porous particles. Fechler and co-workers developed a facile and sustainable strategy to prepare hierarchically porous carbon particles.[157] Polyphenols can chelate with metal ions through coordination interaction allowing the formation of metal–phenolic complexes. After complexing with Zn^{2+}, ellagic acid monomers were directed into a well-organized framework, which assembled into mesocrystals. Finally, the high-temperature treatment enabled the thermal carbon conversion and removed the phenol–metal crystal, which transformed the as-prepared particles into a hierarchically porous carbon. The ellagic acid–Zn complex served as a carbon precursor and porogen in one unit—the so-called "salt-templating" strategy.

Recently, Caruso and co-workers reported a templating strategy using sacrificial polymer cubosomes (PS-*b*-PEO) to prepare ordered mesoporous metal–phenolic particles (Fig. 12f).[158] The polymer cubosomes (PCs) has a bicontinuous triply periodic minimal surface structures leading to a water channel networks with a long-range cubic crystalline order. Importantly, this "soft template" was stable in aqueous solution and could be readily removed by tetrahydrofuran. Thus, the metal–phenolic complexes (*i.e.*, EGCG and gallic acid; Fe^{3+}, Cu^{2+} and Zr^{4+}) fused with the PCs and subsequently assembled *in situ*. Finally, highly ordered mesoporous metal–phenolic particles with a large pore size of *ca.* 40 nm could be obtained (Fig. 12g and h). Relative to PDA of different porosities, fewer mesoporous polyphenol particles have been investigated. However, there are numerous studies focusing on polyphenol-based capsules with unique hollow structures that will be discussed in Section 3.2.2.

3.1.3 Anisotropic particles. Colloidal anisotropic particles with controlled and tuneable internal architecture have gained great research attention due to their structure-dependent advantages in various applications including energy conversion and biomedicine. However, the accurate engineering of anisotropic particles at the nanoscale level remains challenging. PEN provides a relatively facile method for the fabrication of anisotropic nanoparticles. Driven by molecular interactions with either soft or hard template substrates, phenolic materials can be readily assembled for the manipulation of anisotropic nanoparticles with unique structures such as patchy surfaces.[159]

The precise control of intermolecular interactions makes anisotropic growth easier. PDA–Au Janus particles could be

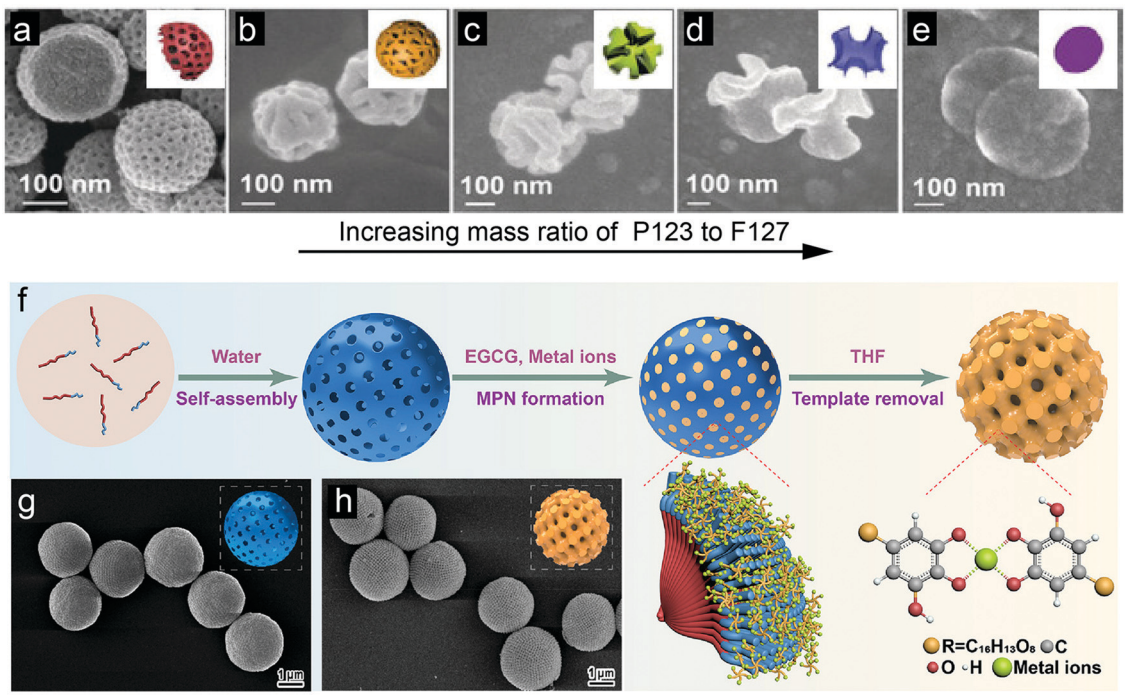

Fig. 12 "Soft template"-directed synthesis of mesoporous phenolic particles. (a–e) SEM images of PDA particles prepared with different mass ratios of P123 to F127: (b) 0 : 1; (c) 1 : 15; (d) 1 : 3; (e) 1 : 1; (f) 5 : 3. Insets: Schematic representation of mesophase transition of PDA particles at different P123/F127 mass ratio. (a–e) Reproduced with permission. Copyright 2018, Wiley-VCH. (f) Schematic illustration of synthesis of the mesoporous MPN particles using polymer cubosomes (PCs) as templates. SEM images of (g) PCs and (h) mesoporous MPN-coated PCs after template removal. (f–h) Reproduced with permission. Copyright 2020, American Chemical Society.

obtained by simply adding $HAuCl_4$ to a PDA particle solution.[160] Controlled electrostatic repulsion is key to formation of the Janus nanoparticles which could be only prepared in a narrow pH range of 2.5–3.0. The as-synthesized PDA–Au Janus particles could spontaneously self-assemble at oil/water interfaces as a result of the hydrophilic PDA and hydrophobic Au surface. In another study, various anisotropic PDA particles including nanobelts and nanofibers were prepared with the aid of folic acid.[161] The authors hypothesized that folic acid may participate in the self-polymerization process of dopamine molecules. The π–π stacking interaction and hydrogen bonding between folic acid and proto-molecules of PDA may contribute to the formation of PDA nanobelts and nanofibers. Anisotropic nanoparticles with similar nanofibrous structures were obtained by co-assembly of dopamine and pyrrole.[162,163] The oxidative co-polymerization of dopamine and pyrrole in alkaline solutions could produce hybrid nanostructures including nanospheres, nanofibers, nanorods, and nanoflakes by simply changing the molar ratio of two monomers.

Polymer–inorganic nanoparticles are a series of novel hybrid materials for multifunctional applications. Wang and co-workers utilized poly(acrylic acid) (PAA) particles as a structure-directed template for anisotropic growth of dopamine.[164] Different from conventional examples where dopamine molecules could deposit on the surface to form a complete coating shell, the PDA coating on the PAA particles only occurred on one side of particles, as also confirmed by time-dependent electron microscopy observation. This is probably due to the island nucleation of PDA on PAA to reduce the number of interfaces, which is similar to the Volmer–Weber growth mode. Thus, after asymmetric PDA coating on PAA nanoparticles, the deposition of mesoporous calcium phosphate on the other side of the particles could be achieved by introducing $CaCl_2$ leaving the PDA domain untouched. The resulting anisotropic particles could be further modified with PEG and ICG for cancer therapy.

Wang and co-workers developed hollow MOF-PDA Janus nanoparticles using a similar strategy, suggestive of its general applicability for diverse anisotropic particles of different compositions.[165] Using the PAA-directed strategy for anisotropic particles synthesis, they further prepared a monstera flower-like Au nanorod (AuNR)/PDA bowl with spadix-bract nanostructure.[166] The anisotropic structure is composed of AuNRs and bowl-like PDA shells, which allowed cargo loading of both hydrophobic and hydrophilic drugs. To the best of our knowledge, most phenolic-based anisotropic particles were derived from PDA; other phenolic-based materials are rarely reported. More effort should be paid to deciphering the underlying mechanisms so that different anisotropic PEN-particles can be used in the future.

3.2 Particle surface coating using phenolic-based materials

3.2.1 Surface coating on pre-formed particles. Surface coating is a straightforward method to modify or functionalize pre-formed particles. It can alter their surface chemistry and allow for secondary functionalization. Inspired by nature, phenolic-based materials have been widely used for surface coating. Mussels adhere strongly to rocks, ships, and other seashells in wet conditions because they can secrete the adhesive *Mytilus edulis* foot protein that contains many catecholic amino acids.[13] Therefore, phenolic compounds with a high content of catechols and pyrogallols could be a multifunctional coating on the substrate surface *via* strong interfacial bonding.[80,167]

Phenolics show a high affinity towards metallic substrates, leading to depositional coating in which the coordination bond is the main driving force. The surface coating of phenolic assembles could be applied in a variety of metal/metal oxide/metallic composite particles such as Au,[168,169] Ag,[170] magnetic nanoparticles (Fe_3O_4),[171] manganese oxide (Mn_3O_4),[172] molybdenum oxide (MoO_3),[173] aluminium oxide (Al_2O_3) particles,[174,175] and MOF.[176] The nature-inspired coating strategy significantly improves the stability, biocompatibility, and adhesion of the pre-formed particles. Duan and co-workers prepared PDA-coated magnetic nanochains by simply mixing Fe_3O_4 nanoparticles and dopamine molecules in alkaline buffer. Driven by a homogeneous magnetic field, the nanoparticles aligned in a row while the adhesive PDA concurrently formed a conformal coating on the nanochains. This surface coating not only acted as a scaffold to fix the chain structure but also allowed for further surface functionalization such as PEGylation.[177]

PDA-coated magnetic microswimmers were fabricated by dip-coating of magnetic nanoparticles on *Spirulina* and subsequent PDA coating on the outer shell surface.[178] The latter coating enhanced the photoacoustic signal and photothermal effects of the microswimmer, which facilitated real-time tracking of photothermal therapy (PTT). The intrinsic quenching effect and the versatile surface reactivity of PDA also provided an off–on fluorescence diagnosis with sensitive probes. This could be a facile yet productive method to functionalize micro/nanorobots. Core–shell Au nanochains were prepared by dopamine mediation and subsequent self-polymerization.[179] The resulting nanochain consisted of 4–5 Au cores and a PDA coating shell (Fig. 13a and b). The authors claimed that the interactions between the citrates on the Au surface and the protonated primary amines and catechols of PDA were key factors underlying assembly.

Hussain and co-workers functionalized AuNRs with TA for efficient endosomal uptake.[180] The TA-coated nanorods showed strong affinity to serum proteins and formed a strong protein corona matrix that protected the particles. Retention of the nanorods was observed following endocytosis into keratinocyte cells, which may result from the tight association between TA and cellular membrane proteins. TA overcoats the whole nanorods with no direct interaction with the Au surface because the nanorods were coated with cetyltrimethyl ammonium bromide (CTAB) during the synthesis. Unlike thiols, the pyrogallol groups of TA are not sufficiently strong to remove CTAB from the surface—this is a key point in TA coating.

Polyphenol-coated titania particles have been developed by tannic adhering *via* metal–organic coordination.[181] The slightly rough polyphenol surface showed additional reducing capacity enabling *in situ* deposition of Ag nanoparticles onto the shell surface. The pyrogallols could also react with thiol-terminated molecules for further modification.

Phenolic-based materials also showed conformational adhesion to other inorganic substrates such as silica particles,[182] graphene

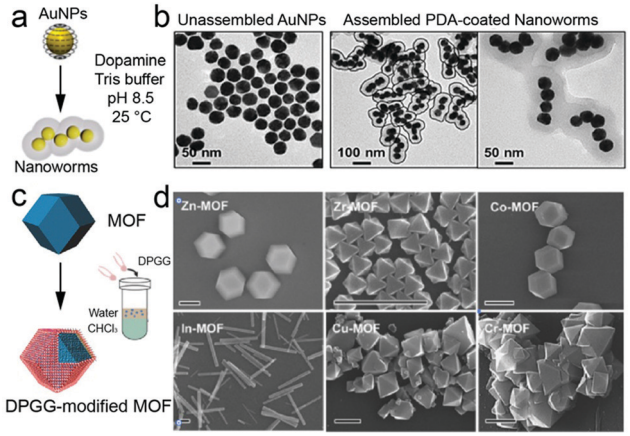

Fig. 13 *In situ* deposition of adhesive phenolic coating on pre-formed nanomaterials. (a) Schematic illustration of dopamine-mediated assembly of Au nanoparticles (AuNPs) into PDA-coated nanoworms. (b) TEM images of unassembled AuNPs and assembled nanoworms. (a and b) Reproduced with permission. Copyright 2019, American Chemical Society. (c) Schematic illustration of the surface functionalization of MOF particles by a phase transfer reaction. (d) SEM images of the DPGG-modified MOF particles of different metal ions. Scale bar:1 μm. (c and d) Reproduced with permission. Copyright 2017, Wiley-VCH.

QDs,[183] carbon materials,[184,185] and black phosphorus.[76,186] MSNs have been used in a wide range of biomedical applications (*e.g.*, drug delivery) due to their excellent chemical and mechanical stability, high pore volume, and surface area.[187] Although MSNs are well-known for their high drug loading capacity, the unfunctionalized particles cannot release cargo in a controlled manner. Thus, the phenolic compounds deposited on MSN could act as a "gate keeper" blocking drug molecules inside MSN and releasing them under specific stimuli. In one example, Mei and co-workers modified DOX-loaded MSN with a mussel-inspired PDA coating and further attached D-α-tocopheryl polyethylene glycol 1000 succinate (TPGS) to the PDA surface through Michael addition.[188] pH-Responsive drug release was observed; the resulting nanoparticles could release 38.9% and 47.7% of DOX molecules at pH = 6.5 and at pH = 5.0, respectively. Only moderate release (19.5%) was recorded when the nanoparticles were dispersed in neutral solutions over six days. The TPGS modification gave the nanoparticles the ability to overcome multidrug resistance. In this case, PDA exerts more than one functionality onto the pre-formed MSNs. Similarly, fluorescent nanodiamonds,[189] graphene nanosheets,[190] and carbon nanotubes[185] were also incorporated into a PDA shell for surface coating of carbon particles showing enhanced physiochemical properties.

Black phosphorus is a novel two-dimensional material that has recently attracted great attention of researchers for its good compatibility, photothermal conversion, and drug loading. However, phosphorus is sensitive to oxygen and water, which hinders its potential in biomedicine. PDA coatings can protect interior black phosphorus from environmental damage largely improving its stability.[77]

The surface coating of phenolic materials has also been used to engineer MOFs. MOFs are of great interest in a number of host–guest interactions and applications. However, most MOFs (*e.g.* zeolitic imidazolate framework) possess vulnerable intermolecular interactions between metal ions and organic ligands, which are often unstable under acidic conditions. The surface coating is applied to improve the stability and biocompatibility of MOF particles. A biocompatible and biodegradable core–shell MOF nanoparticle for tumor photothermal-chemotherapy was developed by PDA coating on MOFs particles.[191] The cytotoxicity and *in vivo* acute toxicity were evaluated and demonstrated that the biocompatibility of the MOF nanoparticles was greatly improved. Meanwhile, the degradation time was extended and regulated at a moderate rate. A novel strategy for the functionalization of MOFs was developed *via* a phenolic-inspired lipid molecule (1,2-dipalmitoyl-*sn*-glycero-3-gallol) as a coating shell. In particular, the intrinsic hydrophilicity of the MOF surface was altered to be hydrophobic and thus form various nanoarchitectures due to the amphiphilic particles (Fig. 13c).[192] Density Functional Theory calculations showed that strong chelation of the metallic skeleton and trihydroxylphenol groups was the basis for the synthesis of amphiphilic MOFs. A variety of metal ion (Zn^{2+}, Co^{2+}, Zr^{4+}, Fe^{3+}, Cu^{2+}, Cr^{3+}, In^{3+}, Al^{3+}, and Eu^{3+})-based MOFs have been used to prove the generality of this coating strategy (Fig. 13d). Queen and co-workers revealed that the PDA coating strategy offered stability improvements for a diverse set of MOFs with varying metals, ligands, and topologies including ZIF-8, ZIF-8, UiO-66, Cu-TDPAT, Mg-MOF-74, MIL-100-Fe, and HKUST-1.[193] However, phenolic compounds such as TA and gallic acid are weak organic acids that could release free protons and destroy MOFs. Much attention has been paid to the reaction conditions when preparing phenolic surface coatings on MOFs to avoid etching.[80]

Through covalent and non-covalent interactions, phenolic compounds can deposit on the polymeric particles and form a tight surface coating. For example, to facilitate the interactions with biological interfaces, polymeric nanoparticles usually need pre-functionalization, which is complicated and inefficient. Using phenolic-based materials as a surface coating is an easy and efficient method. Yeo and co-workers fabricated PDA-coated poly(lactic-*co*-glycolic acid) (PLGA) nanoparticles in a weak alkaline condition (pH = 8–8.5).[194] The authors speculated that PDA deposits on the polymeric surface as a thin film rather than particulate aggregates. After the prime-coating, PLGA nanoparticles could be further conjugated with amine- or thiol-terminated functional ligands such as small molecules, peptides, and other polymer ligands.

Recently, a PDA-coated nucleic acid nanogel has been prepared for gene-mediated cancer therapy.[195] The nanogel particles were first obtained by DNA-grafted polycaprolactone assembly with siRNA hybridization. PDA could also form a conformational coating on the hybrid polymeric particles to protect the bioactive particles from enzyme degradation and give the particles strong absorbance in the near-infrared. Thus, the delivered siRNA downregulated the expression of heat shock proteins and induced cellular apoptosis under mild photothermal treatment.

As mentioned above, phenolic compounds show adhesion on virtually any particle substrates thus serving as a multifunctional

shell for particle engineering. A facial synthetic strategy on the basis of polyphenol coating could be used in a number of particles with different sizes, shapes, structures, and composition. These are novel building blocks to create various superstructures. Moreover, the chemical activity and structural flexibility can be tuned on demand by incorporating different metal ions into the assembly. This phenolic coating strategy opens an avenue to the fabrication of hybrid and complex materials.[196] Surface coating is the most straightforward strategy to modify or functionalize the pre-formed particles. Further discovery of novel phenolic-based materials and investigation of the kinetics and mechanisms of phenolics will improve particle nanoengineering.

3.2.2 Hollow capsules. As mentioned, adhesive phenolic-based materials form conformational surface coatings on various particle substrates. Thus, by using sacrificial templates as the particle core, hollow capsules could be readily obtained. Emulsion droplets,[197] SiO_2 microspheres,[198] $CaCO_3$ particles,[199] and MOF particles[200] are frequently-used sacrificial cores that could be removed by treatment with ethanol, hydrofluoric acid, and ethylenediaminetetraacetic acid (EDTA). Depending on the original size of pre-formed particles, nano- and micro-hollow capsules could be prepared in a facile manner. The film thickness of coating shell could also be controlled by optimizing the reaction conditions.

With assistance of metal ions, phenolic hollow capsules could be easily prepared through MPNs. Caruso and co-workers developed a series of TA based phenolic capsules with a wide range of metal ions including Al, V, Cr, Mn, Fe, Co, Ni, Cu, Zn, Zr, Mo, Ru, Rh, Cd, Ce, Eu, Gd, and Tb.[16,26] Due to the strong coordination between TA and metal ions, robust metal–phenolic films were deposited on the $CaCO_3$ particles and could later be removed. The film thickness may vary according to the doped metal ions and is determined by the molar ratio of TA to metal ions. Further demonstrations of pH-responsive disassembly suggested that the hollow capsules have potential in responsive drug delivery.[201] A bilayered hollow nanoparticle of MPN-coated $CaCO_3$ was developed for cancer treatment by phenolic coating and core etching.[202] Specifically, the hollow particles were synthesized by simply mixing the gallic acid and Fe^{2+} with amorphous $CaCO_3$ particles. By extending the reaction time, a cavity was found inside the template particles and gradually enlarged leaving only the MPN shell. The resulting capsule exhibited high loading capacity of anticancer drugs, pH-responsive size shrinkage and drug release, and Fenton catalytic activity enabling enhanced tumor penetration and therapy.

Another example of EGCG–Cu(II) MPN capsule for peripheral artery disease was reported by using $CaCO_3$ as sacrificial core.[203] After several repetitive deposition cycles of EGCG–Cu(II) MPN onto $CaCO_3$ particles, EDTA was used to remove the templates (Fig. 14a–c). Such a metal–polyphenol capsule remarkably combined the anti-inflammatory and antioxidant activities of EGCG and the angiogenic activity of copper ions demonstrating the great advantages of PEN. Phenolic hollow capsules could be obtained with MOF particles (ZIF-8) as

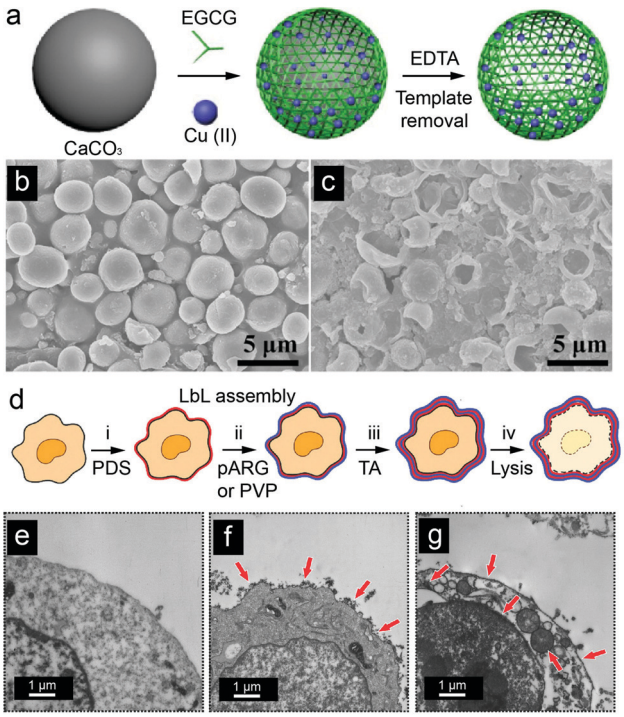

Fig. 14 Hollow phenolic particles prepared through phenolic coating and template removal. (a) Schematic illustration of synthesis of EGCG–Cu(II) capsules. SEM images of (b) EGCG–Cu(II)@$CaCO_3$ nanoparticles and (c) EGCG–Cu(II) capsules. Reproduced with permission. Copyright 2020, Elsevier. (d) Schematic illustration of preparation of LbL-coated bio-hybrid cancer cell-templated capsules with alternating layers (step i–iii) of either the electrostatically interacting polyelectrolytes dextran sulfate (PDS), poly-L-arginine (pARG) or poly(*N*-vinylpyrrolidone) (PVP), and TA *via* hydrogen bonding followed by cell lysis upon hypo-osmotic treatment (iv). TEM images of (e) uncoated cells, (f) bilayers of PVP/TA-coated cells, and (g) bilayers of TA/PVP-coated cells. The red arrows indicate LbL coating. (d–g) Reproduced with permission. Copyright 2014, Wiley-VCH.

sacrificial templates and ellagic acid/TA as etching agents.[192] Under basic conditions, the phenol coordination of metal accompanied by etching/dissolution of the MOF core leads to polyhedral hollow cages that mimic the parent particles. The authors revealed that the dimensions of the hollow cages were dependent on the solution pH, etching time, and parent cores making the hollow interiors tuneable. It was demonstrated that phenolic acids could release free protons to destroy the framework of MOF particles during the coating.[204] Their relatively large size helped protect the MOFs from fully collapsing by blocking the pores. The MOF surface was thus changed from hydrophobic to hydrophilic which let free protons penetrate the MOF cores.

Typically, hollow PDA capsules could be obtained by spontaneous self-assembly of dopamine monomers in the absence of metal ions. The universal surface coating on a wide range of sacrificial templates allows for the synthesis of PDA hollow films with varying thickness under optimized conditions.[205] For instance, a robust PDA microcapsule with varying thickness was developed using $MnCO_3$ particles as sacrificial template.[206] Dopamine concentration, solution pH, and deposition time all

impact the morphology and shell thickness. In addition to solid particles, both emulsion and non-emulsion systems could successfully be used to prepare PDA capsules. However, this remains a challenge because most PDA capsules are at the micrometer level, which might limit their *in vivo* applications.

To prepare nanometer PDA capsules, a 200 nm hollow PDA capsule was developed utilizing a miscible tetrahydrofuran–Tris buffer mixture.[207] Sun and co-workers introduced sodium dodecyl sulfate to the dimethyldiethoxysilane systems of which emulsion droplets were reduced.[208] The minimized PDA hollow nanocapsules retained the capacity for photoacoustic imaging and photothermal conversion from PDA nanoparticles. They also had significantly improved loading capacity for anticancer drugs. This PDA nanocapsule could be used as a multifunctional nanoplatform for both *in vitro* and *in vivo* cancer treatment.

A similar strategy could also be applied for PDA coating on MOF particles. The deposition process of PDA growth on the surface of zeolitic imidazolate framework-8 (ZIF-8) was investigated in detail: MOF templates are automatically etched off during the coating.[209] The self-etching started with a truncated cubic shape in a crystalline facet-dependent fashion. The material then turned into an intermediate yolk–shell structure with ZIF-8 cargo loaded inside. Longer incubation resulted in a cubic PDA nanocapsule comparable to TA etching process. This study not only illustrates the possible etching mechanism of PDA coating on MOF particles but also paves the way to prepare non-spherical nanocapsules.

Mixing synthetic functional polymers during self-polymerization is an effective route to strengthen the phenolic surface coating. The versatile chemistry of phenolics permits various molecular interactions including hydrogen bonding, electrostatic interactions, and hydrophobic interactions with functional polymers. Many studies have evaluated the LbL technique using a mixture of phenolic compounds and synthetic polymers to prepare hollow capsules. PVPON is a representative polymer for multilayer assembly. This hydrophilic, non-ionic polymer can form strong hydrogen bonding with TA. For example, LbL assembly of TA and PVPON can be used to synthesize bio-hybrid capsules (Fig. 14d).[210] In this case, live cancer cells were encapsulated within the hybrid coating, and the cell templates could be removed by hypo-osmotic treatment leaving cell lysates inside (Fig. 14e–g). The authors claimed that improved membrane integrity was observed when using PVPON as starting materials rather than TA.

Polyphenol could serve as an antioxidant to scavenge free radicals. This could in turn reduce radical-induced oxidation and elicit immunomodulation. Therefore, to maximize the benefits of coating materials, islet encapsulation with polyphenol coatings were investigated to restore euglycemia for diabetes therapy.[211] First, LbL surface coating of TA/PVPON was performed on sacrificial silica particles of 4 μm. After dissolution of the template cores, a hollow shell with a thickness of around 40 nm was obtained. The *in vivo* results demonstrated that the hybrid capsule could maintain islet function, immnuo-suppression, regulation of pro-inflammatory chemokines, and decreased T cell trafficking. Moreover, the TA/PVPON microcapsules could also be decorated with metal/metal oxide nanoparticles through coordination between metallic substrates and TA. The ultrasmall iron oxide nanoparticle-modified capsules exhibited excellent T_1 and T_2 contrast for magnetic resonance imaging.[212] Together with the drug loading capacity, this hybrid biocapsule holds potential for traceable drug delivery and image-guided cancer therapy.

It is also feasible to incorporate organometallic compounds in TA/PVPON hollow capsules to prepare metal–organic hybrid coatings.[213] The authors produced LbL assemblies of TA, PVPON, and a manganoporphyrin (MnP) modality to mimic the enzymatic antioxidant superoxide dismutase. Inclusion of an MnP outer layer significantly increased the antioxidant effect of the capsule. A phenolic-enabled capsule containing two kinds of synthetic polymers was developed *via* LbL assembly.[214] The dopamine-modified poly(acrylic acid) (PAA–Dopa) and PVPON complex could diffuse into the PDA pre-layer during LbL assembly. Through hydrogen bonding between polymers and PDA, the PDA–PAA–Dopa–PVPON hybrid capsules could be obtained and showed pH-responsive swelling–shrinking behaviour. The volume swelling ration was confirmed to be 1.34 from pH 2.0 to pH 8.5, which is considered responsive for drug delivery.

PEN is a useful toolkit to integrate various functional modalities in a single platform. Considering the nature-inspired features and its intrinsic biocompatibility, PEN is also an effective method to assemble bio-active molecules when preparing hollow capsules. Recently, Caruso and co-workers established a polyphenol-mediated technique for protein assembly.[215] The authors demonstrated that more than 10 types of proteins could be assembled with different phenolics including TA, gallic acid, and EGCG. Through multiple non-covalent interactions (hydrogen bonding, hydrophobic, and ionic interactions), the protein–polyphenol networks were formed on the sacrificial particles, and the free-standing hollow capsules could be obtained after dissolution of the spherical templates. This PEN-based strategy could be employed in bioactive surface coatings, protein interaction studies, protein engineering for catalysis, imaging, and cell targeting. Interestingly, Messersmith and co-workers developed a template-free approach to prepare PDA nanocapsule in the presence of bioactive molecule resveratrol. Nanocapsules with varying shell thickness could be obtained by tuning the synthesis conditions including solvent, dopamine/resveratrol ratio, and dopamine concentration. The resulting nanocapsules had excellent free radical scavenging activity.[216]

3.2.3 One-step synthesis of core–shell particles. Core–shell particles have been widely used in biomedicine due to their unique structure and attractive versatility. In a typical synthesis, core–shell particles are prepared by surface coating or growth on pre-formed core particles. Importantly, PEN provides a novel strategy for the one-step synthesis of core–shell particles. A tea polyphenol-based method of core–shell particle synthesis by one-pot preparation within minutes was developed (Fig. 15a).[217] The tea polyphenol was extracted from the broadleaf holly leaves that were then reacted with metal precursors ($AgNO_3$). Under microwave irradiation, heterogeneous nanoparticles (Ag@TP) with a 60 nm Ag core and 8 nm polyphenol shell were obtained. Confocal laser scanning microscopy (CLSM) results confirmed

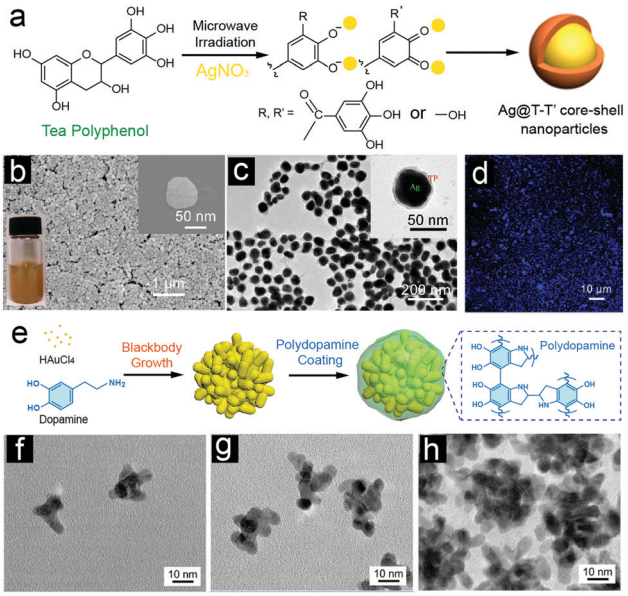

Fig. 15 Interfacial assembly of metal–phenolic hybrid nanoparticles through one-step synthesis. (a) Schematic illustration of self-assembly of polyphenol-based core@shell nanostructures within 1 min using microwave-assisted green chemistry. (b) SEM images and (c) TEM images of Ag@TP with lower and higher magnification. Inset: Optical image of Ag@TP suspension. (d) Confocal laser scanning microscopy image of Ag@TA nanoparticles. (a–d) Reproduced with permission. Copyright 2014, American Chemical Society. (e) Schematic illustration of one-step synthesis of AuPBs. TEM images of AuPBs at different growth times: (e) 1 h, (f) 2 h, and (g) 4 h. (e–h) Reproduced with permission. Copyright 2018, American Chemical Society.

the autofluorescence of the as-prepared nanoparticles (Fig. 15b–d). The authors indicated that the formation mechanism of core–shell particles involved a simultaneous oxidative self-assembly and aggregation under microwave treatment. Moreover, Au plasmonic blackbodies (AuPBs) showed a unique core–shell structure with a hyperbranched internal core as prepared *via* a PDA-enabled one-step synthesis (Fig. 15e).[218] The growth of AuPBs was performed by simply mixing $HAuCl_4$ and dopamine molecules together. Triggered by the alkaline solution, dopamine molecules began to self-polymerize and reduce the Au precursor at the same time leading to a highly adhesive PDA coating on the hyperbranched Au cores with abundant built-in electromagnetic hot-spots (Fig. 15f–h). Star-like branched plasmonic nanostructures with strong enhancement could be prepared by using gallic acid as a reducing and stabilizing agent.[219] By tuning the polyphenol concentration, the particle morphology changed from spherical to highly branched proving the importance of gallic acid for one-step synthesis. In conclusion, phenolic-enabled one-step synthesis is a surfactant-free method to easily synthesize metal–polymer core–shell nanoparticles.

3.3 Engineered secondary nanostructures using phenolic-based templates

3.3.1 Versatile platform for secondary organic molecule modification. The multifaceted physicochemical reactivity of phenolics can provide versatile ad-layers or templates for surface modification of secondary organic molecules. Diverse organics could be anchored on the phenolic surface through either non-covalent or covalent bonding. PEN-based secondary modification is a simple but attractive strategy to functionalize the particles while integrating kaleidoscopic modalities of organics into the particle system. Protective polymer growth on the phenolic-based templates is a representative study of secondary organic molecule modification. Functional polymers such as thiol/amino-terminated PEG have been widely used for *in vivo* studies of bioactive particles showing prolonged blood circulation and less binding with serum proteins of the PEGylated particles.[220] While one end of PEG was terminated with thiol/amino groups, the other end could be functionalized according to meet the desired properties. Some targeting PEG polymers such as folic acid-terminated PEG has been used for surface modification of phenolic particles greatly improving the targeting efficiency of nanoparticles in a facile manner.[221] Recently, several studies focusing on organic modifications on phenolic surface have emerged including novel uses of phenolic-based templates.

Polymer-modified phenolic particles could be directly obtained by surface conjugation of functional polymers *via* a "grafting to" method. Similar to PEGylation, the functional group-terminated polymers can be grafted on the particle surface through covalent interactions. For instance, cationic polymers were conjugated to the particle surface to construct a phenolic-based gene carrier.[222–224] Park and co-workers developed a multifunctional nanoparticle capable of magnetic resonance imaging (MRI), fluorescence imaging, and genetic manipulation. The particle was fabricated by coating caffeic acid, PDA, and PEI layer on Zn/Fe magnetic nanoparticles sequentially.[225] The amino groups of PEI covalently bound catechol groups through a Schiff's base reaction leading to a core–shell metal–organic nanoparticle. The resulting particles showed a higher loading capacity of plasmid DNA than conventional non-viral transfection agents (*e.g.*, lipofectamine) and could deliver the genetic materials into cells for expression. In this case, PDA serves as a "biological glue" to impart different modalities into the single particle system.

The surface-initiated polymerization on phenolic particles is typically considered a "grafting from" method for polymer modification. The polymer initiators could be immobilized on the phenolic templates as starting points and further chain growth was performed by adding polymer monomers and a polymerization trigger. Dendritic poly(amidoamine) (PAMAM) growth on the surface of PDA-coated magnetic particles was reported. Methyl methacrylate conjugated with catechols as an initiator was reacted with ethylenediamine *via* amidation reaction for growth of PAMAM. By simply repeating the growth process, high generation of dendritic PAMAM could be grafted onto the PDA shell.[226] In addition, a ring-opening reaction was conducted on the PDA coating as a reaction scaffold.[227] The catechol groups of PDA could initiate the ring-opening polymerization of glycidol to form a hyperbranched polymer coating.

Atom transfer radical polymerization (ATRP) has also been applied on phenolic particle surfaces for polymer growth leading to densely packed polymer brushes. Zhou and co-workers

demonstrated successful surface-initiated polymerization from a PDA-coated surface.[228] The authors revealed that PDA itself could generate radicals under light irradiation to trigger the radical polymerization of a number of vinyl monomers including methacrylates, acrylates, and styrene. Thanks to the universal adhesion of PDA on virtually any substrate, this phenolic-based surface-initiated polymerization could be performed "anywhere" under sunlight.

"Grafting from" polymerization of PNIPAM on hollow PDA spheres was also developed for construction of hybrid polymer nanocapsules with controlled architecture.[229] After introduction of 2-bromoisobutyryl bromide initiators on PDA through a nucleophilic substitution reaction, the activators regenerated by electron transfer ATRP were used to synthesize PNIPAM polymer brushes. Both inward and outward polymer growth from PDA hollow particles could be manipulated by hydrothermal treatment. The unique structure and thermal-responsive features make the phenolic/polymer particles a good candidate for drug delivery. Phenolic surfaces such as PDA could be a versatile platform for ATRP in a "grafting from" method. There are many other polymer brushes that are candidates for polymer modification on phenolic-based templates.[230,231]

Protein corona modification is another effective way to camouflage engineered particles and improve their bioavailability in biological systems. However, not all particles can adsorb the proteins. Caruso and co-workers fabricated a library of hyaluronic acid-based MPN capsules (HA-MPN) and investigated the targeting effect of protein corona.[232] The HA-MPN was first obtained by co-assembly of hyaluronic acid, polyphenol, and metal ions. The incorporation of hyaluronic acid improved the binding affinity of capsules toward CD44-overexpressing cells. Interestingly, the modification of a protein corona (human serum) on HA-MPN did not disrupt the interaction between capsules and cells. On the contrary, the increased specificity of the targeting system was observed because the protein corona reduced the non-specific cell interactions and retained targeting affinity. However, the adsorption of different proteins on phenolic-based templates and the solution to protein fouling still remained elusive. To address this issue, the interactions between the MPN films and specific functional proteins including were investigated.[233] Bovine serum albumin (BSA), immunoglobulin G, and fibrinogen were selected as individual protein samples, and fetal bovine serum (FBS) was the complex biological medium. The authors claimed that the amount of complex serum proteins adsorbed on the Fe(III)-terminated MPN surface was significantly larger than that of the TA-terminated template. However, the absorbed masses of three individual proteins are larger on the TA-terminated MPN with smaller mass differences when the protein molecular weight increases. This result suggests that TA-terminated templates are preferred when using MPN materials *in vivo* because many blood proteins could unexpectedly adsorb on a Fe(III)-terminated MPN.

Although non-specific binding of proteins on phenolic-based templates is spontaneous and rapid, the immobilized proteins are commonly in a random orientation, which is an important consideration in some biomedical uses such as

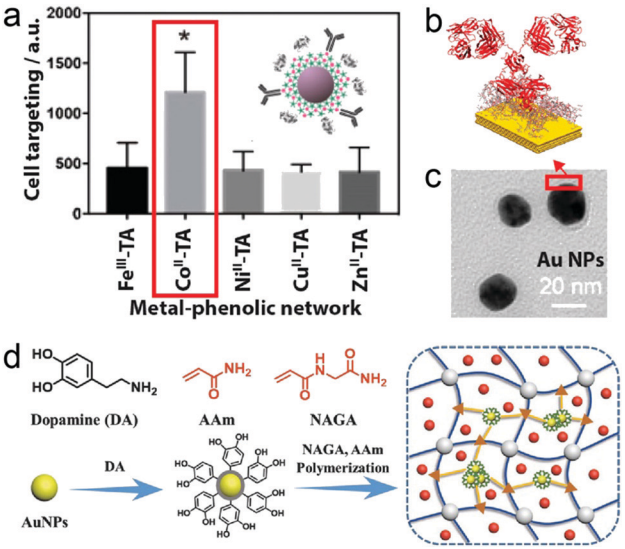

Fig. 16 Versatile phenolic-based platform for secondary organic molecule modification. (a) Cell targeting performance of MPNs of different metal ions. Inset: AuNP@MPNs with protein corona layer coating and antibody tag. (b) Schematic presentation of antibody-anchored AuNPs with specific protein orientation. (c) TEM image of antibody-anchored AuNPs. Reproduced with permission. Copyright 2020, American Chemical Society. (d) Schematic illustration of the fabrication of AuNP@PDA and AuNP@PDA-cross-linked hydrogel. Reproduced with permission. Copyright 2018, Wiley-VCH.

antibody–antigen recognition. The fragment crystallizable (FC) region should be immobilized on the template surface and the Fab binding regions should face outward. For example, MPN coating on Au substrate could be used as a potential candidate for antibody immobilization (Fig. 16a–c).[234] Upon physisorption of antibodies, all particle systems (Fe^{3+}, Co^{2+}, Ni^{2+}, Cu^{2+}, Zn^{2+}) exhibited enhanced association with target antigens, with Co^{2+} systems demonstrating more than 2-fold greater association. The solvent-exposed Co^{2+} directly and preferably coordinated to the histidine-rich portion of FC region allowing for enhanced antigen targeting.

In addition to single particle engineering, the phenolic particles could also serve as crosslink points inside the polymer networks providing a useful method to construct three-dimensional polymer networks (Fig. 16d).[235] An injectable thermo-responsive hydrogel with photothermal capabilities was developed for light-controlled drug release. The hydrogel network was fabricated by assembly of poly(*N*-acryloylglycinamide-*co*-acrylamide), PDA-functionalized AuNPs, and anticancer drugs. The introduction of core–shell particles distinctively enhanced the mechanical properties of hydrogels due to the increased crosslinking density. PDA-linked AuNPs with the thermoresponsive hydrogels due to its universal adhesion and chemical reactivity enabling near-infrared light-controlled drug release.

Modification of small organic molecules on phenolic surfaces could easily be achieved through either chemical reaction or direct physical adsorption. However, some studies reported modification of small organic molecules by other strategies. Wei and co-workers synthesized phthalocyanine(photosensitizer)-modified

PDA nanoparticles *via* complementary base pairing rules.[236] The adenine-modified PDA and thymine-modified zinc phthalocyanine effectively bound to each other. Importantly, the thymine-modified photosensitizer could be released upon near-infrared irradiation due to the excellent photothermal conversion capability of PDA.

3.3.2 Direct the growth of inorganic materials. As a result of the presence of phenolic groups, PEN allows for diverse interactions between phenolic-based templates and inorganic materials particularly metal chelation and reduction. The strong binding with inorganic materials, particularly metal/metal ions, enables *in situ* growth or direct modification of metal/metal oxide particles on template surfaces. The facile process, green chemistry, and good biostability of the final particles can lead to rapid synthesis of hybrid particles such as core–shell particles, core–satellite particles, and nano-gapped particles (NPPs) with promising results in biomedicine.

The high intermolecular affinity of phenolic groups toward metal ions permits easy immobilization of metallic precursors on template surfaces and directs *in situ* growth of inorganic materials. Chen and co-workers prepared branched nanoporous Au nanoshells on redox-active polymer poly(vinylphenol)-*b*-(styrene) (PVPH-*b*-PS) nanoparticles which served as both a reducing agent and coating template.[237] The self-assembly of amphiphilic PVPH-*b*-PS gave rise to polymeric nanoparticles with phenol groups exposed outward. In alkaline solution, the phenol groups featured strong reductive properties thus reducing Au(III) precursors to form AuNPs *in situ*. By extending the reaction time, branched Au nanoshells with a high nanoporosity were formed on the particle template. The original polymeric core could be removed by dispersing the particles in organic solvent leading to the formation of a hollow cavity. The branched nanoporous Au nanoshells were further attached with PNIPAAms for photothermal-triggered drug release.

PDA templates either as a particle core or coating shell on a pre-formed particle could act as a stabilizer to direct the growth of inorganic materials. PDA offers *in situ* reduction of metal ions on the template surface. However, further addition of reducing agents may be required depending on the metal ions and the proposed particle structure. A core–petal nanostructure was fabricated by oxidative nano-peeling chemistry based on PDA coating and templating by Nam and co-workers.[238] PDA-coated AuNPs were first obtained by self-assembly of dopamine molecules. The oxidative disruption and peeling of PDA as well as budding of the petal Au nanostructure was conducted by adding metal precursor ($HAuCl_4$), PVP, and reducing agent (hydroxyl amine). The Au(III) precursor turned the catechol groups into quinones and undermined the assembled PDA layer. This led to protruding Au petals reduced by hydroxyl amine. To validate the versatility of phenolic-mediated secondary growth, Caruso and co-workers developed a strategy on the basis of TA and aromatic dithiol (BDT) for particle surface engineering including the growth of inorganic materials (Fig. 17).[105] In basic aqueous solutions, TA and BDT monomers spontaneously co-polymerized into supramolecular particles (pBDT–TA), and the phenolic groups of TA on the surface enabled further

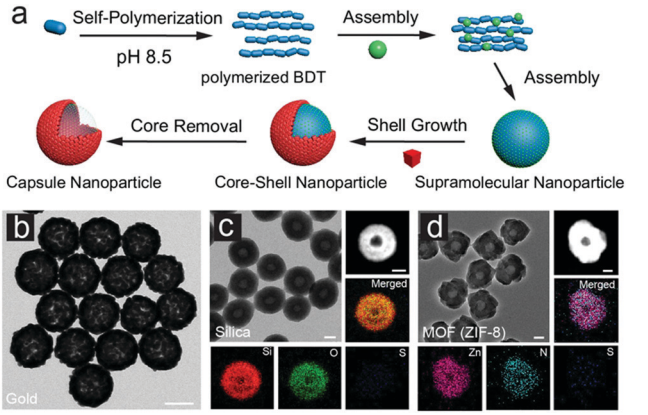

Fig. 17 (a) Synthetic strategy for particle engineering using pBDT–TA supramolecular networks. The polyphenol-stabilized particles subsequently allow for the growth of diverse shell materials on the particles. TEM images of (b) Au (c) silica, and (d) MOF hollow structures after removal of the pBDT–TA core. Insets in image (c) and (d): HAADF-STEM images of representative silica and MOF hollow particles and their corresponding EDX mapping results. Reproduced with permission. Copyright 2020, Nature Publishing Group.

interactions of various inorganic precursors such as silica and metal salts. Interestingly, the BDT–TA particles could also be removed as sacrificial templates. Due to the diverse chemistry of phenolic groups, this strategy was also effective for the growth of organic materials.

A similar strategy could be applied to construct core–satellite particles with compositional diversity. *In situ* growth of AuNPs on PDA-coated carbon nanotubes could be performed without treatment of reducing agents.[239] The small Au nanoparticles (diameter: *ca.* 8 nm) were randomly deposited on the PDA sidewalls. In addition to Au, the phenolic-based templates could also direct the growth of Ag for bacterial killing.[240] After the addition $AgNO_3$ in the suspension of PDA-coated AuNRs, bimetallic Au@Ag nanorods were obtained in the absence of other reducing agents. Further, Au@Ag nanorods demonstrated high cell killing performance due to plasmonic photothermal conversion and Ag release upon irradiation. The authors also used the PDA shell to conjugate anti-bacterial antibodies to improve the targeting efficiency.

Zhang and co-workers demonstrated that PDA nanoparticles also exhibited reductive ability toward Pt^{4+} by generating platinum nanoparticle-decorated PDA particles.[241] Pt nanoparticles with a diameter of 3 nm were uniformly distributed on the surface of 200 nm PDA nanoparticles. The satellite particles could be used for further modification of zirconium–porphyrin shells for enhanced tumor therapy. Due to the strong interaction between phenolic molecules and metal precursors, ultrasmall copper sulphide (CuS) nanoparticles with an average diameter of 3 nm were synthesized *in situ* on the surface PDA-coated UCNPs (PDA-UCNPs).[242] The color change of the suspension from light blue to dark green after addition of $CuCl_2$ clearly indicated the formation of Cu^{2+}–PDA complexes. The authors compared this growth method with a simple mix of CuS nanoparticles and PDA-UCNPs. The *in situ* growth routine created more uniform and

stable hybrid particles. With such a method, the core, phenolic shell, and secondary inorganic satellites could be integrated into a single system for multifunctional uses in biomedicine. Some studies also reported the preparation of satellite nanoparticles by mixing the pre-formed satellite metallic particles with the core phenolic-based cores such as PDA@AuNP and PDA@UCNP;[243,244] these are discussed elsewhere.

NPP is another representative particle obtained *via* PEN. Typically, NPPs are constructed by at least one cycle of linker molecules (*i.e.* polymer, DNA) coating on the metal core and then metal deposition on the coating shell.[245] Phenolic-based polymers are good candidates for gap molecules that could be used for NPP synthesis due to their adhesive nature and controllable growth kinetics. A PDA-enabled synthesis of MOF-contained NNPs was reported by Duan and co-workers.[62] Because of the universal adhesion, PDA could form a conformational coating on a wide range of nanoparticles regardless of size, shape, and composition. Thus, the PDA-coated nanoparticles could be prepared for secondary modification of MOF because PDA could further drive the heterogeneous nucleation and growth of MOF. We note that PDA coatings gave the particles good colloidal stability while avoiding particle aggregation during MOF growth. The resulting NPPs showed a combined physicochemical property from the core and the shell, which demonstrates a useful strategy to construct MOF-coated nanohybrids. Moreover, this strategy could be utilized for the synthesis of NNPs with multiple concentric shells.[246] The PDA-coated core–shell nanoparticles were first prepared by self-polymerization of dopamine on the functional cores. The high density of catechols on the PDA surface offers metal chelation and reduction to particles facilitating the nucleation and *in situ* growth of a secondary metallic layer. Importantly, the coating and metallization cycles could be simply repeated to obtain tailored NNPs with double or even triple shells. Importantly, the gap distance could be tuned by controlling the reaction time of PDA coating. The PDA-enabled NNPs provide great potential for bacteria detection and bio-catalysis. Choi and co-workers further explored the synthesis of Ag-containing NNPs *via* PDA.[247] The authors reported the key structural parameters of concentric NNPs including gap thickness, core–shell composition, and geometrical configuration.

In addition to the use of PDA, a bimetallic Au@Ag core–shell particle with a polyDOPA interlayer has been developed.[248] After co-assembly of DOPA and Au(III) seeds under weak alkaline condition, Au@polyDOPA nanoparticles were obtained. The polyDOPA shell with a high density of catechol chains showed strong reducing capability when the catechols were oxidized into quinones thus directing the growth of a secondary Ag shell. The final polyDOPA NNPs showed good performance in surface-enhanced Raman scattering (SERS) thanks to the hot spots embedded in the polyDOPA gap. Overall, the phenolic-directed growth method largely enriched the library of PEN-based particles to further expand their potential applications in biomedicine.

3.3.3 Possibilities for miscellaneous materials. By balancing the interactions between phenolics and other functional molecules, miscellaneous particle systems with multiple components and unique structures have been developed for specific applications. Zhou and co-workers obtained dopamine-derived cross-linked vesicles by terminal functionalization of amphiphilic hyperbranched copolymers.[249] The vesicles could be readily obtained by self-assembly of amphiphilic block copolymers. The vesicles could subsequently be readily self-crosslinked into stable vesicles in alkaline solution due to the self-polymerization of dopamine. Unlike surface coating on pre-formed particles, this study demonstrated a new way to fabricate hollow particles with functional coatings on both the inner and outer surface. Further functionalization like carboxylation, AuNPs growth, protein loading, and DNA conjugation could be achieved in a simple "mixing and grafting" process.

Nanoscale MOFs have also attracted great attention in various applications thanks to their hierarchical structure and tuneable pore space. Traditional hybrid MOF-phenolic nanomaterials required either surface modification of phenolics on a MOF core or secondary growth of a MOF on phenolic substrates. A simple one-spot method to synthesize MOF/PDA-based hybrid nanogels has been reported.[250] The phenolic hydroxyl groups coordinate with metal ions to further form a MOF skeleton with organic linkers encapsulating dopamine monomers in the pores of MOF. Importantly, the dopamine molecules could also interact with organic linkers through π–π stacking forming a MOF–dopamine intermediate. After polymerization in basic conditions, the resulting hybrid nanoparticles showed enhanced photothermal effects together with T_1 positive magnetic resonance imaging capability. A similar MOF–dopamine hybrid structure was reported by Queen and co-workers.[251] The dopamine monomers were first loaded inside the MOF structure consisting of Fe^{3+}, and 1,3,5-benzenetricaboxylate underwent spontaneous polymerization to PDA. This *in situ* polymerization-enabled MOF/PDA hybrid nanomaterial had extrinsic porosity that improved its surface chemistry. Interestingly, the Fe^{3+} not only chelated with dopamine molecules for encapsulation but also promoted the anaerobic oxidation of dopamine. Such encapsulation-based strategies are an illuminating method to synthesize heterogeneous particles with multifunctional potentials.

Through one or combined molecular interactions, phenolics have numerous possibilities for an array of materials. The PEN toolkit can lead to a larger library of phenolic-based particle systems with unique structures and excellent properties prepared *via* a wide range of biomedical applications.

4. PEN for biomedical applications

Naturally occurring phenolics are well-known for their excellent biocompatibility and negligible toxicity. In biological systems, phenolic-based materials participate in diverse biochemical pathways and metabolic activities leading to intrinsic biological properties such as ultraviolet-visible light absorption, anti-oxidation, free radical scavenging, chelating capability to metal ions, *etc.*[252] Due to phenolics' versatile chemistry, PEN can integrate different functional motifs into a single particle

system. These multifunctional particle systems have potential in a variety of biomedical applications. Next, we will discuss particle–cell interactions, pharmacokinetics, and the toxicology of phenolic particle derivatives. Biomedical applications based on PEN platforms including biosensing, bioimaging, and therapy will be introduced.

4.1 Particle–cell interactions, pharmacokinetics, and toxicology profiles

4.1.1 Cellular interaction. Many endeavors have been made to construct various PEN-base particle systems for biomedicine. It is necessary to understand the particle–cell interactions prior to their biomedical uses. The particle–cell interactions including cellular absorption/targeting, internalization, trafficking, processing, and degradation are largely affected by the physicochemical properties of particles, and these are crucial to therapeutic efficacy. A thorough and precise investigation of particle–cell interactions between phenolic materials and biological systems would surely enhance the therapy and reduce side effects. Natural phenolic materials have unique properties when participating in biomedical processes. For instance, the natural polyphenolic pigment melanin is excreted from melanocytes and transferred to neighboring keratinocytes to form perinuclear melanin caps and protect cells from irradiation damage.[253]

The intrinsic adhesion of phenolic surfaces improves the cellular membrane adsorption of particles. For example, EGCG molecules bind to cell membranes before cellular uptake leading to a colored cell surface, *i.e.*, the "a cell sealing effect".[254] The assembled phenolic particles with terminal functional groups retained their adhesive characteristics. Gianneschi and co-workers prepared PDA nanoparticles to mimic natural melanin, which showed an adhesive feature at high concentration when treated with cancer cells (Fig. 18a–d).[255] The interactions between phenolic groups and the cell membrane, especially the membrane proteins, dramatically impact the cellular adsorption. To increase the specific cellular uptake, targeting molecules (*e.g.*, antibody, targeting peptide) could be anchored on the phenolic surface either through covalent conjugation or non-covalent binding.[256,257] The cellular uptake efficiency is usually time- and concentration-dependent suggesting that longer incubation times and higher concentrations resulted in more internalized particles. Optimization of particle properties and surface chemistry may help to improve the uptake efficiency and determine the uptake pathways (*e.g.* phagocytosis, macropinocytosis and receptor-mediated endocytosis, *etc.*).[258,259]

Surface modification of phenolic materials on pre-formed particles is an effective strategy for cellular delivery enhancement. A PDA coating facilitated cellular uptake of both inorganic (SiO_2, Au) and organic (polystyrene) particles.[255,260,261] After PDA coating, nanoparticles were internalized through Caveolae-, Arf6-dependent endocytosis, and Rab34-mediated macropinocytosis.[262] *Versus* conventional surface modification methods such as PEGylation, phenolic coating enabled higher uptake of the particles.[261,263] This suggests that the improved uptake by PDA could be attributed to the electrostatic interactions between amino groups of PDA and phosphate groups of the membrane as well as the interaction between catechol groups of PDA and choline groups of the membrane. Further experimental and computational studies are needed to confirm the mechanism.

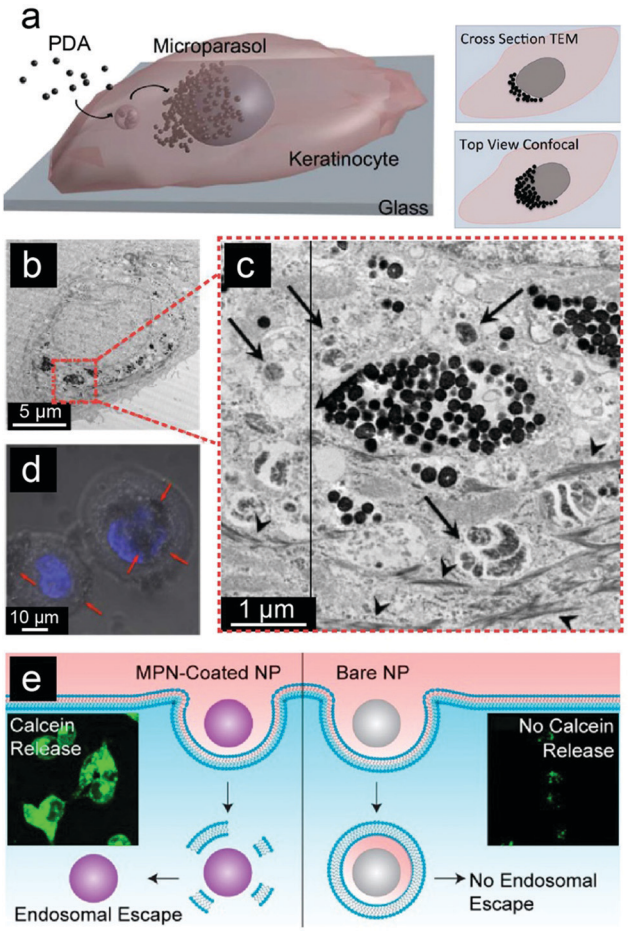

Fig. 18 Cellular uptake study of phenolic nanoparticles. (a) Scheme for the uptake, transportation, and accumulation of PDA nanoparticles in cells. (b) TEM image, (c) enlarged TEM image, and (d) confocal laser scanning microscopy image of cells incubated with PDA nanoparticles for 3 days. (a–d) Reproduced with permission. Copyright 2017, American Chemical Society. (e) Scheme and fluorescence microscopy image of endosomal escape of bare and MPN-coated nanoparticles. Reproduced with permission. Copyright 2019, American Chemical Society.

Phenolic materials have been proven to successfully trigger endosomal escape of particles. After cellular uptake, internalized particles, particularly with diameters from 50 nm to 500 nm, are transported to lysosomes *via* endosomes.[264,265] However, particles are exposed to an acidic environment, reducing agents, and degradation enzymes due to endosomal entrapment, which may severely reduce the therapeutic bioavailability. Thus, the therapeutic efficacy improves when more particles can escape from the endosomes. Caruso and co-workers reported that the use of MPNs for surface coating could promote the escape of nanoparticles from endo/lysosomal compartments (Fig. 18e).[266] MPNs assembled from TA and Fe^{3+} or Al^{3+} possessed a "proton-sponge effect" similar to traditional polycationic polymers such as PEI.[267] This effect resulted in the

transition of TA–metal ion complexation state from tris to bis and would disrupt the endo/lysosomal membranes thus facilitating the escape of particles. Yao and co-workers prepared a phenolic-based nanocarrier by assembly of TA, DOX, and indocyanine; these could be internalized by tumor cells through a hydrophobic transition. The hydrophobic particles became larger in acidic conditions within lysosomes leading to lysosome rupture and particle escape.[268] PDA-coated nanoparticles could also partially escape from the endo/lysosomes to cytosol due to the "proton-sponge effect" from the amino groups on PDA shell.[168] Interestingly, the PDA-coated nanoparticles were observed to accumulate in the perinuclear area after endosomal escape, sharing a similar pathway to natural melanin. Finally, the residual particles were transported out of cells *via* exocytosis pathway or degradation.

Most therapeutics designed for cellular regulation can function well only if efficient uptake and endosomal escape are achieved. Thus, the use of PEN may be an effective strategy for particle engineering to modulate the particle–cell interactions.

4.1.2 Pharmacokinetics of PEN-derivate particle systems. Many efforts have been made to investigate the pharmacokinetic parameters including blood circulation, organ/tumor accumulation, and clearance of PEN-based particles in *in vivo* studies.[269,270] The pharmacokinetics of the particles are mainly determined by their size, shape, composition, and surface chemistry. The US Food and Drug Administration requires that all administrated agents be cleared from the body to avoid the possible toxicity.[271] However, particles for drug delivery should have a prolonged circulation time and efficient targeting. Thus, a balance between therapeutic efficacy and biosafety is required.

Versus unmodified particles, phenolic coatings give the particles a hydrophilic surface and the potential for secondary modification. Particles will be tagged by opsonin proteins once they enter the bloodstream making them recognizable to the mononuclear phagocytic system (MPS) and/or reticuloendothelial system (RES).[272] Capture by MPS and/or RES may lead to a rapid clearance of uncoated particles within a short time after injection. Phenolic materials including PDA, TA, EGCG, and gallic acid are relatively hydrophilic and can mask the hydrophobic unmodified surface thus avoiding possible particle aggregation. The drug delivery system obtained by TA polymerization showed distinctively prolonged blood circulation *versus* free small molecules drugs.[268] After two days of injection, DOX concentration of the delivered group was 5.04-fold greater than the free drug group. However, the latent reactivity of the phenolic coating toward various substrates may increase the potential of non-specific absorption leading to non-specific accumulation. About 85% of PDA-coated AuNPs (core: 50 nm; PDA shell: 10 nm) will be cleared out in 5 min after intravenous injection.[168] The rapid clearance caused low therapeutic efficiency.

Therefore, many phenolic particle systems have been further modified with functional polymers to prolong the blood circulation. The conjugation of PEG to the particle surface through Michael addition and/or Schiff's base reaction is one such effective method.[273,274] The polymer chains not only provide steric hindrance against aggregation, but also block the absorption of interfering biomacromolecules, protecting the particles from scavenging by phagocytic system. After PEGylation, the blood circulation of particles was significantly improved. In addition to PEG polymers, chitosan, hyaluronic acid, and other functional polymers could also be decorated on the particle surface for prolonged blood circulation.[75,275,276]

Polymer modification may also simultaneously improve the organ/tumor targeting. As reported, these polymer-modified phenolic particles with a size of >5.5 nm were mainly cleared through the liver and kidneys. The accumulation peaks of liver, kidney, and spleen appeared at 12–24 h after systematic administration. For instance, a metal oxide–polymer hybrid nanoparticle prepared by co-assembly of dopamine, epigallocatechin, pyrrole, and diaminopyridine with a hydrodynamic diameter of 60.9 nm was prepared as a nanotherapeutic agents for tumor treatment.[277] The blood circulation profiles could be fitted to a two-compartment model with a first phase circulation half-time of 0.47 h and a second phase of 6.08 h. This blood circulation time made it possible for the agents to accumulate in tumors achieving a moderate 5.80% ID g^{-1}. At 24 h post-injection, the main accumulation was in the kidneys (12.66% ID g^{-1}) and liver (5.08% ID g^{-1}) proving particle sequestration by MPS.

Polyphenols and small phenolic molecules can penetrate the blood–brain barrier. Due to their ROS scavenging features, they are effective in modulating brain inflammation and neuron protection.[278,279] However, the phenolic-derivate particles without any modifications cannot reach brain cells due to the blood–brain barrier (BBB).[280] To explore the potential applications of phenolic-based particles in brain tissue, short targeting peptides have been conjugated to enhance BBB transportation and improve drug accumulation in brain cells.[281] However, concerns have been raised about the degradation and clearance of such particles.

In contrast to the huge amount of work regarding material synthesis and applications, deep studies on the pharmacokinetics of phenolic particles are rarely reported. There is a true need to map the possible reactions between phenolic materials and important biologics in the body to guide particle engineering for enhanced therapy.

4.1.3 Toxicology of PEN-derivate particle systems. Phenolics feature various therapeutic potential and are well known for their biocompatibility. Thus, there have been many studies concentrating on the toxicology of phenolic monomers.[282,283] Traverso and co-workers recently investigated tissue-directed polymerization by oral administration of dopamine monomers and trace amount of hydrogen peroxide. This could lead to tissue-specific *in situ* growth and enzyme-dependent tissue modifications (Fig. 19a and b).[284] After administration of dopamine solutions, the epithelial layers remained intact with similar histomorphology as the controls suggesting no tissue toxicity. Importantly, the PDA coating showed a high adhesive stability towards tissue. No PDA signal reduction was observed under mechanic stirring and scratching (Fig. 19c and d). However, particle systems may contain different physicochemical properties than phenolic monomers. Thus, a question has been raised about whether there is any difference of toxicology between phenolic monomers and PEN-derived particle systems.

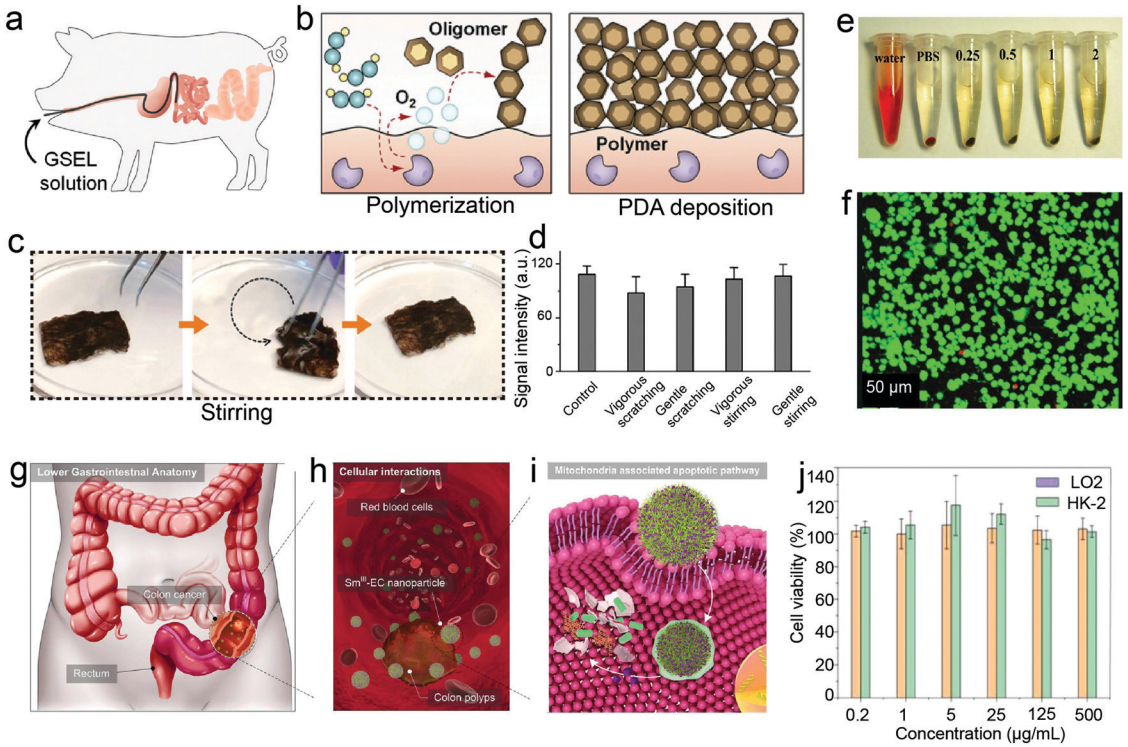

Fig. 19 Pharmacokinetics and toxicology investigation of phenolic-based materials. (a) Schematic illustration of administration of dopamine solution for gastrointestinal synthetic epithelial lining to porcine small intestine through a catheter. (b) Schematic illustration of enzyme-catalysed polymerization and PDA deposition on epithelium. (c) Representative images of fresh resected tissue specimens from the human small intestine with PDA coating under *ex vivo* mechanical stirring and scratching. (d) Quantitative *ex vivo* evaluation of PDA signal intensities of the coated human tissues under a series of physical conditions. (a–d) Reproduced with permission. Copyright 2020, American Association for the Advancement of Science. (e) Hemolysis evaluation of Fe_3O_4@PDA nanocomposites at varying concentration. (f) Live/dead calcein-AM staining of 4T1 cells treated with Fe_3O_4@PDA nanocomposites (green: live; orange: dead). (e and f) Reproduced with permission. Copyright 2020, Wiley-VCH. (g) Overview of the lower gastrointestinal through the endocytosis of Sm(III)–EC nanoparticles. (h) Cellular interaction between colon polyps and Sm(III)–EC nanoparticles. (i) Intracellular delivery of functional Sm^{3+} and EC molecules through the endocytosis of the nanoparticles. (j) Cell viability of normal healthy cells (LO2 and HK-2 cell) treated with Sm(III)–EC nanoparticles. Reproduced with permission. Copyright 2018, Wiley-VCH.

To answer this question, many efforts have been dedicated to investigating the toxicology of phenolic-based particles. Mrówczyński and co-workers conducted a thorough study on the genotoxicity and cytotoxicity of PDA-coated magnetic nanoparticles *in vitro*.[285] Oxidative stress, apoptosis, and DNA damage assays suggested that PDA-coated magnetic particles had low genotoxicity. The genetic materials in the treated cells were altered after long-term exposure to the particles. Another study of PDA-coated carbon dots re-confirmed that *in vitro* cytotoxicity was reduced after PDA coating.[286] Zhou and co-workers fabricated hemoglobin–PDA particles for biostability enhancement of the oxygen carriers.[287] The cytotoxicity analysis of the particles by cell counting indicated that the as-prepared particles possessed favorable blood compatibility and biocompatibility. After the robust and conformational deposition of PDA, the surface chemistry of core particles such as magnetic nanoparticles, carbon dots, bioactive molecules were changed. This coating strategy provides a straightforward method to improve the biocompatibility of a large number of functional particles.[288] In addition, Kong and co-workers assessed the *in vitro* cytotoxicity of TA–Fe^{3+}/Al^{3+} networks, and cell viability remained even up to 41.7 μg mL^{-1} of added material suggesting good biocompatibility of MPNs.[289]

In vivo toxicity profiles of phenolic particles are key data that should be collected prior to use. Most *in vivo* toxicity results of PEN-derived particles include an introduction of their biomedical applications. An *in vivo* study focused on Fe_3O_4@PDA nanocomposites provided evidence for the good biocompatibility of PDA-coated nanomaterials while investigating their performance for cancer therapy (Fig. 19e and f).[290] Biocompatibility evaluations including MTT cytotoxicity assay, live/dead cell staining, hemolysis study, hematoxylin and eosin (H&E) staining, and blood biochemical analysis were performed. These results proved that the PDA-coated magnetic nanoparticles were biocompatible using an animal model, which agrees with the *in vitro* profiles.

Xu and co-workers recently developed polyphenol-modified starch microparticles by LbL assembly of starch and TA for accelerated hemostasis and bone repair.[291] Due to the presence of an outermost layer of polyphenol, the microparticles exhibited low inflammation/immune responses, high biodegradability, as well as excellent therapeutic performance. Self-assembled metal–phenolic nanoparticles integrated with Sm^{3+} and (−)-epicatechin (EC) have been introduced for synergistic therapy against colon cancer (Fig. 19g–i).[292] The Sm(III)–EC MPNs exhibited significant antitumor effects *via* a mitochondria-associated pathway

whereas reduced side effects were observed in normal cells (Fig. 19j).

Sun and co-workers prepared Fe_2O_3@PDA@MPN nanoparticles for chemo-photothermal therapy.[293] The dual phenolic shell-coated particles were evaluated in an animal study and exhibited satisfactory biocompatibility through body weight recording, H&E staining, and blood biochemical analysis. Although the good biocompatibility of particles with phenolic shells has been reported, most PEN-derived particle systems are further modified with secondary polymer growth for *in vivo* biomedical applications. Polymer conjugation such as PEGylation can significantly improve the colloidal stability of the particles and avoid non-specific protein adsorption.[294–296] After modification, the PEGylated particles maintain biocompatible features and generally show no toxicity *in vivo*. Of course, not all particle systems are suitable for polymer conjugation. The attachment of protective polymers on a phenolic surface would deprive the systems of opportunities for other functional modifications such as antibody-enabled targeting. Particle design strategies differ greatly from one another depending on the requirements of the application. There is currently limited literature to compare the biocompatibility of modified and unmodified phenolic-based particles. Both particle systems have been considered biocompatible platforms in biomedicine. Thus, more precise investigation of the compatibility *in vitro* and *in vivo* should be conducted to better evaluate the toxicity of PEN-derived particle systems.

4.2 *In vitro* biosensing

Many high-quality particle systems are synthesized in a simple and reproducible method *via* PEN. After suitable modifications, these particles can be applied for sensing because they can translate information on a physicochemical level into a measurable readout. Therefore, the design of biosensing materials is often realized *via* additional targeting or detecting ligands such as aptamers and antibodies. Here, we will start with the detection of small molecular targets (such as, H^+, metal ion, and small molecules) before moving to larger targets (such as biomacromolecules, cancer cells, and bacteria).

4.2.1 Detection of small molecules. The role of pH in the polymerization of dopamine is critical because it can trigger an autoxidation reaction. The spontaneous oxidation of dopamine to dopamine semiquinone and dopaminequinone occurs in an alkaline solution. Thermodynamic study explained the influence of pH during oxidation and cyclization of dopamine.[29] This provides pH-responsive properties for PDA in pH monitoring. For example, a PDA coating on glassy carbon electrodes was fabricated by electropolymerization. The obtained redox PDA coating with pH-dependent moieties was then used as a voltammetric pH sensor. This PDA-coated electrode showed a distinct oxidation process in various buffers (pH 1–12). These are ascribed to the two-proton two-electron system of electro-oxidation of catechol groups.[297]

The redox activity of dopamine can be applied for the detection of small biological molecules such as glutathione (GSH) and cysteine (Cys). Jiang and co-workers employed Au@PDA core–shell nanoparticles for detecting biothiols where the nanoparticles were prepared by ultrasonic-assisted polymerization of dopamine on Au nanoparticles.[298] Au@PDA nanoparticle-decorated hydrogels were then obtained by mixing nanoparticles with agarose in solution through microwave-assisted heating. Due to the redox-active catechol groups in the shell layer, Au@PDA nanoparticles can facilitate the *in situ* reduction of Ag^+ into Ag nanoclusters directly on the surfaces of the Au@PDA nanoparticles (Fig. 20a and b). The resulting Ag nanoclusters-Au@PDA had a core–satellites structure that can subsequently blue shift the localized surface plasmon resonance (LSPR) of the nanoparticles, providing a color transition from red to yellow. In the presence of biothiols, (*e.g.*, GSH and Cys), Ag^+ would coordinate with biothiols and form a stable metal–metal polymer in solution that prevents the polymerized Ag^+ from *in situ* reduction on the PDA shell. Therefore, the Ag^+-induced color change of Au@PDA-decorated hydrogel was inhibited leading to a simple colorimetric sensing method for biothiols. Moreover, even a 100-fold higher concentration of interfering metal cations (*e.g.*, Na^+, K^+, Mg^{2+}, Ca^{2+}, Fe^{3+} Ni^{2+}, Cu^{2+}, and Zn^{2+}) cannot impact the Ag^+-response of Au@PDA NPs hydrogel.

It is well-known that the adhesive PDA is a favourable substrate for ssDNA adsorption *via* hydrogen bonding and π–π stacking to further quench the fluorescence of dye-conjugated ssDNA due to fluorescence resonance energy transfer (FRET).[299]

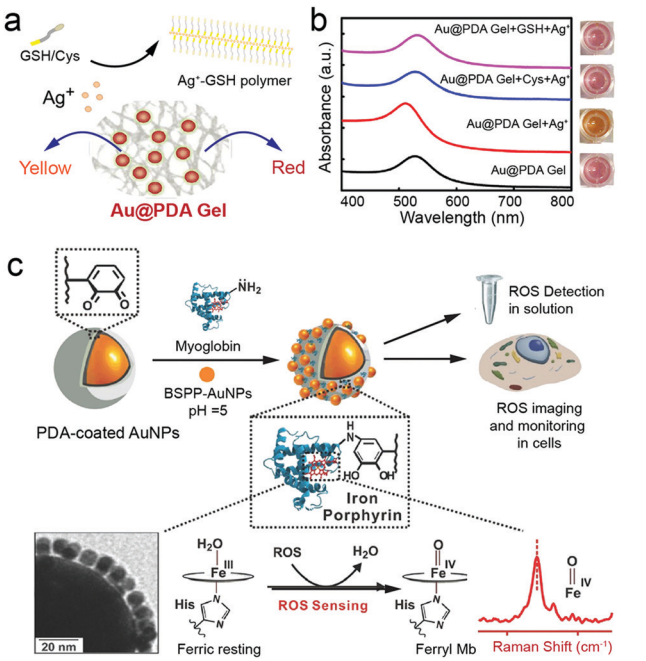

Fig. 20 *In vitro* biosensing of small targets *via* phenolic-based nanoparticles (a) Schematic illustration of the use of Au@PDA hydrogel for sensing biothiols. (b) UV-vis absorption spectra and photos of Au@PDA hydrogel with 200 μM Ag^+ in response to different biothiols (200 μM). (a and b) Reproduced with permission. Copyright 2018, American Chemical Society. (c) Schematic illustration for the synthesis of PDA-mediated SERS nanoprobes for detecting ROS (*e.g.*, H_2O_2, O_2^-, and •OH). The iron–porphyrin site of myoglobin in close proximity to Au core is used as a Raman reporter. Reproduced with permission. Copyright 2017, Wiley-VCH.

Zhang and co-workers further developed a "turn-on" fluorescent assay for detecting antioxidants (*e.g.*, GSH) *via* oxidation-mediated formation of PDA in the presence of a random dye-labelled ssDNA. Under an aerobic and alkaline condition, dopamine molecules were first oxidized to form PDA nanoparticles in the absence of antioxidants. FITC-labelled ssDNA (FITC-ssDNA) were spontaneously absorbed on the surface of the formed PDA nanoparticles. As a result, the fluorescence of FITC-ssDNA was severely quenched by PDA producing a fluorescent "off" state. In contrast, the oxidative polymerization of DA was inhibited in the presence of antioxidants such as GSH and ascorbic acid (AA) allowing for free FITC-ssDNA in solution. This leads to the fluorescent "on" state, enabling the detection of different antioxidants. These results showed a linear detection range of 50 nM to 10 μM for GSH and a limit of detection of 16.8 nM. Moreover, more than 25 potential interferents were tested including metal ions, amino acids, and other biological species (*e.g.*, H_2O_2, GSSG, and glucose); all interferences showed a negligible effect on the sensitivity and selectivity of the sensing system.

Wang and co-workers reported a simple FRET assay for the detection of ROS in living cells where the PDA nanoparticle acted as an energy acceptor and a dye-labelled single-stranded DNA (*i.e.*, Cy5-ssDNA) acted as an energy donor.[300] In this design, the Cy5-ssDNA was adsorbed on the surface of PDA *via* π-stacking forming Cy5-ssDNA–PDA nanocomplexes. If ROS was introduced into the system, then it will cleave the adsorbed Cy5-ssDNAs facilitating the release of free Cy5 molecules into the surroundings and triggering the recovery fluorescence from dyes. This nanosystem can be used to detect ROS generated by glucose oxidase-catalysed oxidation of glucose (100 pM) though a Fenton-like reaction. The increase of Cy5 fluorescence intensity was proportional to the logarithm of glucose concentration (100 pM–1 μM) demonstrating a wide detection range for this FRET assay. Furthermore, ROS was also detected in chemically stimulated HepG-2 cells.

Nam and co-workers described the design of PDA-mediated SERS nanoprobes with myoglobins (MP-SERS) to quantitatively detect ROS (Fig. 20c).[243] In their design, a PDA coating was first deposited on the surface of an Au nanoparticle core (c-AuNP) to facilitate the loading of Raman-active myoglobins and small Au nanoparticle satellites (s-AuNPs) generating plasmonically coupled SERS hot spots between the c-AuNP and s-AuNPs. The six-coordinated Fe(III)–OH_2 of myoglobins present in plasmonic hotspots can react with ROS to produce Fe(IV)=O. Therefore, the change in characteristic Raman peaks from the Fe–porphyrin to Fe(IV)=O was employed to quantify the concentration of ROS. This nanoprobe exhibited fast reaction kinetics with H_2O_2 reaching equilibrium in ~8 min. Moreover, the intensity of Raman peak at 1386 cm^{-1} (Mb–Fe(IV)=O) linearly depended on the logarithm of the concentration of H_2O_2 over a broad of 10^{-2} to 10^{-10} M. This nanosystem can also image ROS levels in living cells in a specific and sensitive manner.

In contrast to the aforementioned random DNA, specific ssDNA aptamers have also been employed to detect targets. For example, Xu and co-workers developed PDA-based nanoparticles for sensing adenosine triphosphate (ATP). In this *in vitro* assay, the introduction of ATP caused dissociation of the dye-labelled aptamer from the PDA nanoparticles leading to fluorescence recovery.[301] The retained fluorescence was found to depend linearly on the concentration of ATP from 0.01 to 2 mM. More importantly, the nucleic acids on biocompatible PDA nanoparticles can be protected from the non-specific enzymatic degradation, which therefore ensured their successful internalization by cells and achieved "signal on" APT sensing within living cells. More recently, Gao and co-workers used Zn^{2+}-responsive hairpin DNA to develop a fluorescent sensor in cells.[302]

PEN can also be used to design some plasmonic nanostructures for label-free SERS detection of small molecules.[303] For example, porous Au nanowaxberry-based SERS substrates were synthesized with PDA nanoparticles as templates. Au seeds were first deposited on the surface of PDA nanoparticles *via* amine groups. Seed-mediated synthesis was therefore used to fabricate the Au nanowaxberry *via* ascorbic acid as an additional reducing agent leading to an Au shell with abundant voids and gaps. These gap nanostructures can facilitate the absorption of analytes for SERS detection. For instance, when malachite green was used as a target analyte, the Au nanowaxberry achieved not only good reproducibility but also high sensitivity with a detection limit down to 1 pM. Moreover, the gap nanostructure was successfully used to detect thiram, benzidine, and 2,4-dinitrotoluene in diverse complex samples such as wastewater, juice, and soil.

PDA coatings are rigid and have been used extensively for molecular imprinting (MIP), generating specific binding sites against various targets.[304,305] This technique provides a strategy for constructing synthetic polymers into artificial receptors that provide binding sites with a specific three-dimensional conformation. This process involves the polymerization of dopamine around a molecular substrate of interest, and the subsequent removal of the substrate leaving behind the imprinted specific recognition domains that contain functionality, size, and shape complementarity to the substrates. *Versus* its biological counterparts (*e.g.*, enzymes, antibodies and hormone receptors), the MIP strategy offers significant advantages due to its high mechanical stability, good chemical resistance, low cost, and easy preparation. For example, a molecularly imprinted PDA coating on an electrode was developed for detection of a widely used antibiotic (sulfamethoxazole, SMX) in the food industry.[306] In this design, the PDA coating was first electrosynthesized on the surface of Au electrodes using cyclic voltammetry in the presence of SMX. The coated electrode was then rinsed with acetic acid to remove the SMX molecular templates in PDA coating. This MIP-based electrochemical sensor exhibited a linear detection range of 0.8 to 170 μM with good selectivity. This platform was validated by analysing spiked SMX in milk samples at a low concentration (*i.e.*, 3.4 μM), demonstrating the potential use for food safety analysis.

4.2.2 Detection of biomacromolecules. Specific targeting moieties are typically required for detecting larger molecules.

Chen and co-workers reported the synthesis of multifunctional Fe_3O_4@PDA nanoparticles for detecting messenger RNA (mRNA). In this design, a 6-carboxyfluorescein (FAM)-labelled hairpin DNA (FAM-hpDNA) containing a 21-base single-stranded loop and a 6-base-pair stem as the recognition segment was first absorbed on the surface of PDA surface. This led to effective quenching of the dye fluorescence.[171] In the presence of the target molecules (*i.e.*, mRNA), the specific affinity between the FAM-labelled ssDNA probe and its target facilitated the formation of a duplex assembly giving rise to the detachment of the probe from the PDA layer with subsequent recovery of the fluorescence. This designed Fe_3O_4@PDA nanoprobes were further used for the *in vitro* detection of mRNA in living cells. Similarly, microRNAs (miRNAs) are single-stranded noncoding RNAs with a typical short length of 21–23 nucleotides, which play an essential role in modulating the expression of specific proteins by controlling mRNA translation in a sequence-specific manner thus offering a feasible pathway for gene regulation.

Bian and co-workers employed PDA-coated Au nanoparticles (Au@PDA) to detect and monitor the expression of miRNAs in human mesenchymal stem cells (hMSCs).[116] The PDA shell on Au facilitated the immobilization of fluorescent dye-labelled hairpin DNA strands (hpDNAs) that can specifically recognize miRNA targets. Both the Au core and PDA shell can efficiently quench the fluorescence of hpDNAs. The specific binding of the hpDNAs to the target miRNAs subsequently triggered the release of hpDNAs from PDA surface and the recovery of fluorescence signals (Fig. 21a). Moreover, the described Au@PDA–hpDNA nanoparticles can enter stem cells without the assistance of additional transfection agents.

More recently, Duan and co-workers used a PDA coating as a tuneable nanoscale spacer to acquire a controllable fluorescence enhancement between the fluorophores and plasmonic nanocrystals.[307] PDA plays multiple roles in their design. First, PDA enables surface coating on different plasmonic Au@Ag nanoparticles with desirable optical properties. Second, the amphiphilic property of PDA allows for the self-assembly of coated nanoparticles at the water–oil interface leading to a densely-packed monolayer of nanoparticles that can be transferred from the interface to a flat substrate. Third, the precisely-controlled thickness of the PDA coating at the nanometer scale (5–25 nm) makes PDA a suitable spacer to modulate the distance between the plasmonic surface and fluorophore. Finally, the DNA detection sequence was conjugated on the PDA coating *via* Michael addition and/or Schiff-base reactions. This PDA-mediated strategy was used to prepare plasmonic substrates with the desired optical properties to selectively match the excitation/emission spectra of the fluorophore of interest providing a simple strategy for controlling FRET (Fig. 21b). Therefore, the biocompatible plasmonic substrate containing a Cy3/Cy5 pair was designed to improve the FRET efficiency in a DNA microarray assay with a sensitivity of 0.74×10^{-9} M towards the target DNA sequence from *Listeria monocytogenes*.

In addition to nucleotide sensing, the utilization of ssDNA with a specific protein affinity offers further applications. For example, Ling and co-workers used a PDA-coated BP nanosystem as a platform to conjugate a FAM-labelled ssDNA for human thrombin aptamer (HTA).[76] In this design, Ca^{2+} were incorporated onto the surface of BP@PDA by forming coordination with the catechol moieties, and then the doped Ca^{2+} mediated the absorption of FAM-labelled ssDNA aptamers on the surface of BP@PDA. This coordination-based interaction is believed to be stronger than van der Waals forces, π–π stacking, and hydrogen bonding existing in conventional 2D nanomaterial-based DNA sensing platforms (*e.g.*, GO, and MoS_2); thus, it can effectively inhibit nonspecific binding of several biological interferences (*e.g.*, bovine serum albumin, bovine thrombin, and mismatched ssDNA sequences) in biomedical applications.[308]

Conventional antibody detection is largely based on enzyme-linked immunoassay (ELISA), which suffers from low sensitivity. Zhu and co-workers used a sandwich-type electrochemical immunosensor for detecting α-fetoprotein (AFP) tumor marker.[309] In their design, PDA nanoparticles were conjugated with detection antibody (PDANP-Ab2), and PDANPs were found to amplify the oxidative charge transfer of the electrochemical mediator (1,1′-ferrocene dimethanol, FDM) as confirmed by cyclic voltammetry (CV). The authors stated that this was the first time PDA nanoparticles were employed as labelling materials for electrochemical immunosensors to increase sensitivity. In addition to its excellent reproducibility and selectivity, the AFP immunosensor showed a broad linear detection range (1 pg mL^{-1} to 50 ng mL^{-1}) and a low detection limit (0.3 pg mL^{-1}). Similarly, Tang and co-workers employed PDA nanocapsules to load a signal-generation molecule, thymolphthalein (TP), *via* π-stacking to produce PDA–TP nanocapsules.[310] In the presence of target AFP, PDA–TP nanocapsule-linked immunosorbent assays were implemented to capture antibody-labelled PDA–TP. Under alkaline conditions, the coated hydrophobic TP on the PDA was deprotonated into a hydrophilic TP^{2-} ion and released into solution resulting in a deep blue color. This strategy offered a linear range of 10–1000 pg mL^{-1} at a low detection limit of 2.3 pg mL^{-1}.

To further develop stable, sensitive, and specific approaches to detect antibodies, Gao and co-workers developed a horseradish peroxidase (HRP)-mediated oxidation of dopamine technique to supplement the current enzyme-linked immunosorbent assay.[311] This method relies on the ultrafast *in situ* deposition of PDA at the target sites, which allows for a dramatically enhanced capture of reporter molecules (*e.g.*, enzymes and QDs). Consequently, the detection limits have been improved by more than three orders of magnitude. For example, the application of this technique in ELISA-based detection of the HIV antigen (*i.e.*, p24 antigen) can afford a sensitivity lower than 3 fg mL^{-1}, which is in stark contrast with the unsatisfactory sensitivity (10 pg mL^{-1}) in conventional ELISA kit. Wang and co-workers reported a MPN capsule-based electrochemical immunoassay for detecting a biomarker of nasopharyngeal carcinoma: Epstein–Barr virus capsid antigen IgA (EBVCA-IgA).[312] In their design, the large MPN capsules prepared from $CaCO_3$ particles contained a large amount of metal ions to amplify the electrochemical signals for anodic stripping voltammetry (ASV). One advantage of the soft capsules is that it possesses leukocyte-like behaviour on the electrode surface *versus* its solid counterpart leading to improved analyte-recognition efficiency.

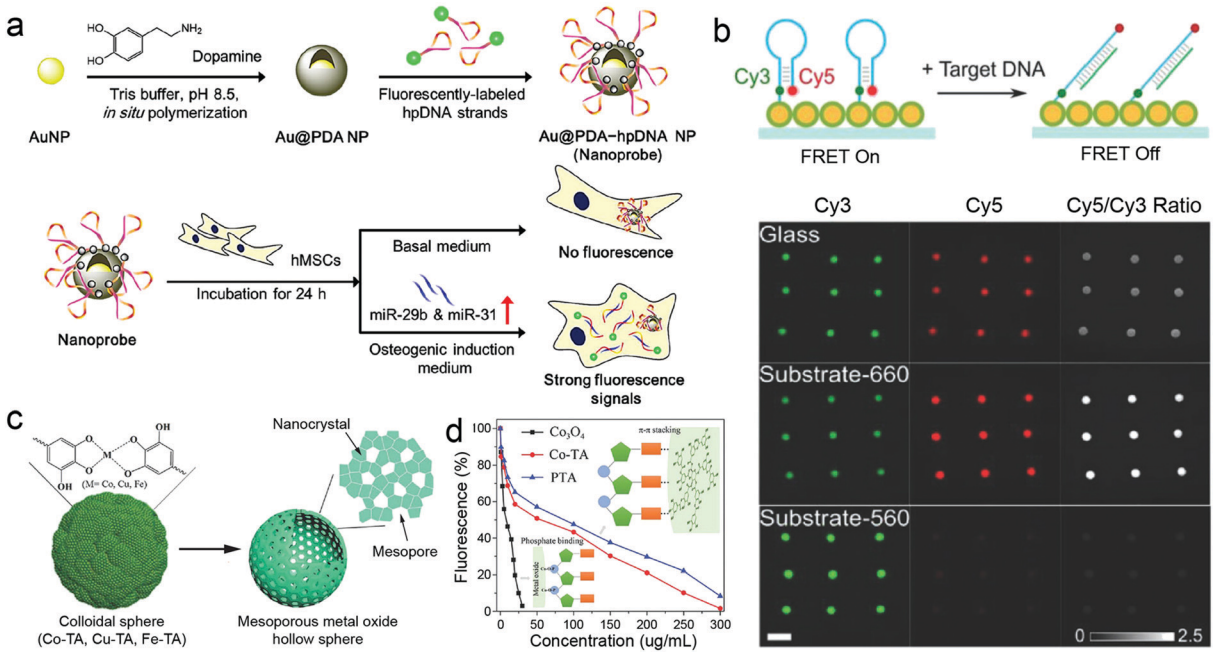

Fig. 21 *In vitro* biosensing of biomacromolecules by using phenolic-based nanoparticles. (a) Schematic illustration of the synthesis of nanoprobes containing PDA-coated Au nanoparticles (Au@PDA NPs) and hairpin-DNA-based (pDNA), and their use for detecting miRNA targets in living hMSCs. Reproduced with permission. Copyright 2015, American Chemical Society. (b) Schematic illustration and fluorescence images of a DNA microarray of Cy3/Cy5 FRET on a plasmonic substrate. After binding a target DNA, the dye pair in the molecular beacon separated. Reproduced with permission. Copyright 2020, Wiley-VCH. (c) Schematic illustration of the synthesis of hollow MMOSs. (d) Fluorescence intensities of probe DNA depended on different concentrations of colloidal spheres. Insets are the schematic illustration of the interactions between probe and materials. (c and d) Reproduced with permission. Copyright 2018, Wiley-VCH.

Once the sandwich structure on the electrode surface is formed, the MPN capsules were disassembled by adding acid, and the released metal ions subsequently acted as analytes to detect EBVCA-IgA down to 0.46 fM.

Phenolic-based materials can be used to synthesize various substrates for signal generation. Wei and co-workers reported a general strategy to design mesoporous metal oxide spheres (MMOSs) with various compositions and structures for detecting miRNA-21.[313] TA and metal ions (*e.g.*, Zn^{2+}, Al^{3+}, Fe^{3+}, and Cu^{2+}) assembled into hybrid nanoparticles by using a formaldehyde-assisted crosslinking strategy. After thermal annealing of metal–phenolic coordination polymer particles, MMOSs containing different metal species could be obtained (Fig. 21c). MMOSs can efficiently quench the fluorescence of a dye-labelled DNA probe and were used to create a "turn-on" fluorescence sensing platform. The fluorescence of FAM-labelled probe ssDNA adsorbed on the surface of MMOSs were efficiently quenched. In the presence of the target miRNA, the nucleic acids hybridized into a double-stranded structure that could shield the phosphates in the double helix structure. Therefore, the double-stranded assembly of DNA could be detached from MMOSs, and the fluorescence of dye-labelled DNA probe was recovered.

4.2.3 Detection of cells. Detecting circulating tumor cells (CTCs) is a minimally invasive method for diagnosing and assessing the efficacy of cancer treatments. However, effectively capturing CTCs is challenging due to their ultralow abundance and various phenotypes. To mimic the structure of the extracellular matrix, Zhou and co-workers developed a necklace-like PDA nanoparticle-decorated alginate nanofiber with a hierarchical nanotopographical structure using electrospinning; the height of the nanotopography was easily modulated by tuning the size of PDA nanoparticles.[314] Four types of cancer cells (*i.e.*, human hepatoma cell line (HepG2), human glioma cell line (U251), human lung epithelial tumor cell line (A549), and human pancreatic carcinoma cell line (PANC-1)) were used to study the cell capture efficiency of the hybrid fibers. The partially exposed PDA on the surface of fiber matrix likely provides chemical signals for capturing CTCs as seen by the improved adsorption of serum proteins that are able to increase cell adhesion. The incorporation of hierarchical nanotopographic structure and surface chemical signaling of PDA in the fiber matrix is believed to promote the capture of CTCs. Moreover, in a blood sample containing spiked cancer cells, the PDA-modified fibers still exhibited good capture indicating its potential for sensing in complex biological environments.

Aptamers or antibodies are typically used for biological targets and can improve the specificity of nanosystems. Wang and co-workers developed an aptamer-based detection strategy for CCRF-CEM cancer cells (Fig. 22a and b). The molecular beacon was designed with three domains: (1) a sgc8 region (blue and black segments) that can specifically bind to PTK7 (strand-sgc8, an overexpressed membrane protein (PTK7) on CCRF-CEM cancer cells), (2) a poly-thymine (poly-T) DNA spacer (green segment), and (3) a hybridization region (red segment)

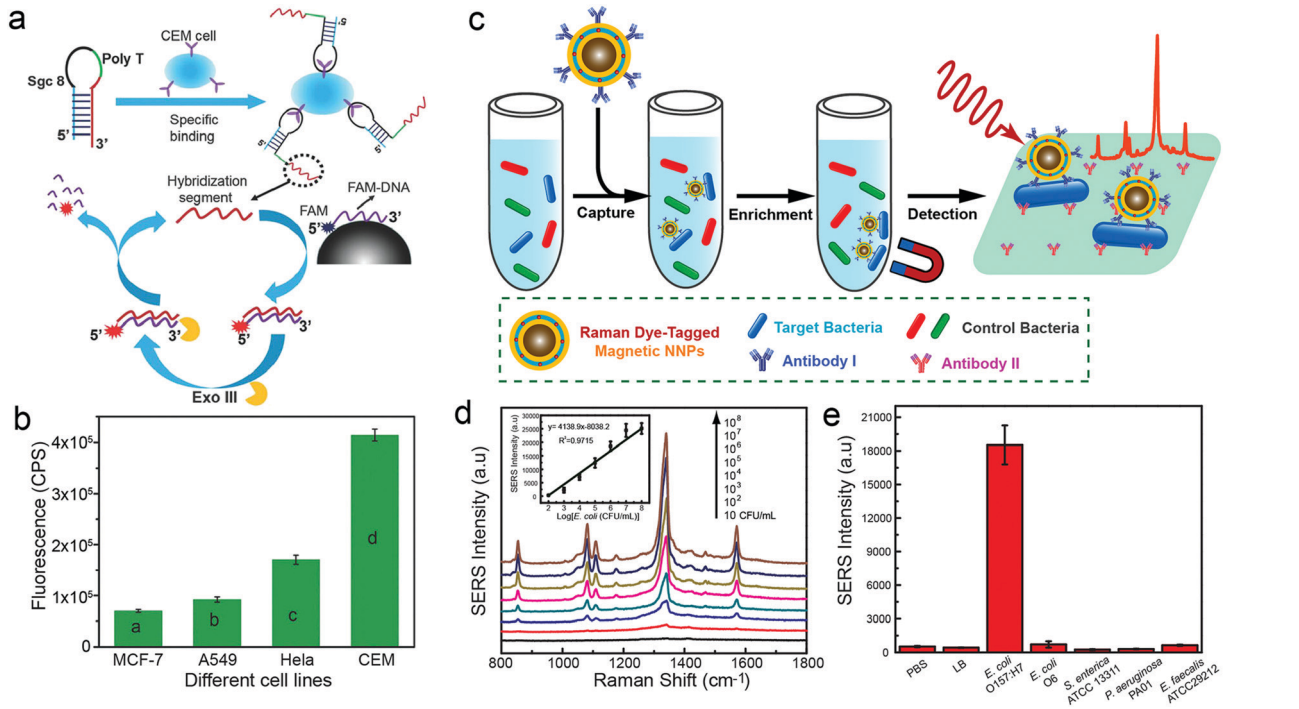

Fig. 22 *In vitro* biosensing of diverse cell types *via* phenolic-based nanoparticles. (a) Proposed mechanism for PDA nanoparticle-based cytosensor for detecting CEM cancer cells. (b) Fluorescence intensity of suspension containing the nanoprobes and different cell lines (*e.g.*, MCF-7, A549, HeLa and CCRF-CEM). (a and b) Reproduced with permission. Copyright 2016, Royal Society of Chemistry. (c) Schematic illustration of the immunoassay using SERS-encoded magnetic nanoprobes for bacterial detection. (d) Raman spectra of *E. coli* O157:H7 at different concentrations after being conjugated with nanoprobes. Inset: Raman intensity at 1341 cm^{-1} depends on the logarithm of the bacterial concentration. (e) The detecting selectivity of this platform by using control buffers and various types of bacteria (10^6 CFU per mL). (c–e) Reproduced with permission. Copyright 2016, American Chemical Society.

to interact with FAM-labelled DNA strands (FAM-DNA) that are pre-absorbed on PDA nanoparticles.[315] The hybridization between the blue and red segments intrinsically maintained the stem-looped structure of the aptamers with a high stability. In contrast, when the nanoprobes were incubated with a CCRF-CEM cell suspension, the sgc8 segment would interact with PTK7 protein on the surface of CCRF-CEM cells and undergo a conformation change releasing the hybridization region. This led to the hybridization between red segments and FAM-DNA on PDA nanoparticles to form a duplex structure; the fluorescence of FAM was then recovered as a result of its detachment from PDA.

In addition to diagnosing cancer, PEN-mediated nanosystems have also been used to detect bacteria and viruses. Duan and co-workers reported a platform strategy for synthesizing diverse core–shell plasmonic nanoparticles with built-in plasmonic nanogaps for bacteria sensing in an immune assay. In this design, the PDA served multiple functions: a nanoscale spacer, a redox-active layer to mediate the *in situ* growth of metal shell, and a reactive scaffold to anchor Raman active molecules inside the nanogap. By introducing a magnetic core and conjugating antibody on the shell surface, SERS-encoded magnetoplasmonic nanogap nanoparticles could be developed to capture bacteria (Fig. 22c–e). This probe-integrated assay showed that the SERS intensity from the bacterial increased linearly from 10 to 10^8 CFU per mL with high sensitivity (10^2 CFU per mL). Moreover, both buffer controls (*e.g.*, PBS and Luria–Bertani culture medium) and other bacterial species (*e.g.*, *E. coli* O6, *S. enterica* ATCC 13311, *P. aeruginosa* PA01, and *E. faecalis* ATCC 29212) produced negligible signals. This high specificity of this platform was ascribed to the presence of targeting antibodies and surface-blocking molecules on the immune sandwich assay.[316] To simplify the detection process, they further employed PDA-glued magnetic nanochains to increase the mixing efficiency streamlining the design of the microfluidic assay where the nanochains act as nanoscale stir bars.[317] Furthermore, by introducing the capture antibodies on the surface of nanochains, this platform could rapidly capture diverse bacteria such as *Escherichia coli* O157:H7 (*E. coli* O157:H7) and *Staphylococcus aureus* (*S. aureus*). After supplementation with SERS nanoprobes in a sandwich structure, the microfluidic assay only required 1 μL of sample showing consistent linear correlation from 10 to 10^4 CFU per μL and suggesting it has excellent sensitivity.

Cai and co-workers reported a resonance light scattering (RLS)-based sensor for detecting trace quantities of Hepatitis A virus using SiO_2@PDA where the PDA shell was molecularly imprinted with HAV templates.[318] The target viruses were selectively captured by virus-imprinted PDA on SiO_2 nanoparticles increasing the RLS intensity that was recorded using a fluorescence spectrophotometer. The enhanced RLS intensity (ΔIRLS) was proportional to the concentration of HAV in the range of 0.04–6.0 nmol L^{-1} with a low detection limit of 8.6 pmol L^{-1}.

4.3 *In vivo* bioimaging

PEN enables the fabrication of diverse imaging probes to diagnose diseases. These particles can accumulate in the site of interest through either passive or active targeting (stealth *vs.* targeting), followed by high-resolution imaging using several techniques. Phenolics can serve as contrast agents for imaging or as tools to integrate imaging tags. In this section, various PEN-based imaging techniques including fluorescence imaging, magnetic resonance imaging, photoacoustic imaging, and other medical imaging technologies will be discussed.

4.3.1 Fluorescence imaging. Fluorescence imaging is a widely-used technique in biomedicine for cellular tracking and organ/tissue imaging.[319] A straightforward method to fabricate fluorescent probes is to conjugate fluorescent dyes with target substrates. Due to the reactive surface chemistry of phenolic materials, many particle systems with phenolic surfaces can be readily tagged with dyes for fluorescent imaging.[320,321] Commercial fluorescent dyes provide a range of colors applicable to different imaging conditions. However, fluorescence quenching may occur *via* FRET and/or photo-induced electron transfer phenomena when the dyes and phenolic molecules are closely packed.[322,323] To solve this problem, researchers utilized polymer-conjugated dyes for fluorescent labelling. Silica coating on the pre-formed phenolic particles could also avoid the direct attachment of dyes onto the phenolics. Interesting "off–on" strategies for fluorescence imaging based on quenching effects were developed.[324,325] Before reaching the targets, the fluorescent molecules were entrapped in the phenolic-based particles and showed no fluorescence. Triggered by external stimuli, the entrapped fluorescent molecules could be released from the systems recovering fluorescence. These two strategies have been applied in many phenolic-based particle systems to circumvent quenching effects to improve bioimaging.

Recently, some PEN-derivative particle systems with intrinsic fluorescence have gained research attention. For example, PDA nanoparticles exhibited wavelength-dependent fluorescence under UV light.[322] However, the fluorescence intensity from PDA is too weak to meet the needs of fluorescence imaging. It was reported that suppressing dopamine polymerization or reducing the π–π stacking could be possible solutions to synthesize fluorescent PDA. Wei and co-workers first obtained fluorescent PDA particles using a concentrated H_2O_2 solution for oxidation.[326] The oxidized PDA nanoparticles retained their solubility and biocompatibility and exhibited excitation wavelength-dependent fluorescence emission from 360 to 500 nm. It was noteworthy that the oxidized PDA particles showed outstanding photostability. No significant photobleaching was observed during continuous excitation for 30 min. Furthermore, fluorescent PDA capsules were prepared through a similar oxidative method on pre-formed PDA capsules.[199] Interestingly, the fluorescence intensity of the capsules was shown to be pH-dependent with the highest intensity at a pH of 3. Further testing demonstrated the internalization of fluorescent capsules for cell visualization.

The π–π stacking between dopamine molecules leads to strong fluorescence quenching. Degradation methods that aim to undermine the π–π stacking interactions could be used to prepare fluorescent PDA. Tseng and co-workers reported that the hydroxyl radicals generated at 100 °C could decompose PDA nanoparticles into fluorescent PDA dots with blue fluorescence in the presence of H_2O_2 and NaOH.[327] In addition to oxidation and degradation methods, fluorescent PDA particles could be prepared by conjugation with PEI.[328] Green fluorescent PDA particles with high stability showed great cell imaging performance. With the assistance of metal ions, polyphenol-based particles can be engineered into fluorescent probes. Caruso and co-workers prepared functional MPN capsules composed of TA and up to 18 different metal ions. Of all MPNs, the authors found that by introducing 2-thenoyltrifluoroacetone (TAA) and acetylacetone into the system, TA–TAA–Eu(III) and TA–acetylacetone–Tb(III) MPN capsules were observed to be red fluorescent (613 nm) and green fluorescent (545 nm).[26] Despite these achievements in phenolic-based fluorescent probes, there is limited research on their applications *in vivo* due to their low quantum yields. The incorporation of fluorescent dye molecules or fluorescent metal complexes within the particle system is still considered the most effective method for *in vivo* fluorescence imaging.[329]

4.3.2 Magnetic resonance imaging. MRI is a powerful imaging technique and has been used for clinical diagnosis. Utilization of MR contrast agents (CAs) such as commercially used Magnevist (Gd–DTPA) improve the imaging sensitivity by altering the longitudinal (T_1) or transverse (T_2) relaxation times of surrounding water protons.[330] However, the relatively low relaxivity of most traditional CAs and the potential risk of metal ion release require the development of novel MRI agents for efficient MRI performance and biosafety. Further, the emergence of imaging-guided therapy for medical use required a multi-functional theranostic system. Due to the strong chelating ability of metal ions and high affinity toward metal/metal oxide substrates, phenolic materials have been used for construction of various theranostic particle systems for MRI functions.

The dihydroxyphenol or trihydroxyphenol groups coordinate with a variety of metal ions including Gd^{3+}, Mn^{2+}, and Fe^{3+}, enabling the formation of metal–phenolic complexes as potential MR CAs for *in vivo* bioimaging. Jokerst and co-workers provided a facile method to fabricate Gd^{3+}-doped particles as MR CAs (Fig. 23a and b).[331] The PDA-based CAs could be integrated with PDA particles either by adding Gd^{3+} salts during dopamine polymerization, or by metal ion exchange with an Mn^{3+}-doped template particle. Transverse MRI images pre- and post-injection showed that the MRI signal increased 2-fold *versus* baseline (Fig. 23c). Mao and co-workers prepared a theranostic particle system using EGCG, anti-cancer drugs, polyphenol-modified copolymers, and Gd^{3+}, giving a higher longitudinal relaxivity (4.95 ± 0.44 mM^{-1} s^{-1}).[142] To reduce the risk of Gd^{3+} release, a Gd^{3+} metallofullerene with three Gd^{3+} encapsulated was used as satellites anchored to the surface of PDA particles.[332] The core–satellite structure of the CDPGM NPs permitted fast exchange of water and thus had a high relaxivity r_1 of 14.06 mM^{-1} s^{-1} and low risk of release of Gd^{3+}. The PDA nanoparticles here served as a platform for assembly of different functional moieties. It is

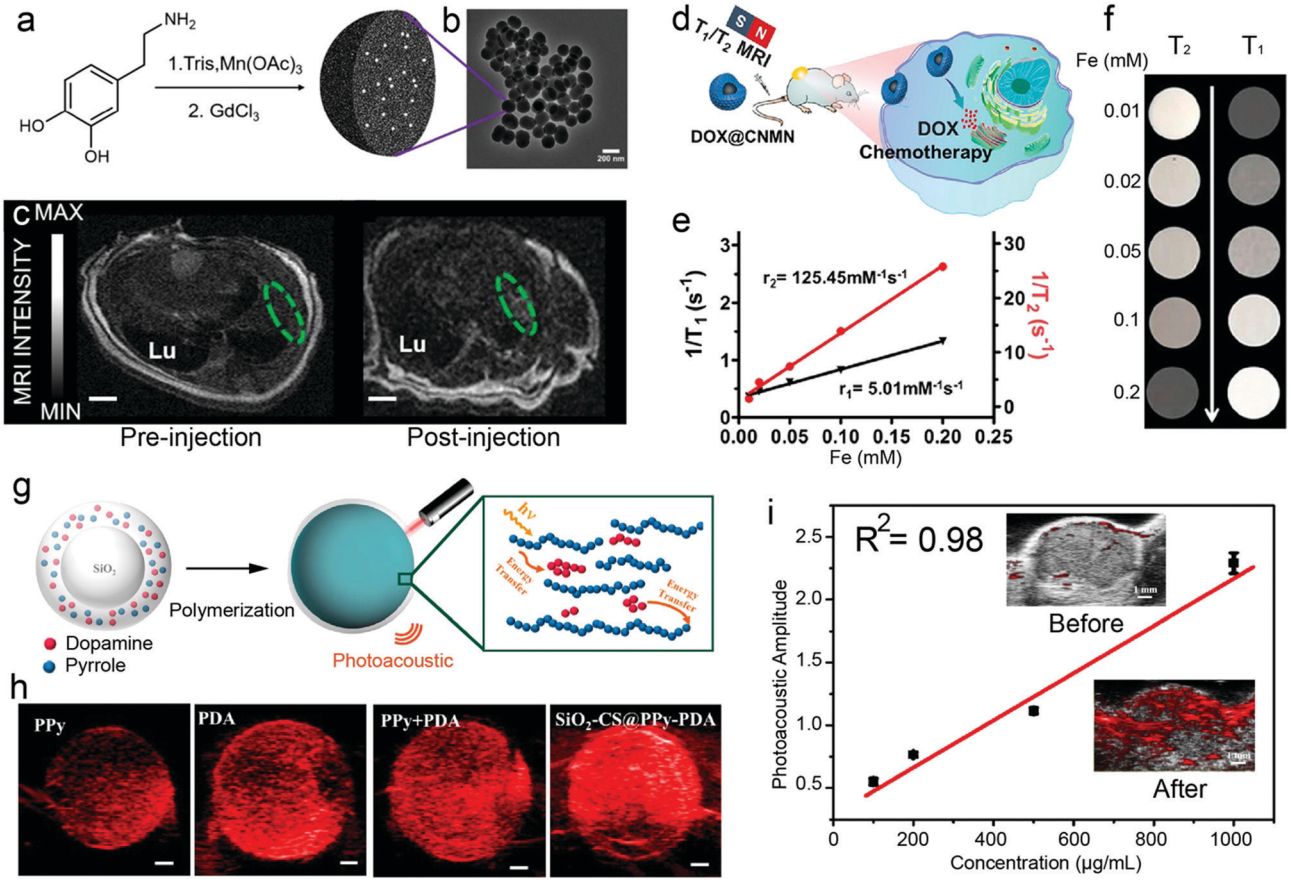

Fig. 23 *In vivo* MRI and PAI performance of phenolic-based nanoparticles. (a) Synthesis and (b) TEM image of Gd^{3+}-doped PDA nanoparticles. (c) Transverse MRI view of a mouse heart before and after injection of the MR CAs. Reproduced with permission. Copyright 2019, American Chemical Society. (d) Schematic illustration of T_1/T_2 MRI-guided cancer therapy by DOX-loaded TA–Fe(III) coordination network (DOX@CNMN). (e) r_1 and r_2 relaxivities of CNMN as a function of the Fe molar concentration in the solution, and (f) the corresponding MR images of CNMN. (d–f) Reproduced with permission. Copyright 2020, American Chemical Society. (g) Schematic illustration of silica nanoparticles with PDA and PPy coating for PAI. (h) Photoacoustic images of suspensions of different particles and (i) photoacoustic amplitude of PPy–PDA-coated silica particles at different concentration. Inset: Photoacoustic images at 700 nm of the tumor before and after injection of the particles. (g–i) Reproduced with permission. Copyright 2018, American Chemical Society.

noteworthy that such particles also showed strong NIR absorption, photoacoustic effects, and positron emission tomography (labelled with ^{64}Cu) performance implying great potential of the particles for multimodal imaging-guided cancer therapy. More recently, a T_1-MRI trackable particle system was fabricated for real-time *in vivo* temperature monitoring. The $NaBiF_4$:Gd@-PDA@PEG particles guaranteed accuracy of temperature mapping with weak local phase susceptibility (1.04×10^{-6} emu g^{-1} Oe^{1-}). Further animal studies verified its capability of dynamic temperature recording in tumor and peritumoral tissue.[333]

In addition to Gd^{3+}, other metal ions such as Mn^{2+} are good candidates to synthesize MR CAs. Caruso and co-workers confirmed that the TA–Mn(II) MPN capsules displayed a relaxivity r_2 on the order of 60 s^{-1} mM^{-1}, which is sufficient for *in vivo* imaging.[26] Liu and co-workers prepared Mn^{2+}-incorporated metal–organic particles composed of Mn^{2+}, a NIR dye (IR825), and PDA for MRI-guided cancer therapy.[334] The obtained particles exhibited a comparable or even higher r_1 relaxivity than that of commercial Gd^{3+}-based CAs. Importantly, the synergistic photothermal effect of IR825 and PDA makes the system a potential photothermal agent for tumor ablation. Thus, the real-time tracking enabled by MRI could reliably guide the subsequent therapy for enhanced efficacy with high spatiotemporal resolution. Self-assembly of phenolic monomers and strong coordination between phenol groups and metal ions both facilitate the development of metal ion-doped MR CAs. The relaxivities of particles derived from different metal ions (Gd^{3+}, Ni^{2+}, Mn^{2+}, Cu^{2+}, Fe^{3+}, Zn^{2+}, *etc.*) are different. Among all metal ions, Gd^{3+}-doped particles exhibited the highest photoacoustic signal intensity.[331,335] Further studies of the interaction forces in the system could provide more information to engineer particles with higher MRI performance.

Metal oxides or metal composites with phenolic coatings represent a series of superior MR CAs with high biocompatibility and satisfactory *in vivo* bioimaging. The core–shell nanoparticles not only retain the contrast enhancement of the cores, but also allow for biocompatible surface coatings and further secondary functionalization. Chen and co-workers demonstrated that

magnetic Fe_3O_4@PDA nanocomposites with a T_2 relaxation rate of 114.7 mM^{-1} s^{-1} could be used as CAs for MRI.[171] However, *in vivo* data was not shown in the report. More recently, Liu and co-workers prepared Fe_3O_4@PDA nanocomposites as T_2-weighted MRI contrast agents for cancer diagnosis.[290] The transverse relaxivity of Fe_3O_4@PDA nanocomposites was determined to be 337.8 mM^{-1} s^{-1}, which is much higher than that of Fe_3O_4@PDA particles with the same components and structure. According to the physicochemical characterization results in both studies, the core size of particles may account for the difference. *In vivo* imaging tests of Fe_3O_4@PDA as a CA was conducted, and significant enhancement of MRI signals in the tumor site was recorded due to high particle accumulation at the tumor site. To functionalize the particle system for different applications, researchers utilized the core–shell Fe_3O_4@PDA as a particle template for further growth of a cationic polymer and DNA attachment for MRI-guided therapy.[225,302] Most of the Fe_3O_4@PDA particles were used as T_2 mode relaxation CAs. Thus, a combination of T_1/T_2 modes for MRI is further considered as a tool with complementary advantages to provide more accurate information.

An avocado-like Fe^{3+}/Fe_2O_3 particle system with T_1/T_2 dual mode was developed by Sun and co-workers (Fig. 23d–f).[293] The Fe_2O_3 particles were coated by PDA first which allowed for TA–Fe(III) MPNs growth, leading to a phenolic-engineered all-iron MR imaging agent. After one hour of intratumoral injection, the MR signal intensity of T_1 increased by nearly 3.5 times, and the T_2 signal intensity decreased to 40%. At 24 h intravenous post-injection, the T_1 and T_2 signal intensities increased by 1.5-fold and decreased to 0.6 of the original showing a clearer tumor boundary. Other metal oxides or metal composites including Mn_3O_4,[172] Co–P,[78] MnO_2,[336] and $Gd_2(CO3)_3$[70] have been developed with phenolic groups for the synthesis of biocompatible MR CAs with multifunctional modalities.

4.3.3 Photoacoustic imaging. PAI is a promising imaging technique for *in vivo* bioimaging with superb spatiotemporal resolution. With external illumination, the imaged tissue absorbs light energy and creates ultrasound (US) waves that could be detected and used for reconstruction of photoacoustic images.[337] To improve the signal contrast, photoacoustic CAs with efficient conversion of light energy and generation of US waves have been developed.[338,339] A NIR laser is typically used for PAI due to the deep tissue penetration of NIR irradiation. Thus, a good photoacoustic CA for *in vivo* bioimaging should possess high NIR absorbance, high molar-extinction coefficient, good photostability, and biocompatibility. To date, various CAs for PAI have been developed including PEN-derived particles.

PDA has a broad extinction spectrum from 650–1300 nm; biological tissue shows a minimum in absorption. Thus, upon pulsed laser irradiation, PDA nanoparticles transfer light into heat fluctuations and sound waves generate high contrast.[340] Photoacoustic signals and PDA concentration is linearly dependent. Thus, the accumulation of PDA nanoparticles at a target of interest could provide high-contrast images for disease diagnosis. Lu and co-workers prepared PDA nanoparticles by modification of a short targeting peptide (arginine–glycine–aspartic–cysteine acid) on the particle surface to improve tumor targeting.[341] Cheng and co-workers functionalized PDA nanoparticles of similar size with an autophagy-inducing peptide (*beclin 1*) and a targeting peptide (arginine–glycine–aspartic) for enhanced therapy.[342] The photoacoustic features successfully enabled real-time tracking and biodistribution study of the nanoparticles. Moreover, PDA materials with a different structure and morphology also offer photoacoustic signal such as PDA nanocapsules.[208] Here, 200 nm hollow PDA capsules with a shell thickness of about 30 nm showed over two-fold higher photoacoustic intensity than solid PDA particles at the same concentration. Further, mesoporous PDA nanoparticles were applied for PAI-guided chemo-photothermal therapy.[343] The PA signals in the tumor region could be recorded at different time points to assess the nanoparticle enrichment after administration.

Metal–phenolic hybrid materials also exhibited satisfactory photoacoustic effects for *in vivo* bioimaging. It was reported that TA–Fe(III) and pyrocatechol–Fe(III) complexes could emit strong photoacoustic signals.[344,345] Other metal–polyphenol complexes such as TA–Mn(II) and EGCG–Fe(III) likewise featured PAI ability and good photostability even when they were deposited as a coating shell on substrates.[346] The photoacoustic signal of metal–phenolic complexes is also proportional to the metal ion concentration indicating that phenols and metal ions both contribute to the photoacoustic features.[345] Consequently, many hybrid particle systems of phenolic materials and metal-based substrates including metal, metal oxides, and metal complexes have been developed for PAI.

Magnetic particles (Fe_3O_4),[171] TiO_2 nanoparticles,[347] AuNRs,[348] Au nanostars,[349] Au nanobones[350] and various metal-based materials can also be used as core substrates for fabrication of core–shell photoacoustic agents. The presence of metal increases the light adsorption into the NIR range, which facilitates the generation of local heat and US emission for high-resolution PAI. Traditional photoacoustic agents showed the highest absorbance band in the first near-infrared window (700–950 nm, NIR-I), which hindered PAI for deep-located tissue because of limited tissue penetration depth.[351] A Au–PDA hybrid nanoparticle obtained by one-pot synthesis offered PAI in the second near-infrared window (950–1700 nm, NIR-II).[218] The compact blackbody had hyperbranched Au, and the PDA had a uniform broadband absorption across 400–1350 nm implying the potential for NIR-II PAI. The *in vivo* study confirmed that the photoacoustic amplitude at the tumor site reached its peak value of 4.7-fold of the tumor background after 24 h of injection underscoring its great PAI ability. This indicates that attention should be paid to both the NIR absorbance intensity and incident light wavelength when designing the photoacoustic agents.[352]

Conjugated polymers are well-known photoacoustic CAs. The assembly of conjugated polymers and phenolics yield novel photoacoustic CAs. Shao and co-workers reported that pyrrole and dopamine monomers could co-deposit onto silica nanoparticles to form a polypyrrole–PDA (PPy–PDA) shell (Fig. 23g).[353] Such core–shell particles showed a broadband adsorption in the NIR region from 700 nm to 1000 nm. The hybrid PPy–PDA coating on SiO_2 template showed significant enhancement in

the PA intensity, which was 340% of PPy and 180% of PDA with the same mass concentrations (Fig. 23h). After intravenous administration, intense photoacoustic signals could be observed in the tumoral region demonstrating its feasibility for *in vivo* PAI (Fig. 23i).

4.3.4 Others imaging modalities. Through PEN, functional particle systems with different imaging modalities could be prepared on the basis of either phenolic materials themselves or various integrated functional motifs. Here, novel optical agents for imaging techniques other than fluorescence imaging, MRI, and PAI will be introduced. However, it should be noted that the PEN-derived particle systems usually possess multiple imaging modalities. The combined bioimaging provided higher resolution for personalized precision medicine.[354]

Chen and co-workers prepared a polyphenol-based nanoplatform for dual-modality imaging of MRI and positron-emission tomography (PET).[355] The polyphenol-based polymer co-assembled with Mn ions or zirconium-89 (^{89}Zr) as cross-linkers to form a particle carrier for anti-cancer drug delivery. The Mn^{2+}-based particle could be used for MRI due to the coordination of Mn^{2+} and polyphenols while the ^{89}Zr-loaded particle served as PET agents to evaluate the biodistribution. *In vivo* imaging results of PET provided precise information of particle accumulation in the tumor region and liver clearance. Another PEN-derivate polymer nanoparticle self-assembled by polyphenol–poloxamer was developed for PET and NIR fluorescence bimodal imaging (Fig. 24a and b).[356] The supramolecular particles were synthesized by self-assembly of TA and amphiphilic block copolymer (poloxamer 407) in the presence of NIR fluorescent dyes (IR780) and were further loaded with metal radionuclides (^{89}Zr) through the coordination interactions with TA. Thanks to the strong chelating ability of TA, ^{89}Zr was highly stable in mouse serum and less than 3% of ^{89}Zr leaked over 72 h. Further *in vivo* PET imaging performed at different time points of post-injection provided quantitative information of particle distribution.

X-ray computed tomography (CT) provides high-resolution and three-dimensional anatomic information and is a widely-used imaging technique in clinical diagnosis. PDA-coated Au nanostars could serve as CT imaging CAs for imaging-guided tumor therapy.[357] However, they suffer from low sensitivity and poor resolution in soft tissues. To improve imaging, europium–phenolic network coated $BaGdf_5$ nanocomposites were developed for tri-modal CT/MRI/luminescence imaging.[145] Specifically, the electrons of Gd^{3+} account for the T_1-weight MRI imaging and the TA–Eu(III) complexes in the particles contributed to the green and red luminescence. The CT property of as-synthesized composites results from the intensive absorption of X-ray by the large atomic

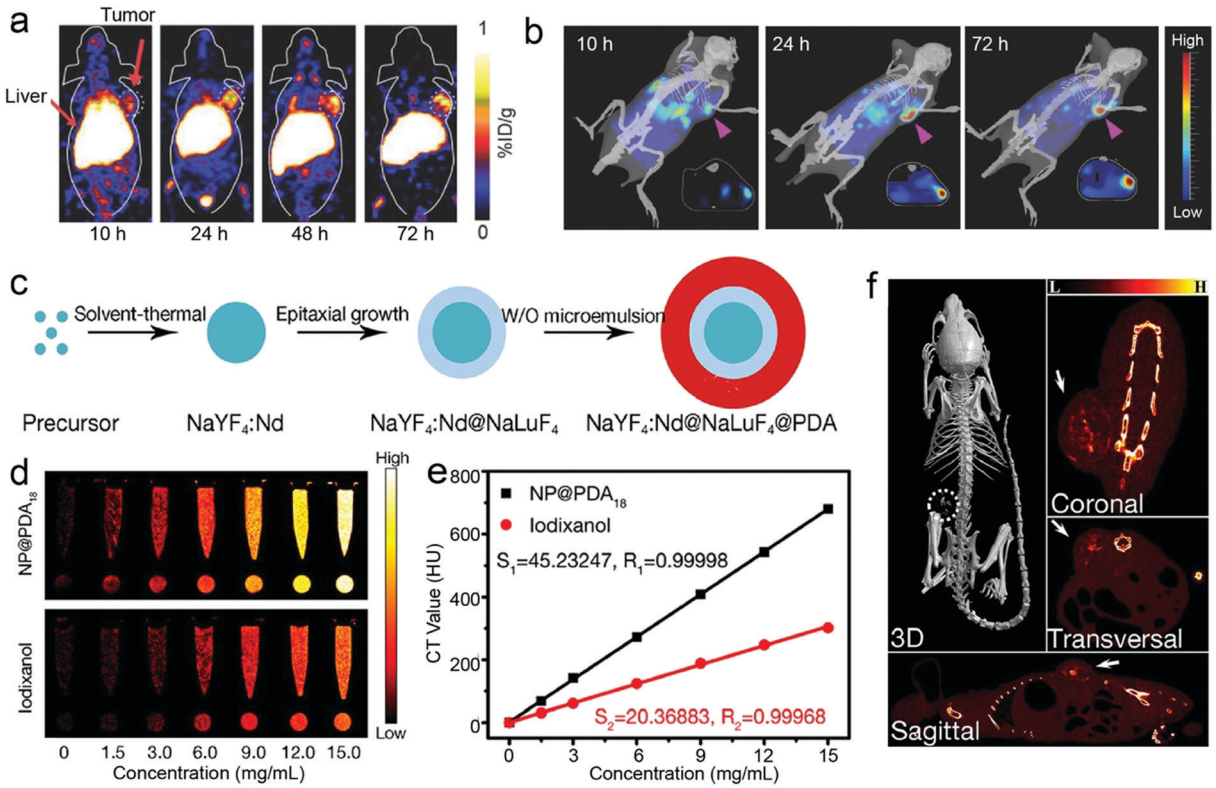

Fig. 24 *In vivo* bioimaging of various imaging techniques on the basis of phenolic-derivate particle systems. (a) Serial coronal PET images at different time points post-intravenous injection of ^{89}Zr-labelled phenolic particles in tumor-bearing mice. (b) 3D fluorescence images reconstructed with the whole body transillumination images. (a and b) Reproduced with permission. Copyright 2017, Wiley-VCH. (c) Schematic illustration of synthesis of PDA-coated La nanoparticles for imaging-guided cancer therapy. (d) X-ray CT images, and (e) HU values of PDA-coated La nanoparticles and iodixanol aqueous solution with different concentrations. (f) X-ray CT images of tumor-bearing mice after intratumoral injection of nanoparticles. (c–f) Reproduced with permission. Copyright 2017, American Chemical Society.

number of elements. This nanocomposite for CT/MR/optical imaging could serve as a superior CA to acquire comprehensive information of deep-located tissues with high resolution. A bimodal CT/NIR-II imaging agent with significant photothermal effects was obtained by fabricating PDA-coated La nanoparticles (Fig. 24c).[358] The $NaYF_4$:Nd^{3+}@$NaLuF_4$ nanophosphor with excellent X-ray attenuation and NIR photoluminescence is well-suited for *in vivo* imaging. The PDA coating on the nanophosphor remarkably improved the biocompatibility and endowed the particles with high photothermal conversion for tumor ablation. This core–shell nanocomposite could be used for both NIR-II optical imaging of the tumor and CT imaging. The increasing slope of the Hounsfield unit (45.23) against the particle concentration is much higher than that for iodixanol (20.37) (Fig. 24d and e). The nanocomposites showed great performance in bimodal imaging-guided therapy for tumor-bearing mice (Fig. 24f).

Medical US imaging is an essential diagnostic technique that allows for enhanced-resolution imaging to track the blood flow rates and examine the pathologic tissues.[359] Like other imaging methods, US imaging could be improved by introducing CAs. Conventional US CAs are inert low-boiling perfluorocarbons entrapped within the phospholipid or protein coatings. However, the short circulation time and poor accumulation in target tissues due to the relatively large particle size limited the imaging resolution. A range of US CAs have been developed for perfluorocarbon encapsulation in a more stable fashion such as phenolic materials. Rinehart and co-workers focused their attention on the investigation of perfluorocarbon-loaded PDA nanoparticles.[360] Fluorine-functionalized PDA nanoparticles (PDA-F) were first prepared through Michael addition with perfluorodecanethiol. The fluorophilicity of the functionalized particles possessed high loading capacity of perfluoropentane droplets which display strong and persistent US contrast. Compared with commercial CAs, PDA-F at a particle size of 135 nm showed favorable color Doppler imaging lifetime of about 1 h. A further *ex vivo* imaging study on fresh porcine liver demonstrated the effective tissue perfusion. Moreover, the same group gave Fe^{3+} in the particle system by chelation to generate photoacoustic signals in addition to US signal.[361] Both *in vitro* and *in vivo* investigations demonstrated the capability of PDA-F particles for bimodal US/photoacoustic imaging.

Lu and co-workers used the Raman molecule-encoded Au@PDA nanoparticles as a probe to detect bone cracks.[362] In their design, an 8 nm-thick PDA coating was chosen as optimized coating to prevent the leaking of the Raman-active molecules and disturbance from hash environment while also minimizing the interference on the SERS signal intensity from the capsulation. The bone crack can be specifically labelled by SERS-encoded Au@PDA by taking advantage of high affinity of PDA towards calcium exposed on the damaged bone and measured by an intense featured Raman signal.

4.4 Disease therapy

While some phenolic molecules themselves can serve as active drugs for certain disease (*e.g.*, antimicrobials, inflammation, Alzheimer's disease), PEN can be used to design dedicated drug delivery systems and provide complementary treatment approaches by introducing more functionalities.[135] In this section, PEN-derivate particle systems for drug delivery will be introduced followed by discussion of PTT, photodynamic therapy (PDT), immunotherapy, and other treatments.

4.4.1 Drug delivery system. The well-designed particle structure and morphology as well as the potential for secondary modification enables PEN-based particle therapeutics to work as protective carriers with specific targeting for drug delivery. A wide spectrum of functional cargos from small molecule drugs to biomacromolecules and other therapeutic agents could be delivered into the target sites for use in PEN.

Successful drug delivery of small molecule drugs requires prolonged blood circulation and efficient targeting for improved disease treatment and reduced side effects. There are two main ways to load cargo for small molecule drug delivery. First, the PEN-based particle carrier could be fabricated in advance for subsequent loading of drug molecules *via* physical adsorption and chemical conjugation. The chemotherapeutic DOX can be efficiently loaded on the surface of PDA particles, EGCG particles, MPNs, and other phenolic-based particles as a model drug for cancer therapy.[363–366] The π–π stacking and hydrogen bonding between DOX and phenolic surface dominates the loading process with some examples of covalent interactions. To improve the loading efficiency, phenolic particles with larger pore size and high surface area such as (meso)porous particles and hollow capsules were used for the delivery.[139,367] Furthermore, the core–shell particles provide an opportunity to impart another functional modality by incorporating the cores of interest. The introduction of Au core by using PDA-coated AuNRs led to a high photothermal conversion thus enabling synergistic chemo-phototherapy.[368] Other core materials include magnetic nanoparticles,[325,369] UCNPs,[50] selenide molybdenum,[44] Mn_3O_4 nanocrystals,[172] and zinc oxide nanocores.[370] These have also been used for core–shell delivery systems that integrated specific functions.

As reviewed, most of core–shell nanoparticles for delivery of small molecule drugs were derived from PDA shell, whereas other phenolic materials could serve as protective shells for drug delivery. Kong and co-workers developed a core–shell MSN@MPN nanoparticles where DOX molecules were loaded inside silica matrix prior to the coating of MPN.[289] Herein, the TA–Fe(III) networks acted as a pH-responsive gatekeeper for on-demand drug release. Li and co-workers functionalized the DOX-loaded UCNP@MSN nanoparticles with TA–Cu(II) network to block the premature release of drug molecules.[371] The cumulative release of DOX molecules could be observed under an acidic environment due to the collapsed MPN shell. Dithio-PDA-coated porous CeO_2 nanorods were fabricated as dual-responsive drug delivery system.[372] Small molecule drugs were well-encapsulated by the protective coating until reaching the target site and were then released in response to either GSH or low pH. In short, the small molecule drugs could be loaded inside pre-formed nanoparticles with phenolic coating for protective delivery.[373]

The second strategy for drug delivery was co-assembly of small molecule drug and phenolic materials into particle systems. Chen and co-workers developed a drug delivery platform by self-assembly of DOX, Fe^{3+}, platinum prodrug polyphenols, and PEG–polyphenols.[374] The hydrophobic DOX coordinated with Fe^{3+}, and Fe^{3+} further interacted with phenolic groups of the monomers. The resultant nanoparticles showed high accumulation in tumor for 72 h where nanoparticles in other organs were gradually cleared out. This effectively inhibited the tumor growth by synergistic therapy of DOX and platinum drugs (Fig. 25a and b). The phenolic materials serving as "biological glue" assembled all functional blocks including drug molecules in one single particle system. Interestingly, these as-prepared particles for drug delivery inherited the capability of assembly–disassembly transformation. The TA-based particles could transform into hydrophobic particles in an acidic environment, and revert to a smaller hydrophilic nano-assembly in cytoplasm, thus achieving precise intracellular payload release.[268] These delivery methods for small molecule drugs have been well-demonstrated by using DOX as a model drug. Besides, the PEN-based strategy was also applied for various drug molecules for specific therapy such as cisplatin,[348] desipramine,[182] hesperetin,[70] imiquimod,[375] and docetaxel,[376] showing great potentials of PEN for precise delivery of small molecules drugs. The physicochemical properties of small molecule drugs are the decisive factors of loading efficiency and capacity. Drug molecules with hydrophobic domains, aromatic rings, polar groups, or negative/positive charges are often used as loading cargos for delivery therapy.

Recent advances in biotechnology and pharmaceuticals have created a large number of functional biomacromolecules like proteins and DNA/RNA to engage specific targets in a wide range of biological processes.[377,378] However, efficient delivery of biomacromolecules is facing several challenges like instability, short circulation time, cellular impermeability, *etc.* The emergence of PEN facilitates the development of carriers with a unique structure and various functions for biomacromolecules delivery.

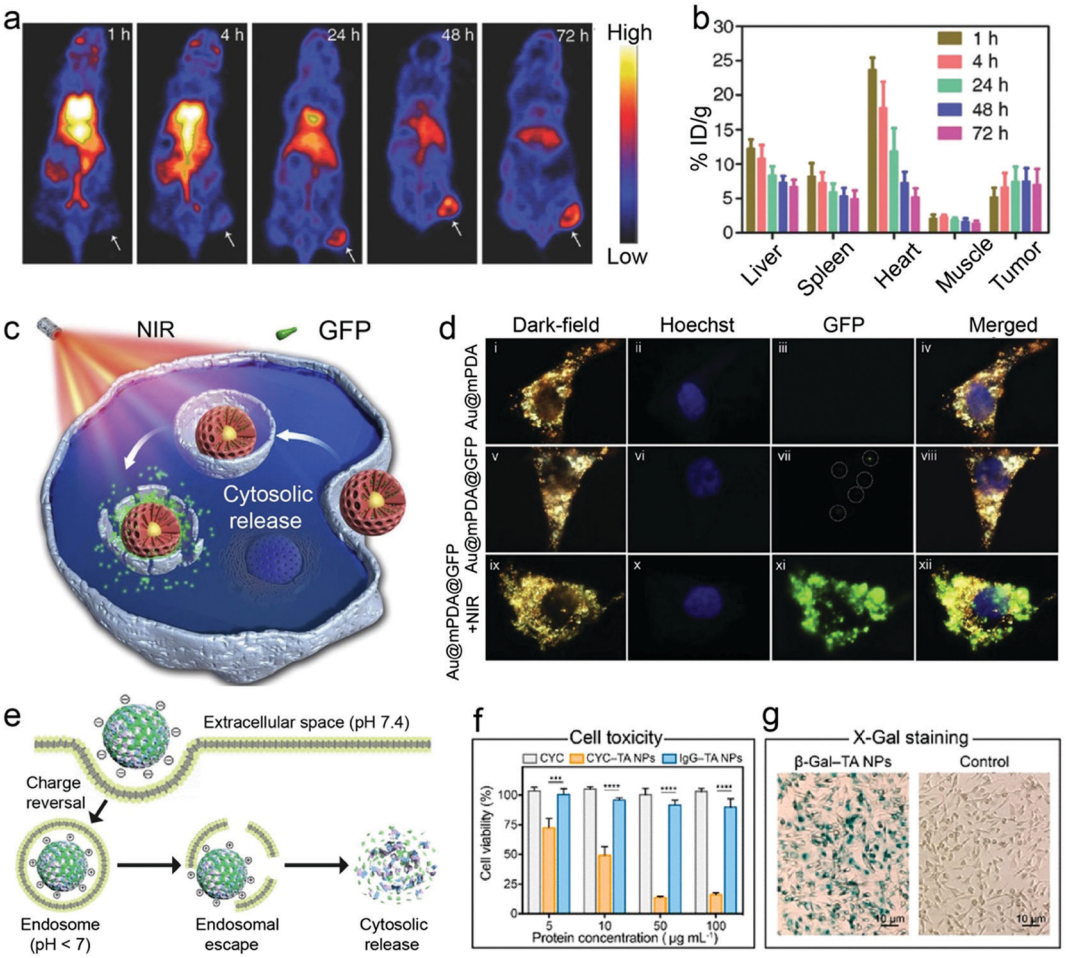

Fig. 25 Drug delivery performance by phenolic-based drug delivery systems. (a) Biodistribution study of ^{89}Zr-labelled phenolic drug delivery system. (b) Quantitative region of interest (ROI) of analysis of major organs and tumor at various time points. (a and b) Reproduced with permission. Copyright 2018, Wiley-VCH. (c) Schematic illustration of green fluorescent protein (GFP) delivery by Au@mPDA. (d) Intracellular GFP delivery enabled by Au@mPDA under NIR irradiation. (c and d) Reproduced with permission. Copyright 2020, Elsevier. (e) Schematic illustration of intracellular protein delivery from a protein–polyphenol nanoparticle. (f) Cell viability of cancers cells incubated in the presence of free anticancer drug (CYC), CYC–TA nanoparticles, or IgG–TA nanoparticles. (g) X-Gal staining of cancer cells treated with β-Gal–TA nanoparticles. (e–g) Reproduced with permission. Copyright 2020, American Chemical Society.

Traditional DNA/RNA delivery or gene transfection could be achieved *via* cationic polymers such as PEI.[379] Thus, the conjugation of cationic polymers with phenolic particles is a straightforward method to fabricate DNA/RNA carriers. The as-prepared carriers could be further modified with either secondary growth or integrated with functional cores making it a multifunctional delivery system. Park and co-workers fabricated PEI-conjugated magnetic nanoparticles with the aid of PDA and caffeic acid for gene delivery.[225] The nanocarrier was an efficient gene transfection tool and useful in cellular tracking by magnetic resonance and fluorescence imaging. Enhanced delivery with stimuli-responsive release could be accomplished *via* MOF-coated PDA nanoparticles.[380] The siRNA and MOF precursors were mixed and co-assembled onto the PDA surface. The siRNA chains would be released at endosomal conditions leading to genetic cytotoxicity.

In contrast, protein delivery and DNA/RNA delivery differ in some ways. Although proteins could be anchored with binding sites on the surface of phenolic materials through non-covalent interactions, or covalent binding in some cases,[232] protective delivery is more preferred. Thus, a growing library of phenolic particles with meso- or macro-pores, channels, and hollow structures have been developed. However, the pore size of these particles should be larger than those for small molecule drugs because of larger hydrodynamic size (usually >5 nm) of biomacromolecules. Duan and co-workers reported a mesoporous PDA with Au nanoparticle core as a multifunctional protein delivery system (Fig. 25c).[381] Mesochannels of *ca.* 30 nm were created with block copolymers as "soft-template" to protect the payload and offer a large loading capacity. Recombinant proteins with polyhistidine tags could be reversibly stored inside the channels through nickel ion chelation and were released upon near-infrared irradiation. This mesoporous PDA system allowed efficient loading and remote control of protein release (Fig. 25d). MPNs with large and ordered mesochannels of >20 nm were also developed for the high loading of various proteins with different shapes, charges, and sizes.[158] Due to the hydrogen bonding, electrostatic, and/or hydrophobic interactions, the MPN derived from phenolics (EGCG or gallic acid) showed high affinity towards high-molecular-weight proteins. In addition to the porous particles, co-assembly of various monomers into particle system could be used for protein delivery. Polyphenols exhibit multiple non-covalent interactions with proteins, which allow robust and responsive polyphenol–protein network. It was demonstrated that TA, gallic acid, and EGCG can co-deposit onto the substrate surface with more than ten proteins.[215] Importantly, the proteins retained their structure and bioactivity after encapsulation. The authors indicated that hydrogen bonding, hydrophobic interactions, and ionic interactions are three main driving forces in network assembly. The physicochemical properties of the proteins such as the isoelectric point markedly affect the final network.

The polyphenol–protein network nanoparticles are also capable of endosomal escape (Fig. 25e–g).[382] At acidic conditions, the network undergoes a surface charge reversal and subsequent disassembly in response to the intracellular glutathione for further protein therapy. Such phenolic-enabled strategies provide opportunities for the development of protein carriers and could offer intracellular protein delivery.

4.4.2 Photothermal therapy. PTT with minimal invasiveness and high spatiotemporal resolution has recently attracted attention in the field of cancer therapy.[383,384] PTAs can convert light energy into heat at a local site. Thus, some intriguing systems to transform heat into other signals have been developed such as photothermal-triggered drug delivery.[385] Due to the unique molecular structure, phenolic materials are good candidates for PTAs.

PDA particles inspired by melanin have been validated in PTT. Pure PDA particles provided a photothermal conversion efficiency of 40% (808 nm), which is sufficient for tumor PTT.[136] PDA has a wide absorption spectrum from ultraviolet to visible and even through the NIR light window. Lu and co-workers confirmed that exposure to 808 nm irradiation at 2 W cm^{-2} for 5 min after intratumoral injection of PDA nanoparticles significantly inhibited tumor growth and caused no damage.

In addition to melanin-like PDA, metal–phenol networks are surprisingly efficient at photothermal conversion and offer good photothermal stability. Chen and co-workers developed a nanosized metal–polyphenol framework composed of EA and Fe^{3+} for PTT.[335] The strong photothermal effect originated from the ligand to the metal charge transfer bond of which a broad band of absorbance in NIR window was observed. *In vivo* studies demonstrated moderate photothermal performance and negligible toxicity. Similarly, the MPNs assembled TA and transition metals including Fe(III), V(III), and Ru(III) – the product had high photothermal efficiency (40%). Feng and co-workers fabricated TA–Fe(III) network capsules *via* silica particle templates.[386] The particle size of TA–Fe(III) nanocapsules was 200 nm with varying thickness from 13 nm to 56 nm. To verify the importance of polyphenol groups in MPN for PTT, Chen and co-workers compared the fundamental physicochemical properties of different Fe(III)–phenol complexes.[344] The authors claimed that *ortho* diphenols and triphenols were key components of MPN complexes for high UV-vis-NIR absorbance, good photothermal performance, and photoacoustic imaging.[279] Phenols with mono-hydroxy groups fail to form stable complexes and thus could not be applied for PTT and PAI. Other polyphenol molecules such as EGCG have been utilized for PTT and showed comparable good performance.[387]

In addition to phenolic-based materials, there are also numerous excellent PTAs derived from metallic materials.[388] Thus, the combination of phenolic-based materials with other metal-based PTAs can improve the PTT effect. Thus far, many hybrid PTAs have been developed for PTT and photothermal-triggered bioregulation. For instance, phenolic material-coated plasmonic nanoparticles are a class of efficient PTAs. Various plasmonic materials (*e.g.*, Au, Ag, Cu) with different particle structures (*e.g.*, sphere, rod, star, ring, cube, bipyramid, sheet, *etc.*) could be modified with phenolic coating. The resulting hybrid particle system offered a more efficient photothermal conversion than either component alone. The absorbance spectrum verified that the hybrid particles showed higher light

absorption at the desired wavelength range. Magnetic particles and MOFs have also been shown to have positive contributions to PTT. These materials can improve the photothermal effect but also provide the potential for bioimaging and pH-responsive properties of each material, respectively.

Some hybrid PTAs with unique structures are worth highlighting. Compact plasmonic blackbody nanoparticles of hyperbranched Au structures coated with a PDA shell were developed by Duan and co-workers and showed extremely high photothermal conversion efficiency.[218] The efficiencies of AuPBs were determined to be 88.6% at 808 nm and 80.8% at 1064 nm, respectively. According to the experimental and simulation results, the superior photothermal conversion originated from higher absorption efficiency and smaller scattering cross-section of AuPBs. The small size and strong coupling of the closely spaced plasmonic branches with compact PDA coating leads to large amplification of the local electric fields, and thus strongly generating heat. Interestingly, the light spectra of AuPBs showed a broadband extinction giving comparable photothermal conversion at both the first and the second NIR bio-window.

Previous PTAs were mainly used to generate local hyperthermia for cancer cell inhibition. More recently, some well-designed PEN-based nanostructures were developed for various photo-triggered bioregulation on the basis energy conversion from heat into signals in other forms. The bioregulation together with PTT could perform synergistic therapy and improve the efficacy. A photothermal-triggered "nanobomb" delivery system was developed by incorporation of NH_4HCO_3 within the DOX@PDA particles reported by Liu and co-workers.[149] Under NIR irradiation, NH_4HCO_3 can be photothermally triggered to generate CO_2 and NH_3 gases and then facilitate the "bomb-like" release of DOX *in situ*. The NIR-induced hyperthermia and DOX molecules synergistically inhibit the tumor growth. Ping and co-workers fabricated a thermophilic enzyme-assisted nanoplatform composed of mesoporous PDA-coated AuNRs for enhanced PTT of deep tumors (Fig. 26a and b).[389] The thermophilic enzyme showed stronger digestive capability toward extracellular matrix at elevated temperatures and was loaded through non-covalent interactions inside the PDA mesopores. Upon NIR irradiation, the loaded enzyme can be spatiotemporally released and activated for on-demand

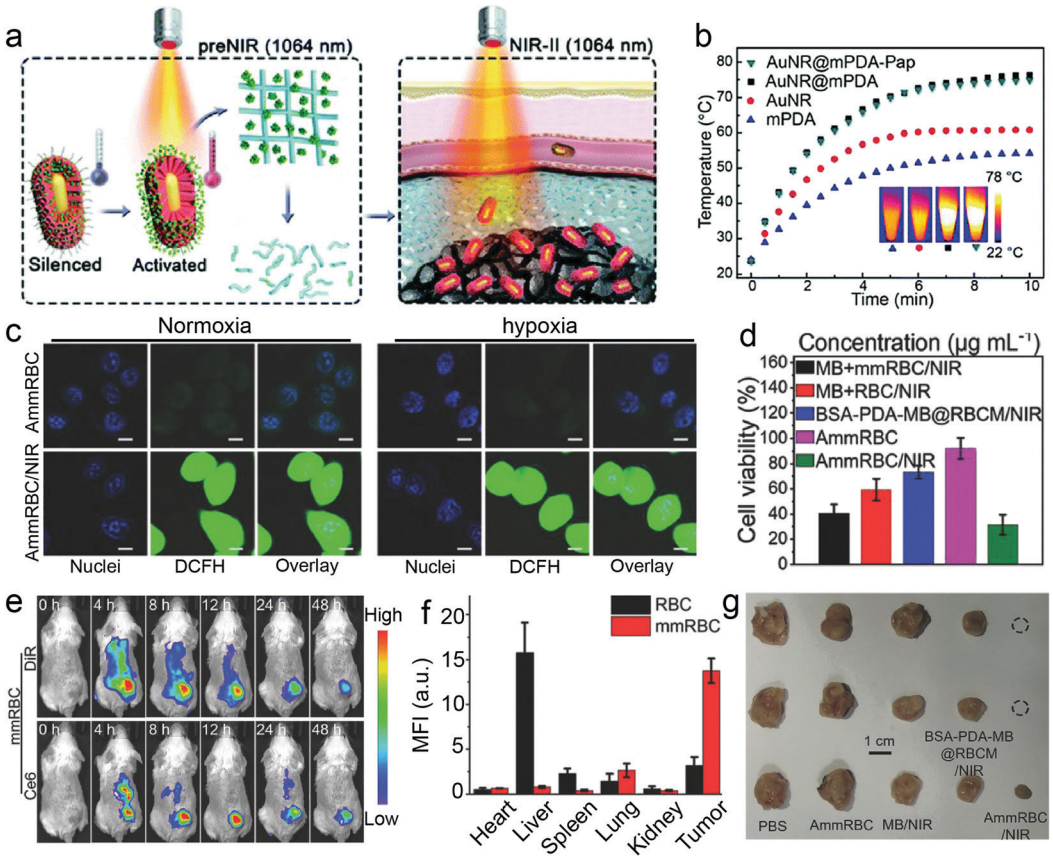

Fig. 26 PTT and PDT performance of phenolic-derivate particle systems. (a) Schematic illustration of NIR-triggered stromal depletion for enhanced tumor PTT. (b) Temperature increasing profiles of different PTAs under 1064 nm NIR-II irradiation. (a and b) Reproduced with permission. Copyright 2020, Royal Society of Chemistry. (c) *In vitro* 1O detection assay of 4T1 cells with different treatment in normoxia and hypoxia conditions. Scale bar: 10 μm. (d) Viability of 4T1 cells after various treatments under hypoxia. (e) *In vivo* fluorescence images of 4T1 tumor bearing mice with different treatments observed at various time points after intravenous injection. (f) The corresponding mean fluorescence intensity (MFI) values of tumor and major organs with different treatment harvested at 48 h post-injection. (g) Photos of the tumors harvested at day 20 post PDT treatments. (c–g) Reproduced with permission. Copyright 2019, Wiley-VCH.

stromal degradation, which induces deeper penetration of AuNRs for efficient PTT at deep-tissue levels.

Moreover, a growing library of therapeutic systems based on PTT and other combinational therapies have been developed for enhanced bioregulation and therapy. Functionalized Fe_3O_4@PDA systems with triphenylphosphonium have been developed to decrease the mitochondrial membrane potential for easier access of DOX to mitochondria.[390] Studies on PTT-integrated immunotherapy by preparing PDA-coated Au nanostars combined with a sub-therapeutic dose of DOX have been reported. The core–shell particles can elicit anti-tumor immune response, providing a possible strategy against metastatic tumors.[391]

Recently, non-metallic materials such as black phosphorous and graphene oxide have emerged as remarkable PTAs for PTT, but their relatively inert chemistry severely hinder their applications in biomedicine. The modification of phenolic materials could further improve their biocompatibility and enhance their PTT performance. For example, black phosphorous QDs could be coated with adhesive PDA, and the resulting core–shell particles exhibited excellent photothermal effect and photoacoustic features.[186] The as-prepared particle systems have great potential for cancer theranostics because of their biocompatibility and biodegradability. After surface coating of PDA, graphene oxide exhibited enhanced photothermal effect and good dispersibility in aqueous solution.[392] A similar phenomenon was also observed by Zhang and co-workers who reduced graphene oxide with a PDA coating to efficiently induce local hyperthermia for cancer cells inhibition.[393] Interestingly, the versatile chemistry of the PDA coating enabled further loading of metallic PTAs (Au nanostars) and chemotherapeutics (DOX). Such PDA-based platform provides a good potential for combined PTT by three kinds of PTAs.

There are three main strategies to improve PTT efficacy: first, to combine PTT with other therapies such as chemotherapy and immunotherapy. Second, to reduce the side effects that may occur during the PTT process such as hyperthermia-caused inflammation. Third, to deal with the intrinsic protections in the target cell such as expression of heat shock proteins. Therefore, PEN with a powerful integrating capability could be used to accomplish these combinational therapies. A combination of different functional motifs in one therapeutic system through PEN is a promising approach to fabricate multifunctional platforms for enhanced PTT.

4.4.3 Photodynamic therapy. PDT is a minimally invasive treatment method for tumor therapy with high specificity. It has gained tremendous attention over the past decade in both pre-clinical investigations and clinical practice.[394] Photosensitizer molecules absorb the external light irradiation at specific wavelengths and can convert the surrounding oxygen into cytotoxic singlet oxygen and ROS.[395] However, the PDT efficacy is often compromised due to less efficient delivery of the photosensitizer; there can be unexpected damage to normal cells. Thus, the phenolic-based materials have been used as a multifunctional platform for photosensitizer delivery and enhanced PDT.

Phenolic materials modified with targeting molecules and a protective shell could improve the accumulation of photosensitizer at the tumor site. A pH-responsive platform composed of PEG–MPN capsules modified with folic acid was developed for the delivery of haematophorphyrin monomethyl ether (HMME).[396] The delivery system showed higher accumulation in target cells *via* folic acid, and the HMME photosensitizer would be released at an acidic pH. With a 638 nm laser, the released HMME in the cytoplasm could generate lethal ROS and induce cell apoptosis demonstrating the applicability of phenolic-based delivery.

Due to the unique structure of the tumor vasculature, the oxygen surrounding the cells was quickly consumed leading to an oxygen shortage that limited ROS generation.[395] To avoid an oxygen shortage, functional motifs that supply oxygen could be incorporated. For example, Zhang and co-workers coated both platinum and a zirconium–porphyrin shell on PDA particle cores making the combined systems a nanofactory for enhanced PDT.[241] The platinum interlayer could catalyse the endogenous H_2O_2 to oxygen, and the outer zirconium–porphyrin shell could convert the oxygen into ROS. Mao and co-workers incorporated both platinum and ruthenium in PDA-based particle system for oxygen-sustained PDT where ruthenium complexes could produce ·OH through Fenton reaction.[397] Mesoporous manganese-based MOFs with PDA modification and Ce6 loading were proved to alleviate tumor hypoxia for PDT.[398] The MOFs acted as a nanoenzyme to catalyse the conversion of endogenous H_2O_2 to oxygen, and the Ce6 triggered the generation of ROS for PDT. Additionally, bioactive molecules such as enzymes could be co-delivered with photosensitizers as an oxygen supply. Zhang and co-workers created man-made red blood cells (RBCs) by encapsulating hemoglobin and methylene blue inside the RBC membrane coated-PDA vehicles (Fig. 26c–g).[147] The introduced PDA could prevent oxygen-carrying hemoglobin from degradation before accumulation at the tumor site. Upon NIR irradiation, this man-made pseudo-RBC permits an *in situ* oxygen supply to combat the hypoxia-mediated resistance of cancer cells to PDT. Both *in vitro* and *in vivo* studies demonstrated the superior tumor inhibition of the RBCs. A MOF-gated PDA nanoparticles for simultaneous delivery of catalase and methylene blue was also reported.[399] In acidic conditions, the cargo would be responsively released allowing oxygen-supplied PDT.

Recently, some studies have reported that increasing the ROS concentration in mitochondria could improve the therapeutic effect suggesting that mitochondria targeting could improve PDT performance. With the aid of phenolic carriers, mitochondria-targeting molecules were further modified with photosensitizer delivery systems. Triphenyl phosphonium (TPP), a mitochondria-targeting molecule, was conjugated with PDA-coated black phosphorus nanosheets *via* covalent interaction to improve the targeting efficiency.[400] Thus, the photosensitizer Ce6 could be delivered into mitochondria and generate ROS upon NIR irradiation, which remarkably enhanced cell killing efficiency. Wang and co-workers conjugated a targeting motif (indolium group) with a photosensitizer (tetraphenylethene)

achieving mitochondria targeting and ROS generation at the same time.[401]

To improve the photodynamic effects and therapeutic selectivity, phenolic-based materials are used to construct a multifunctional platform for imaging-guided therapy and combined therapy. Liu and co-workers developed a dopamine-mediated biomineralization method to construct $CaCO_3$–PDA hollow particles for multimodal imaging-guided PDT.[69] Due to the pH sensitivity of the hollow particles, the pre-loaded Ce6 could be released under reduced pH. More importantly, the release of photosensitizer was accompanied by fluorescence recovery, which was quenched by PDA at first. Mn could be attached for magnetic resonance imaging *via* the strong chelation of PDA to metal ions. Together with the photoacoustic property of PDA and the fluorescence of Ce6, this biomineralized particle system demonstrated a multimodal imaging-guided PDT.

In addition, a TiO_{2-x} theranostic PDA-based nanoplatform has been developed for biomodal imaging-guided triple therapy.[347] The titanium oxide–PDA core–shell nanoparticles permitted drug loading and fluorescent tags modification, which facilitated fluorescence imaging, photoacoustic tomography, and photodynamic/photothermal/chemotherapy. Many studies have investigated the combined therapy of PTT and PDT for tumor treatment where local hyperthermia and cytotoxic ROS/singlet oxygen synergistically inhibit tumor growth.[402–404] In these systems, phenolic materials offered functional integration, and their intrinsic good biocompatibility made them suitable components for various PDA agents.

4.4.4 Immunotherapy. Natural phenolics have been widely investigated for their pharmacological activities including immunomodulatory actions. Phenolic molecules such as curcumin, resveratrol, wogonin, EGCG, and other polyphenols have demonstrated high efficacy in inhibiting large tumor growth. Recently, many phenolic-engineered particles have been developed to engage with specific targets for immune system regulation.[405]

Phenolic-based particle systems could promote the maturation of dendritic cells (DCs) that play important roles in tumor pathology. Phenolic materials such as PDA particles can serve as vaccine vectors for enhanced immune response. Antigen-ovalbumin-coated PDA nanoparticles exhibited higher cellular uptake and accumulation at lymph nodes.[406] The upregulated expression of major histocompatibility complex and the activation of $CD8^+$ T cells were observed. Furthermore, after covalent conjugation with PDA nanoparticles, tumor cell lysate could be delivered in a very efficient manner.[407] Interestingly, the empty PDA nanoparticles could facilitate the maturation of DCs and delay the tumor growth making PDA an excellent material for immunotherapy. In contrast to surface loading, an encapsulation strategy enabled by depositing EGCG–Al(III) network layer onto the living cells was developed as vaccine carriers.[408] Thus, almost 100% of cell proteins could be entrapped within the particles providing highly efficient loading for antigen delivery. The EGCG–Al(III) could protect the antigens from degradation during circulation and improve cellular uptake. Modulated expression of a co-stimulation marker on DCs and up-regulation of key cytokines were observed. Similar particle systems for efficient loading for immunotherapy such as mesoporous PDA nanoparticles have also been reported. Cai and co-workers loaded R837, a toll-like receptor agonist, into mesoporous PDA and modified the particles with PVP.[409] The resulting delivery system showed higher targeting to the lymph node because of the enhanced lymphatic drainage ability of PVP. Further release of R837 at lymph nodes effectively activated DCs and led to a $CD8^+$ T-cell response. Yeo and co-workers focused their attention on sustained delivery of chemotherapeutic carfilzomib (CFZ) for safe and effective immunotherapy.[410] A supramolecular assembly of TA and Fe^{3+} supplemented with albumin coating was developed for CFZ entrapment. Upon intratumoral injection, the TA–Fe(III) MPN assemblies allowed for prolonged tumor retention of CFZ, enhancement of $CD8^+$ T cell population, and development of stronger tumor-specific immune responses.

Due to the presence of phenolic materials, PEN-based immunotherapy is often combined with PTT for improved therapy. Tumors may recur after PTT due to the presence of residual tumor located at untreated margins. Therefore, the combination of PTT and immunotherapy is an ideal strategy for complete tumor therapy and can use PEN. For instance, PDA-coated Al_2O_3 nanoparticles were developed for simultaneous PTT and delivery of CpG—an adjuvant to trigger immune response.[175] The authors emphasize that the delivery of CpG could contribute to the secretion of antibodies and cytokines as well as the immune cell proliferation, which distinctively prevented tumor recurrence after PTT. Core–shell PDA@MSN nanoparticles prepared as vehicles for immunomodulatory drug delivery have also been reported.[411] Due to the photothermal conversion of PDA cores, local hyperthermia could kill cancer cells and trigger drug release. This leads to synergistic photothermal immunotherapy.

Oh and co-workers modified PDA nanoparticles with anti-PDL1 (programmed cell death 1 ligand 1) antibody and loaded imiquimod into the PDA matrix (Fig. 27a–c).[375] The antibody tag increased the binding of nanoparticles to cancer cells overexpressing PDL1, which could enable greater photothermal effect against tumors. The presence of imiquimod efficiently promoted the activation of DCs and converted naïve T cells to cytotoxic T cells. The authors described the particle system as an in situ-assembled vaccine, which is promising for the treatment of tumors overexpressing PDL1. PDA nanoparticles again serve as a platform to assemble various functional blocks.

A similar combination of PTT and immunotherapy was also obtained with polyphenol-coated magnetic particle system.[412] A combination of even three therapies including PTT, immunotherapy, and chemotherapy was demonstrated in a PDA-based system.[413] In current delivery systems, phenolic materials are emerging as multifunctional drug delivery platform for immunotherapy. In the view of their natural anti-tumor and anti-inflammation effects, even more work with PEN-based immunotherapy is expected in the future.

4.4.5 Other therapies. PEN offers great potential for various other disease therapies. Inspired by traditional medicine or combined with other strategies, PEN provides a powerful toolkit in biomedicine. In this section, some emerging therapeutic methods using PEN-based particles will be introduced.

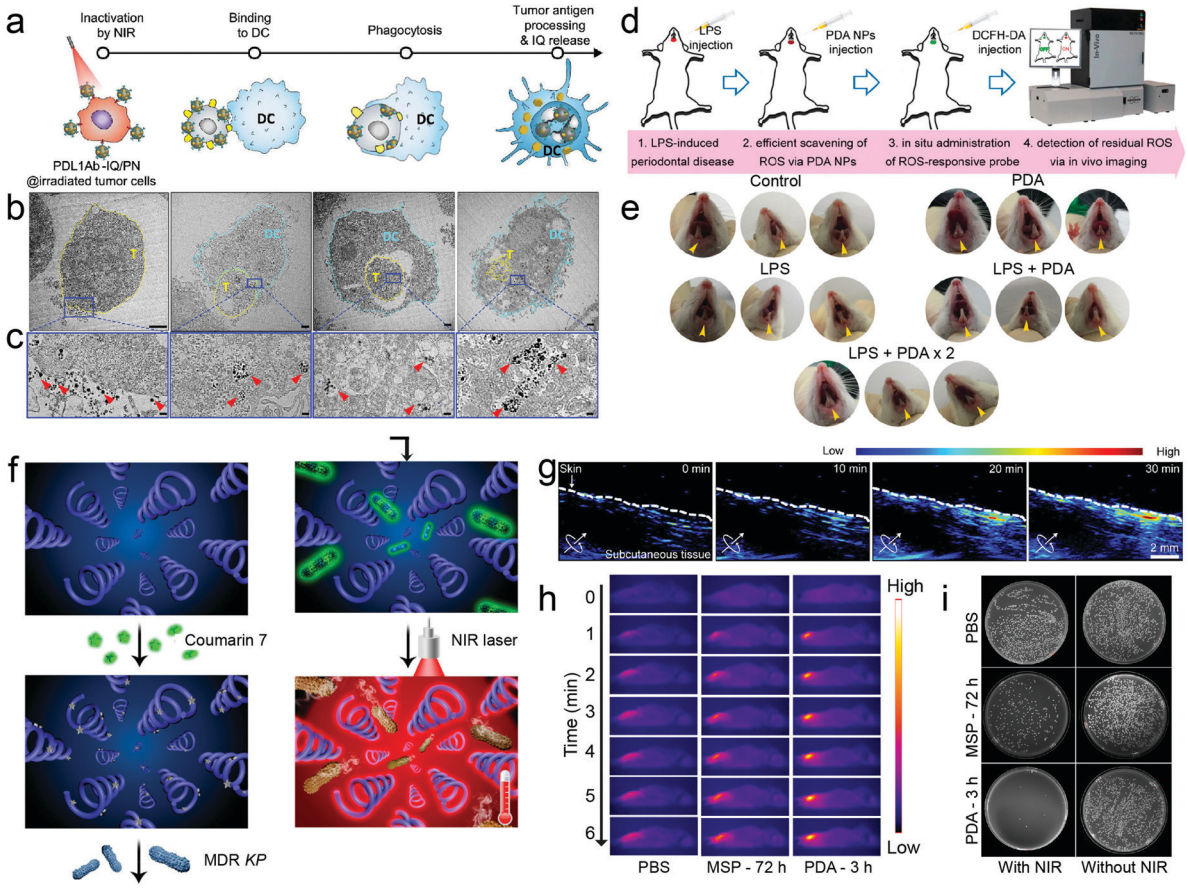

Fig. 27 Diseases therapy performance of PEN-derivate particle systems. (a) Schematic illustration of DC binding, phagocytosis, and digestion of tumor cells treated with PDL1-loaded PDA nanoparticles (PDL1Ab-IQ/PN) under NIR irradiation. (b) TEM images of the phagocytosis of tumor cells upon coculture with DCs. Scale bar: 2 μm. (c) Enlarged images of corresponding blue-lined box areas in (b). Scale bar: 200 nm. Reproduced with permission. Copyright 2019, American Chemical Society. (d) Schematic illustration of lipopolysaccharide (LPS)-induced periodontal disease and design of ROS scavenging. (e) Photographic images of Kunming mice 3 days after various treatments. (d and e) Reproduced with permission. Copyright 2018, American Chemical Society. (f) Schematic illustration of the protocol for a test including the grafting coumarin probe, bacterium (MDR *KP*) fluorescence detection, and photothermal treatment. (g) Time-lapse PA images captured at an interval of 10 min with an 808 nm NIR light. Scale bar: 2 mm. (h) Thermal images of the infection regions irradiated with 808 nm NIR irradiation. (i) Photographs of the *MDR KP* colonies on the plate count agar plates. (f–i) Reproduced with permission. Copyright 2020, American Chemical Society.

Phenolic materials are efficient ROS scavengers.[414,415] Abnormally elevated levels of ROS have been involved in the development of many diseases including cerebral ischemia, neuronic disorder, and inflammatory diseases.[416] The functional groups in phenolic materials can eliminate excessive and toxic ROS. PDA is a typical phenolic material used as a ROS scavenger. PDA nanoparticles have been reported to reduce 2,2-diphenyl-1-picrylhydrazyl suggesting the free-radical-scavenging property of PDA.[417] Liu and co-workers demonstrated that PDA nanoparticles displayed a significant anti-inflammation effects on acute inflammation-induced injury.[418] PDA nanoparticles remarkably reduced ROS level both *in vitro* and *in vivo*. Moreover, the potential of PDA nanoparticles for periodontal disease treatment was investigated.[419] A murine periodontitis model clearly demonstrated the feasibility of PDA nanoparticles as robust antioxidants to remove multiple ROS and decrease periodontal inflammation without any side effects (Fig. 27d and e). The antioxidative property of PDA was also proved in the treatment of diseases in central nervous system such as ischemic stroke.[420] PDA nanoparticles showed satisfactory anti-oxidative characterization against reactive oxygen and nitrogen species.

TA is also a well-known anti-oxidant that can scavenge ROS. With the aid of polymeric phenylboronate, TA could be assembled into nanogels showing strong anti-inflammatory effects. The assembly of TA with metal ions could be engineered into particles of different sizes and shape for specific uses.[421] TA–Cu(II) coordination nanosheets were prepared as a potent nanoenzymes for scavenging ROS from cigarette smoke by Wei and co-workers.[422] Thanks to the superoxide dismutase-like activity, catalase-like activity, and hydroxyl radical elimination capacity, the TA–Cu(II) nanosheets placed in a commercial filter allowed for remarkable ROS scavenging in smoke aerogel reducing the acute lung injury by smoking.

The versatile use of PEN provides potential in anti-bacterial applications by effective delivery of anti-bacterial materials or combined photo-triggered therapy. Upon irradiation, an

increased local temperature induced by photothermal conversion of phenolic materials could efficiently and quickly kill bacteria and pathogens. To improve the anti-bacterial performance of PTT, Fe_3O_4@PDA nanoparticles modified with an HSP inhibitor (2-phenylethynesulfonamide, PES) were fabricated to reduce the tolerance of bacterial to photothermal effect.[423] The PES ligands could be responsively released due to the weakened molecular interactions giving enhanced therapeutic performance. Messersmith and co-workers prepared bimetallic PDA-gapped nanorods with conjugation of anti-bacterial antibodies for combined photo-triggered therapy.[240] The hybrid nanorods featured high efficiency of photothermal conversion leading to both plasmonic heating and NIR-triggered release of Ag. The conjugation of antibodies and PEG polymers allowed the particles to have specific targeting to Gram-negative and Gram-positive bacteria. These effects could cooperatively contribute to the excellent cell killing. Integrating PTT with antibiotic drug delivery in one system was achieved with polyphenol-based nanosheets for antibiofilm activity.[43] The transition metal dichalcogenide nanosheets exfoliated by polyphenol have superior biostability and high loading capacity of antibiotic drugs (penicillin) for synergistic anti-bacterial treatment. Particles systems with unique structures such as microswimmers for pathogenic bacterial infection treatment were constructed by PDA coating on magnetized *Spirulina* matrix (Fig. 27f–i).[178] Under NIR irradiation, the microswimmers showed enhanced photothermal effect and photoacoustic features leading to trackable pathogenic treatment. The microswimmers could be accumulated at the site of interest upon application of magnetic actuation. The outstanding anti-bacterial performance of PEN-based particle systems demonstrates their wide range of cell killing from cancer cells to bacteria.

Along with a deeper investigation into materials science, novel particle systems engineered by PEN have been developed to meet the requirements of an everchanging biomedical field. On the one hand, the intrinsic properties of phenolics allow for the direct uses of phenolic-based materials for specific disease therapy. On the other hand, the versatile chemistry and integrating capability of phenolics provides a platform to impart a variety of functional motifs into a single system for multifunctional applications.

PEN-based particle systems have also aroused interest in other areas of biomedicine. For example, ionic liquids-loaded hollow PDA particles could be used for microwave thermal therapy.[424,425] Under microwave power irradiation, the ionic liquids could convert microwave energy into local heat for tumor ablation suggesting a different remote-triggered thermal therapy. Radionuclides such as ^{99m}Tc and ^{131}I could be loaded inside the PDA particles for radioisotope therapy.[363] Liu and co-workers used PDA nanoparticles as an efficient carrier for simultaneous delivery of radionuclides and DOX. In addition to the combined radioisotope therapy and chemotherapy, single-photon emission computed tomography can track the therapeutic delivery in real-time. PDA-coated silica nanoparticles were also investigated for rapid hemostasis.[426] The authors indicated that the highly porous network structure with a variety of functional groups of PDA surface could facilitate cell aggregation and clotting. Importantly, low exothermic effects and antimicrobial properties were observed together with a remarkably reduced blood loss. After lipid coating, the intracellular uptake of PDA nanoparticles in neuronal cells could be observed. A recent study reported that PDA nanoparticles could serve as neuroprotective agents and a PTA for intracellular neuron stimulation.[427] Under NIR laser irradiation, the temperature increase induced by PDA caused a Ca^{2+} influx paving a new way for neuronal regulation.

5. Conclusion and outlook

Phenolic compounds have shown great potential in nanotechnology especially for the design of multifunctional nanosystems. This work builds on the excellent summaries of phenolic-based hydrogels or monolithic coatings already published. Here, we overviewed the development of multifunctional nanosystems (*e.g.*, core–shell nanoparticles, mesoporous nanoparticles, Janus nanoparticles, *etc.*) that are engineered by phenolic compounds *via* covalent bonds or supramolecular interactions with various building blocks (*e.g.*, small molecules, DNA, peptides, protein, metal, semiconductors, *etc.*). Along with the biocompatibility of the phenolics, the unique physicochemical properties of these nanosystems can further dictate their functionality in biomedicine. Extensive achievements have been made in the research community but a better understanding of the complex material–material interactions (*i.e.*, between phenolics and other diverse building blocks) and their complex bio–nano interactions (*e.g.*, between PEN nanoparticles and distinct biological environment) is still needed. Listed below are future research opportunities.

(a) A deeper understanding of the formation mechanisms for phenolic-based assemblies including their kinetics and dynamics (*e.g.*, polymerization, metal coordination, *etc.*) is needed. For example, although the proposed molecular mechanism for dopamine polymerization is well accepted and can explain most PDA systems, a more complete understanding of the mechanism can facilitate the manipulation of PEN in a controlled manner. Furthermore, tuning the ratio of covalent bonds and supramolecular interactions with PDA may give more opportunities for morphology control and the final optical properties of the final products. A clear view of chemical formation would also help to modulate the biodegradability of phenolic-based nanoparticles.

(b) The interactions between phenolics and other chemical building blocks should be identified. The scientific community typically considers such interactions empirical; however, a holistic view at the molecular level is lacking. Computational modelling could provide more insight on the underlying mechanisms which could expand the capability of PEN-based materials.

(c) Work should be done to modulate the morphology of phenolic-based particle systems beyond conventional nanostructures. Taking advantage of wet-chemical synthesis as well as the regioselective activity and molecular rigidness of phenolics, anisotropic particles (*e.g.*, rod-like, ring-like nanostructures) may demonstrate even greater robustness in nanomedicine.

(d) Therapeutics based on phenolics other than dopamine and TA should be developed. The intrinsic chemical versatility

of phenolics allows for secondary conjugation *via* organic chemistry thus creating diverse candidates for complex applications. For example, the design of new synthetic phenolics with specific functional groups or moieties (*e.g.*, a fluorescent tag) could significantly improve their versatility. Other materials (*e.g.*, carbon materials) can also be derived from phenolic materials extending the potential of phenolic-based materials.

(e) Scalability and reproducibility should be improved. High quality and throughput are bottlenecks to nanomaterial development and other techniques such as microfluidics and electrospray could solve this problem. New methodologies will make phenolic-based nanoparticles more accessible for practical use.

(f) Although PEN has created many nanoparticles for biomedicine, the details of the pharmacokinetics, biocompatibility, and biodegradability still need considerable investigation even though some phenolics are FDA-approved (*e.g.*, TA, EGCG). The safety of phenolic-based nanomaterials (*e.g.* long-term toxicity) should be further studied.

Although many researchers have developed and applied phenolic-based materials in the past decades, there are still significant advances that could be made for promising biomedical applications. We envision that the concerted efforts of researchers in nanotechnology, organic chemistry, and medicine will deliver higher controllability of phenolic-based nanoparticles that expand their applications in biomedicine and beyond.

Conflicts of interest

There are no conflicts to declare.

Acknowledgements

This work was supported by National Natural Science Foundation of China (81630098, 82003666), and China Postdoctoral Science Foundation (2020M671773, 2020TQ0266). J. V. J. acknowledges NIH funding under mechanism DP2 HL137187, DP2 HL137187-S1, and R21 DE029917 as well as NSF funding under award 1845683. M. N. C. acknowledges fellowship support from NIH under award T32 CA153915. P. B. M. acknowledges support from NIH under awards R37 DE014193 and R01 EB022031.

Notes and references

1 L. Bravo, *Nutr. Rev.*, 1998, **56**, 317–333.
2 S. Quideau, D. Deffieux, C. Douat-Casassus and L. Pouysegu, *Angew. Chem., Int. Ed.*, 2011, **50**, 586–621.
3 Y. Liu, K. Ai and L. Lu, *Chem. Rev.*, 2014, **114**, 5057–5115.
4 L. R. He, C. D. Mu, J. B. Shi, Q. A. Zhang, B. Shi and W. Lin, *Int. J. Biol. Macromol.*, 2011, **48**, 354–359.
5 J. H. Waite and M. L. Tanzer, *Science*, 1981, **212**, 1038–1040.
6 H. Lee, N. F. Scherer and P. B. Messersmith, *Proc. Natl. Acad. Sci. U. S. A.*, 2006, **103**, 12999.
7 J. Yu, W. Wei, E. Danner, R. K. Ashley, J. N. Israelachvili and J. H. Waite, *Nat. Chem. Biol.*, 2011, **7**, 588–590.
8 G. P. Maier, M. V. Rapp, J. H. Waite, J. N. Israelachvili and A. Butler, *Science*, 2015, **349**, 628–632.
9 Y. Li, M. Qin, Y. Li, Y. Cao and W. Wang, *Langmuir*, 2014, **30**, 4358–4366.
10 Y. Li, T. Wang, L. Xia, L. Wang, M. Qin, Y. Li, W. Wang and Y. Cao, *J. Mater. Chem. B*, 2017, **5**, 4416–4420.
11 Y. Li, J. Cheng, P. Delparastan, H. Wang, S. Sigg, K. G. DeFrates, Y. Cao and P. B. Messersmith, *Nat. Commun.*, 2020, **11**, 1–8.
12 B. P. Lee, P. B. Messersmith, J. N. Israelachvili and J. H. Waite, *Annu. Rev. Mater. Res.*, 2011, **41**, 99–132.
13 H. Lee, S. M. Dellatore, W. M. Miller and P. B. Messersmith, *Science*, 2007, **318**, 426–430.
14 J. H. Ryu, P. B. Messersmith and H. Lee, *ACS Appl. Mater. Interfaces*, 2018, **10**, 7523–7540.
15 Q. Ye, F. Zhou and W. M. Liu, *Chem. Soc. Rev.*, 2011, **40**, 4244–4258.
16 H. Ejima, J. J. Richardson, K. Liang, J. P. Best, M. P. Van Koeverden, G. K. Such, J. Cui and F. Caruso, *Science*, 2013, **341**, 154–157.
17 M. A. Rahim, S. L. Kristufek, S. Pan, J. J. Richardson and F. Caruso, *Angew. Chem., Int. Ed.*, 2019, **58**, 1904–1927.
18 J. Zhou, Z. Lin, Y. Ju, M. Rahim, J. Richardson and F. Caruso, *Acc. Chem. Res.*, 2020, **53**, 1269–1278.
19 W. Fan, B. Yung, P. Huang and X. Chen, *Chem. Rev.*, 2017, **117**, 13566–13638.
20 Q. Hu, H. Li, L. Wang, H. Gu and C. Fan, *Chem. Rev.*, 2019, **119**, 6459–6506.
21 C. Zhang, B. Wu, Y. Zhou, F. Zhou, W. Liu and Z. Wang, *Chem. Soc. Rev.*, 2020, **49**, 3605–3637.
22 H. A. Lee, Y. Ma, F. Zhou, S. Hong and H. Lee, *Acc. Chem. Res.*, 2019, **52**, 704–713.
23 W. Cheng, X. Zeng, H. Chen, Z. Li, W. Zeng, L. Mei and Y. Zhao, *ACS Nano*, 2019, **13**, 8537–8565.
24 G. Chen, J. Seo, C. Yang and P. N. Prasad, *Chem. Soc. Rev.*, 2013, **42**, 8304–8338.
25 J. A. Jackman, D. Cho, J. Lee, J. Chen, F. Besenbacher, D. A. Bonnell, M. C. Hersam, P. S. Weiss and N. Cho, *ACS Nano*, 2016, **10**, 5595–5599.
26 J. Guo, Y. Ping, H. Ejima, K. Alt, M. Meissner, J. J. Richardson, Y. Yan, K. Peter, D. von Elverfeldt, C. E. Hagemeyer and F. Caruso, *Angew. Chem., Int. Ed.*, 2014, **53**, 5546–5551.
27 M. A. Rahim, K. Kempe, M. Mullner, H. Ejima, Y. Ju, M. P. Van Koeverden, T. Suma, J. A. Braunger, M. G. Leeming, B. F. Abrahams and F. Caruso, *Chem. Mater.*, 2015, **27**, 5825–5832.
28 J. Chen, S. Pan, J. Zhou, Q. Zhong, Y. Qu, J. J. Richardson and F. Caruso, *Chem. Mater.*, 2020, **32**, 6975–6982.
29 M. Salomaki, L. Marttila, H. Kivela, T. Ouvinen and J. Lukkari, *J. Phys. Chem. B*, 2018, **122**, 6314–6327.
30 C. Zhang, Y. Ou, W. X. Lei, L. S. Wan, J. Ji and Z. K. Xu, *Angew. Chem., Int. Ed.*, 2016, **55**, 3054–3057.
31 H. Lee, W. I. Kim, W. Youn, T. Park, S. Lee, T. S. Kim, J. F. Mano and I. S. Choi, *Adv. Mater.*, 2018, **30**, 1805091.
32 H. B. Na, G. Palui, J. T. Rosenberg, X. Ji, S. C. Grant and H. Mattoussi, *ACS Nano*, 2012, **6**, 389–399.

33 C. Xu, K. Xu, H. Gu, R. Zheng, H. Liu, X. Zhang, Z. Guo and B. Xu, *J. Am. Chem. Soc.*, 2004, **126**, 9938–9939.
34 D. Ling, W. Park, Y. I. Park, N. Lee, F. Li, C. Song, S. G. Yang, S. H. Choi, K. Na and T. Hyeon, *Angew. Chem., Int. Ed.*, 2011, **50**, 11360–11365.
35 W. Tang, G. M. Policastro, G. Hua, K. Guo, J. J. Zhou, C. Wesdemiotis, G. L. Doll and M. L. Becker, *J. Am. Chem. Soc.*, 2014, **136**, 16357–16367.
36 J. Li, C. Sun, P. An, X. Liu, R. Don, J. Sun, X. Zhang, Y. Xie, C. Qin, W. Zheng, H. Zhang and X. Jiang, *J. Am. Chem. Soc.*, 2019, **141**, 8816–8824.
37 A. M. Chiorcea-Paquim, T. A. Enache, E. D. Gil and A. M. Oliveira-Brett, *Compr. Rev. Food Sci. Food Saf.*, 2020, **19**, 1680–1726.
38 S. Du, Y. Luo, Z. Liao, W. Zhang, X. Li, T. Liang, F. Zuo and K. Ding, *J. Colloid Interface Sci.*, 2018, **523**, 27–34.
39 T. Zeng, X. L. Zhang, Y. Y. Guo, H. Y. Niu and Y. Q. Cai, *J. Mater. Chem. A*, 2014, **2**, 14807–14811.
40 J. Song, B. Duan, C. Wang, J. Zhou, L. Pu, Z. Fang, P. Wang, T. T. Lim and H. Duan, *J. Am. Chem. Soc.*, 2014, **136**, 6838–6841.
41 G. Fichman, L. Adler-Abramovich, S. Manohar, I. Mironi-Harpaz, T. Guterman, D. Seliktar, P. B. Messersmith and E. Gazit, *ACS Nano*, 2014, **8**, 7220–7228.
42 W. Wei, L. Petrone, Y. P. Tan, H. Cai, J. N. Israelachvili, A. Miserez and J. H. Waite, *Adv. Funct. Mater.*, 2016, **26**, 3496–3507.
43 C. Zhang, D. Hu, J. Xu, M. Ma, H. Xing, K. Yao, J. Ji and Z. Xu, *ACS Nano*, 2018, **12**, 12347–12356.
44 C. Wang, J. Bai, Y. Liu, X. Jia and X. Jiang, *ACS Biomater. Sci. Eng.*, 2016, **2**, 2011–2017.
45 A. Calzolari, A. Ruini and A. Catellani, *J. Phys. Chem. C*, 2012, **116**, 17158–17163.
46 M. Bloemen, D. Debruyne, P. J. Demeyer, K. Clays, A. Gils, N. Geukens, C. Bartic and T. Verbiest, *RSC Adv.*, 2014, **4**, 10208–10211.
47 Y. Lee, H. Lee, P. B. Messersmith and T. G. Park, *Macromol. Rapid Commun.*, 2010, **31**, 2109–2114.
48 I. L. Medintz, M. H. Stewart, S. A. Trammell, K. Susumu, J. B. Delehanty, B. C. Mei, J. S. Melinger, J. B. Blanco-Canosa, P. E. Dawson and H. Mattoussi, *Nat. Mater.*, 2010, **9**, 676–684.
49 T. Debnath, D. Sebastian, S. Maiti and H. N. Ghosh, *Chem. – Eur. J.*, 2017, **23**, 7306–7314.
50 F. Liu, X. He, Z. Lei, L. Liu, J. Zhang, H. You, H. Zhang and Z. Wang, *Adv. Healthcare Mater.*, 2015, **4**, 559–568.
51 Y. Han, L. Shen, Z. Li and Z. Liu, *Anal. Methods*, 2018, **10**, 3933–3938.
52 H. Gao, Y. Sun, J. Zhou, R. Xu and H. Duan, *ACS Appl. Mater. Interfaces*, 2013, **5**, 425–432.
53 Y. Liu, F. Chen, W. Ye, M. Zeng, N. Han, F. Zhao, X. Wang and Y. Li, *Adv. Funct. Mater.*, 2017, **27**, 1606034.
54 Y. Lei, Z. Tang, R. Liao and B. Guo, *Green Chem.*, 2011, **13**, 1655–1658.
55 Q. Huang, L. Hao, J. Xie, T. Gong, J. Liao and Y. Lin, *ACS Appl. Mater. Interfaces*, 2015, **7**, 20893–20901.
56 D. H. Lin and B. S. Xing, *Environ. Sci. Technol.*, 2008, **42**, 5917–5923.
57 D. H. Lin and B. S. Xing, *Environ. Sci. Technol.*, 2008, **42**, 7254–7259.
58 F. Liu, J. Fan, S. Wang and G. Ma, *Chem. Eng. J.*, 2013, **219**, 450–458.
59 S. A. Mian, L. M. Yang, L. C. Saha, E. Ahmed, M. Ajmal and E. Ganz, *Langmuir*, 2014, **30**, 6906–6914.
60 L. Zhang, J. Wu, Y. Wang, Y. Long, N. Zhao and J. Xu, *J. Am. Chem. Soc.*, 2012, **134**, 9879–9881.
61 R. Liu, S. M. Mahurin, C. Li, R. R. Unocic, J. C. Idrobo, H. J. Gao, S. J. Pennycook and S. Dai, *Angew. Chem., Int. Ed.*, 2011, **50**, 6799–6802.
62 J. Zhou, P. Wang, C. Wang, Y. Goh, Z. Fang, P. B. Messersmith and H. Duan, *ACS Nano*, 2015, **9**, 6951–6960.
63 T. Zhao, X. Zhu, C. Hung, P. Wang, A. Elzatahry, A. A. Al-Khalaf, W. Hozzein, F. Zhang, X. Li and D. Zhao, *J. Am. Chem. Soc.*, 2018, **140**, 10009–10015.
64 X. Zheng, J. Zhang, J. Wang, X. Q. Qi, J. M. Rosenholm and K. Cai, *J. Phys. Chem. C*, 2015, **119**, 24512–24521.
65 Z. Gao and I. Zharov, *Chem. Mater.*, 2014, **26**, 2030–2037.
66 Y. Zhang, Y. He, C. X. Shi, M. D. Sun, C. Yang, H. J. Li, F. M. Chen, Z. M. Chang, X. Zheng, Z. Wang, W. F. Dong, J. J. She and D. Shao, *ACS Sustainable Chem. Eng.*, 2020, **8**, 1695–1702.
67 J. Luo, G. Panzarasa, A. Osypova, F. Sorin, F. Spano, R. M. Rossi, A. Sadeghpour and L. F. Boesel, *Chem. Mater.*, 2019, **31**, 3192–3200.
68 X. Zheng, F. Chen, J. Zhang and K. Cai, *J. Mater. Chem. B*, 2016, **4**, 2435–2443.
69 Z. Dong, L. Feng, Y. Hao, M. Chen, M. Gao, Y. Chao, H. Zhao, W. Zhu, J. Liu, C. Liang, Q. Zhang and Z. Liu, *J. Am. Chem. Soc.*, 2018, **140**, 2165–2178.
70 Z. Ouyang, T. Tan, C. Liu, J. Duan, W. Wang, X. Guo, Q. Zhang, Z. Li, Q. Huang, P. Dou and T. Liu, *Biomaterials*, 2019, **205**, 50–63.
71 W. O. Yah, H. Xu, H. Soejima, W. Ma, Y. Lvov and A. Takahara, *J. Am. Chem. Soc.*, 2012, **134**, 12134–12137.
72 L. Han, X. Lu, K. Liu, K. Wang, L. Fang, L. Weng, H. Zhang, Y. Tang, F. Ren, C. Zhao, G. Sun, R. Liang and Z. Li, *ACS Nano*, 2017, **11**, 2561–2574.
73 G. San Lee, T. Yun, H. Kim, I. H. Kim, J. Choi, S. H. Lee, H. J. Lee, H. S. Hwang, J. G. Kim, D. W. Kim, H. M. Lee, C. M. Koo and S. O. Kim, *ACS Nano*, 2020, **14**, 11722–11732.
74 H. Huang, J. Cui, G. Liu, R. Bi and L. Zhang, *ACS Nano*, 2019, **13**, 3448–3456.
75 J. Necas, L. Bartosikova, P. Brauner and J. Kolar, *Vet. Med.*, 2008, **53**, 397–411.
76 H. Jiang, Q. Xia, D. Liu and K. Ling, *Anal. Chim. Acta*, 2020, **1121**, 1–10.
77 X. Zeng, M. Luo, G. Liu, X. Wang, W. Tao, Y. Lin, X. Ji, L. Nie and L. Mei, *Adv. Sci.*, 2018, **5**, 1800510.
78 J. Liu, L. Jin, Y. Wang, X. Ding, S. Zhang, S. Song, D. Wang and H. Zhang, *Small*, 2018, **14**, 1702431.
79 L. Zhang, Q. Wang, R. K. Jian and D. Y. Wang, *J. Mater. Chem. A*, 2020, **8**, 2529–2538.

80 L. Q. Xu, K. G. Neoh and E. T. Kang, *Prog. Polym. Sci.*, 2018, **87**, 165–196.
81 Z. Wang, H. Yang, F. He, S. Peng, Y. Li, L. Shao and S. Darling, *Matter*, 2019, **1**, 115–155.
82 J. Fu, Z. Chen, M. Wang, S. Liu, J. Zhang, J. Zhang, R. Han and Q. Xu, *Chem. Eng. J.*, 2015, **259**, 53–61.
83 Z. Dong, D. Wang, X. Liu, X. Pei, L. Chen and J. Jin, *J. Mater. Chem. A*, 2014, **2**, 5034–5040.
84 Z. Dong, H. Gong, M. Gao, W. Zhu, X. Sun, L. Feng, T. Fu, Y. Li and Z. Liu, *Theranostics*, 2016, **6**, 1031–1042.
85 H. Wu, H. Hu, J. Wan, Y. Li, Y. Wu, Y. Tang, C. Xiao, H. B. Xu, X. Yang and Z. Li, *Chem. Eng. J.*, 2018, **349**, 129–145.
86 D. Zhang, M. Wu, Y. Zeng, L. Wu, Q. Wang, X. Han, X. Liu and J. Liu, *ACS Appl. Mater. Interfaces*, 2015, **7**, 8176–8187.
87 Z. Wang, S. Ji, F. He, M. Cao, S. Peng and Y. Li, *J. Mater. Chem. A*, 2018, **6**, 3391–3396.
88 S. Hong, Y. Wang, S. Park and H. Lee, *Sci. Adv.*, 2018, **4**, eaat7457.
89 Q. A. Besford, Y. Ju, T. Wang, G. Yun, P. Cherepanov, C. E. Hagemeyer, F. Cavalieri and F. Caruso, *Small*, 2018, **14**, 1802342.
90 W. Shim, C. E. Kim, M. Lee, S. H. Lee, J. Park, M. Do, J. Yang and H. Lee, *J. Controlled Release*, 2019, **307**, 413–422.
91 K. Kim, M. Shin, M. Y. Koh, J. H. Ryu, M. S. Lee, S. Hong and H. Lee, *Adv. Funct. Mater.*, 2015, **25**, 2402–2410.
92 Y. Chen, L. Peng, T. Liu, Y. Wang, S. Shi and H. Wang, *ACS Appl. Mater. Interfaces*, 2016, **8**, 27199–27206.
93 D. Lee, H. Hwang, J. S. Kim, J. Park, D. Youn, D. Kim, J. Hahn, M. Seo and H. Lee, *ACS Appl. Mater. Interfaces*, 2020, **12**, 20933–20941.
94 V. Kozlovskaya, E. Kharlampieva, I. Drachuk, D. Cheng and V. V. Tsukruk, *Soft Matter*, 2010, **6**, 3596–3608.
95 Y. Takemoto, H. Ajiro and M. Akashi, *Langmuir*, 2015, **31**, 6863–6869.
96 H. Lomas, A. P. R. Johnston, G. K. Such, Z. Y. Zhu, K. Liang, M. P. van Koeverden, S. Alongkornchotikul and F. Caruso, *Small*, 2011, **7**, 2109–2119.
97 T. Shutava, M. Prouty, D. Kommireddy and Y. Lvov, *Macromolecules*, 2005, **38**, 2850–2858.
98 M. Ocwieja, Z. Adamczyk and M. Morga, *J. Colloid Interface Sci.*, 2015, **438**, 249–258.
99 V. Ball, *RSC Adv.*, 2015, **5**, 55920–55925.
100 P. Ren, H. Yang, H. Liang, X. Xu, L. Wan and Z. Xu, *Langmuir*, 2015, **31**, 5851–5858.
101 S. Chen, Y. Xie, T. Xiao, W. Zhao, J. Li and C. Zhao, *Chem. Eng. J.*, 2018, **337**, 122–132.
102 Z. Wang, S. Zhao, R. Song, W. Zhang, S. Zhang and J. Li, *Sci. Rep.*, 2017, **7**, 9664.
103 Y. Wang, E. J. Jeon, J. Lee, H. Hwang, S. W. Cho and H. Lee, *Adv. Mater.*, 2020, **32**, 2002118.
104 L. Bai, Y. Lim, J. Zhou, L. Liang and H. Duan, *Langmuir*, 2019, **35**, 9878–9884.
105 J. J. Zhou, Z. X. Lin, M. Penna, S. J. Pan, Y. Ju, S. Y. Li, Y. Y. Han, J. Q. Chen, G. Lin, J. J. Richardson, I. Yarovsky and F. Caruso, *Nat. Commun.*, 2020, **11**, 4804.
106 J. M. Mcrae and J. A. Kennedy, *Molecules*, 2011, **16**, 2348–2364.
107 A. Barrett, T. Ndou, C. A. Hughey, C. Straut, A. Howell, Z. Dai and G. Kaletunc, *J. Agric. Food Chem.*, 2013, **61**, 1477–1486.
108 J. E. Chung, S. Tan, S. J. Gao, N. Yongvongsoontorn, S. H. Kim, J. H. Lee, H. S. Choi, H. Yano, L. Zhuo, M. Kurisawa and J. Y. Ying, *Nat. Nanotechnol.*, 2014, **9**, 907–912.
109 J. P. Vanburen and W. B. Robinson, *J. Agric. Food Chem.*, 1969, **17**, 772–777.
110 A. Shukla, J. C. Fang, S. Puranam, F. R. Jensen and P. T. Hammond, *Adv. Mater.*, 2012, **24**, 492–496.
111 J. C. Isenburg, D. T. Simionescu and N. R. Vyavahare, *Biomaterials*, 2004, **25**, 3293–3302.
112 Y. Han, Z. Lin, J. Zhou, G. Yun, R. Guo, J. J. Richardson and F. Caruso, *Angew. Chem., Int. Ed.*, 2020, **59**, 15618–15625.
113 H. O. Ham, Z. Liu, K. H. A. Lau, H. Lee and P. B. Messersmith, *Angew. Chem., Int. Ed.*, 2011, **50**, 732–736.
114 G. Loget, J. B. Wood, K. Cho, A. R. Halpern and R. M. Corn, *Anal. Chem.*, 2013, **85**, 9991–9995.
115 C. Wang, J. Zhou, P. Wang, W. He and H. Duan, *Bioconjugate Chem.*, 2016, **27**, 815–823.
116 C. K. K. Choi, J. Li, K. Wei, Y. J. Xu, L. W. C. Ho, M. Zhu, K. K. W. To, C. H. J. Choi and L. Bian, *J. Am. Chem. Soc.*, 2015, **137**, 7337–7346.
117 P. Winterwerber, S. Harvey, D. Y. W. Ng and T. Weil, *Angew. Chem., Int. Ed.*, 2020, **59**, 6144–6149.
118 M. Shin, J. H. Ryu, J. P. Park, K. Kim, J. W. Yang and H. Lee, *Adv. Funct. Mater.*, 2015, **25**, 1270–1278.
119 Y. Tokura, S. Harvey, C. Chen, Y. Z. Wu, D. Y. W. Ng and T. Weil, *Angew. Chem., Int. Ed.*, 2018, **57**, 1587–1591.
120 N. Li, X. Yang, W. Liu, G. Xi, M. Wang, B. Liang, Z. P. Ma, Y. Feng, H. Chen and C. Shi, *Macromol. Biosci.*, 2018, **18**, 1800209.
121 A. I. Neto, A. C. Cibrao, C. R. Correia, R. R. Carvalho, G. M. Luz, G. G. Ferrer, G. Botelho, C. Picart, N. M. Alves and J. F. Mano, *Small*, 2014, **10**, 2459–2469.
122 A. D. Dwivedi, N. D. Sanandiya, J. P. Singh, S. M. Husnain, K. H. Chae, D. S. Hwang and Y. S. Chang, *ACS Sustainable Chem. Eng.*, 2017, **5**, 518–528.
123 K. Sawamura, Y. Tobimatsu, H. Kamitakahara and T. Takano, *ACS Sustainable Chem. Eng.*, 2017, **5**, 5424–5431.
124 Q. Zhong, J. J. Richardson, S. Li, W. Zhang, Y. Ju, J. Li, S. Pan, J. Chen and F. Caruso, *Angew. Chem., Int. Ed.*, 2020, **59**, 1711–1717.
125 S. Yang, S. Kang, K. Lee, T. Chung, H. Lee and I. Choi, *J. Am. Chem. Soc.*, 2011, **133**, 2795–2797.
126 J. H. Park, K. Kim, J. Lee, J. Y. Choi, D. Hong, S. Yang, F. Caruso, Y. Lee and I. S. Choi, *Angew. Chem., Int. Ed.*, 2014, **53**, 12420–12425.
127 J. Guo, M. Suastegui, K. K. Sakimoto, V. M. Moody, G. Xiao, D. G. Nocera and N. S. Joshi, *Science*, 2018, **362**, 813–816.
128 X. Li, H. Sun, X. Mao, Y. Lao and F. Chen, *ACS Sustainable Chem. Eng.*, 2020, **8**, 7600–7608.
129 T. T. Nguyen, T. T. Pham, H. T. Nguyen, M. R. Nepal, C. D. Phung, Z. W. You, N. Katila, N. T. Pun, T. C. Jeong,

D. Y. Choi, P. H. Park, C. S. Yong, J. O. Kim, S. Yook and J. H. Jeong, *Biomaterials*, 2019, **221**, 119415.
130 X. Zhang, Z. Li, P. Yang, G. Duan, X. Liu, Z. Gu and Y. Li, *Mater. Horiz.*, 2021, **8**, 145–167.
131 M. Shin, H. A. Lee, M. Lee, Y. Shin, J. J. Song, S. W. Kang, D. H. Nam, E. J. Jeon, M. Cho, M. Do, S. Park, M. S. Lee, J. H. Jang, S. W. Cho, K. S. Kim and H. Lee, *Nat. Biomed. Eng.*, 2018, **2**, 304–317.
132 X. Wang, J. Yan, L. Wang, D. Pan, R. Yang, Y. Xu, J. Sheng, Q. Huang, H. Zhao and M. Yang, *Chem. Mater.*, 2018, **30**, 4073–4080.
133 E. Haslam, *Practical polyphenolics: from structure to molecular recognition and physiological action*, Cambridge University Press, 1998.
134 T. S. Sileika, D. G. Barrett, R. Zhang, K. H. A. Lau and P. B. Messersmith, *Angew. Chem., Int. Ed.*, 2013, **125**, 10966–10970.
135 M. Shin, E. Park and H. Lee, *Adv. Funct. Mater.*, 2019, **29**, 1903022.
136 Y. Liu, K. Ai, J. Liu, M. Deng, Y. He and L. Lu, *Adv. Mater.*, 2013, **25**, 1353–1359.
137 Y. Li, Y. Xie, Z. Wang, N. Zang, F. Carniato, Y. Huang, C. M. Andolina, L. R. Parent, T. B. Ditri and E. D. Walter, *ACS Nano*, 2016, **10**, 10186–10194.
138 Z. Wang, Y. Xie, Y. Li, Y. Huang, L. R. Parent, T. Ditri, N. Zang, J. D. Rinehart and N. C. Gianneschi, *Chem. Mater.*, 2017, **29**, 8195–8201.
139 H. Quang Tran, M. Bhave and A. Yu, *ChemistrySelect*, 2020, **5**, 5537–5551.
140 J. Wei, Y. Liang, Y. Hu, B. Kong, J. Zhang, Q. Gu, Y. Tong, X. Wang, S. P. Jiang and H. Wang, *Angew. Chem., Int. Ed.*, 2016, **128**, 12658–12662.
141 C. Wang, H. Sang, Y. Wang, F. Zhu, X. Hu, X. Wang, X. Wang, Y. Li and Y. Cheng, *Nano Lett.*, 2018, **18**, 7045–7051.
142 Z. Ren, S. Sun, R. Sun, G. Cui, L. Hong, B. Rao, A. Li, Z. Yu, Q. Kan and Z. Mao, *Adv. Mater.*, 2020, **32**, 1906024.
143 Y. Wu, J. Deng, Y. Zhou, Y. Huang and Y. Li, *Nanoscale Horiz.*, 2020, **5**, 501–506.
144 J. Qin, G. Liang, B. Feng, G. Wang, N. Wu, Y. Deng, A. A. Elzatahry, A. Alghamdi, Y. Zhao and J. Wei, *Chin. Chem. Lett.*, 2020, DOI: 10.1016/j.cclet.2020.05.021.
145 W. Zhu, S. Liang, J. Wang, Z. Yang, L. Zhang, T. Yuan, Z. Xu, H. Xu and P. Li, *J. Mater. Sci.: Mater. Med.*, 2017, **28**, 74.
146 C. Liu, W. Shen, B. Li, T. Li, H. Chang and Y. Cheng, *Chem. Mater.*, 2019, **31**, 1956–1965.
147 W. Liu, T. Liu, M. Zou, W. Yu, C. Li, Z. He, M. Zhang, M. Liu, Z. Li and J. Feng, *Adv. Mater.*, 2018, **30**, 1802006.
148 K. Liang, J. E. Chung, S. J. Gao, N. Yongvongsoontorn and M. Kurisawa, *Adv. Mater.*, 2018, **30**, 1706963.
149 M. Li, X. Sun, N. Zhang, W. Wang, Y. Yang, H. Jia and W. Liu, *Adv. Sci.*, 2018, **5**, 1800155.
150 C. Li, Q. Li, Y. V. Kaneti, D. Hou, Y. Yamauchi and Y. Mai, *Chem. Soc. Rev.*, 2020, **49**, 4681–4736.
151 P. Qiu, B. Ma, C. T. Hung, W. Li and D. Zhao, *Acc. Chem. Res.*, 2019, **52**, 2928–2938.
152 C. Wang, H. Zhou, H. Niu, X. Ma, Y. Yuan, H. Hong and C. Liu, *Biomater. Sci.*, 2018, **6**, 3318–3331.
153 J. Tang, J. Liu, C. Li, Y. Li, M. O. Tade, S. Dai and Y. Yamauchi, *Angew. Chem., Int. Ed.*, 2015, **127**, 598–603.
154 B. Guan, L. Yu and X. Lou, *J. Am. Chem. Soc.*, 2016, **138**, 11306–11311.
155 B. Guan, S. Zhang and X. Lou, *Angew. Chem., Int. Ed.*, 2018, **130**, 6284–6288.
156 L. Peng, C. T. Hung, S. Wang, X. Zhang, X. Zhu, Z. Zhao, C. Wang, Y. Tang, W. Li and D. Zhao, *J. Am. Chem. Soc.*, 2019, **141**, 7073–7080.
157 S. J. Yang, M. Antonietti and N. Fechler, *J. Am. Chem. Soc.*, 2015, **137**, 8269–8273.
158 Z. Lin, J. Zhou, C. Cortez-Jugo, Y. Han, Y. Ma, S. Pan, E. Hanssen, J. J. Richardson and F. Caruso, *J. Am. Chem. Soc.*, 2019, **142**, 335–341.
159 K. J. Lee, J. Yoon and J. Lahann, *Curr. Opin. Colloid Interface Sci.*, 2011, **16**, 195–202.
160 H. Xu, X. Liu, G. Su, B. Zhang and D. Wang, *Langmuir*, 2012, **28**, 13060–13065.
161 X. Yu, H. Fan, L. Wang and Z. Jin, *Angew. Chem., Int. Ed.*, 2014, **53**, 12600–12604.
162 W. Zhang, Y. Zhou, K. Feng, J. Trinidad, A. Yu and B. Zhao, *Adv. Electron. Mater.*, 2015, **1**, 1500205.
163 W. Zhang, Z. Pan, F. K. Yang and B. Zhao, *Adv. Funct. Mater.*, 2015, **25**, 1588–1597.
164 M. Zhang, L. Zhang, Y. Chen, L. Li, Z. Su and C. Wang, *Chem. Sci.*, 2017, **8**, 8067–8077.
165 S. Li, L. Zhang, X. Liang, T. Wang, X. Chen, C. Liu, L. Li and C. Wang, *Chem. Eng. J.*, 2019, **378**, 122175.
166 M. Zhang, X. Chen, L. Zhang, L. Li, Z.-M. Su and C. Wang, *Chem. Mater.*, 2018, **30**, 3722–3733.
167 T. G. Barclay, H. M. Hegab, S. R. Clarke and M. Ginic-Markovic, *Adv. Mater. Interfaces*, 2017, **4**, 1601192.
168 X. Liu, J. Cao, H. Li, J. Li, Q. Jin, K. Ren and J. Ji, *ACS Nano*, 2013, **7**, 9384–9395.
169 A. B. Polito, E. I. Maurer-Gardner and S. M. Hussain, *J. Nanopart. Res.*, 2015, **17**, 485.
170 I. I. Niyonshuti, V. R. Krishnamurthi, D. Okyere, L. Song, M. Benamara, X. Tong, Y. Wang and J. Chen, *ACS Appl. Mater. Interfaces*, 2020, **12**, 40067–40077.
171 L. S. Lin, Z. X. Cong, J. B. Cao, K. M. Ke, Q. L. Peng, J. H. Gao, H. H. Yang, G. Liu and X. Y. Chen, *ACS Nano*, 2014, **8**, 3876–3883.
172 X. Ding, J. Liu, J. Li, F. Wang, Y. Wang, S. Song and H. Zhang, *Chem. Sci.*, 2016, **7**, 6695–6700.
173 J. Wang, Y. Yang, H. Li, J. Gao, P. He, L. Bian, F. Dong and Y. He, *Chem. Sci.*, 2019, **10**, 6330–6335.
174 D. Renard, S. Tian, A. Ahmadivand, C. J. DeSantis, B. D. Clark, P. Nordlander and N. J. Halas, *ACS Nano*, 2019, **13**, 3117–3124.
175 W. Chen, M. Qin, X. Chen, Q. Wang, Z. Zhang and X. Sun, *Theranostics*, 2018, **8**, 2229–2241.
176 H. Yan, H. Ni, J. Jia, C. Shan, T. Zhang, Y. Gong, X. Li, J. Cao, W. Wu and W. Liu, *Anal. Chem.*, 2019, **91**, 5225–5234.

177 J. Zhou, C. Wang, P. Wang, P. B. Messersmith and H. Duan, *Chem. Mater.*, 2015, **27**, 3071–3076.
178 L. Xie, X. Pang, X. Yan, Q. Dai, H. Lin, J. Ye, Y. Cheng, Q. Zhao, X. Ma and X. Zhang, *ACS Nano*, 2020, **14**, 2880–2893.
179 C. K. K. Choi, Y. T. E. Chiu, X. Zhuo, Y. Liu, C. Y. Pak, X. Liu, Y. L. S. Tse, J. Wang and C. H. J. Choi, *ACS Nano*, 2019, **13**, 5864–5884.
180 E. A. Untener, K. K. Comfort, E. I. Maurer, C. M. Grabinski, D. A. Comfort and S. M. Hussain, *ACS Appl. Mater. Interfaces*, 2013, **5**, 8366–8373.
181 S. Huang, Y. Zhang, J. Shi and W. Huang, *ACS Sustainable Chem. Eng.*, 2016, **4**, 676–681.
182 D. Chang, Y. Gao, L. Wang, G. Liu, Y. Chen, T. Wang, W. Tao, L. Mei, L. Huang and X. Zeng, *J. Colloid Interface Sci.*, 2016, **463**, 279–287.
183 M. Nurunnabi, Z. Khatun, M. Nafiujjaman, D. G. Lee and Y. K. Lee, *ACS Appl. Mater. Interfaces*, 2013, **5**, 8246–8253.
184 B. Wang, Y. Zhai, S. Li, X. Liu, T. Wang and C. Li, *J. Colloid Interface Sci.*, 2020, **574**, 122–130.
185 H. Hu, B. Yu, Q. Ye, Y. Gu and F. Zhou, *Carbon*, 2010, **48**, 2347–2353.
186 Z. Li, H. Xu, J. Shao, C. Jiang, F. Zhang, J. Lin, H. Zhang, J. Li and P. Huang, *Appl. Mater. Today*, 2019, **15**, 297–304.
187 Z. Li, J. C. Barnes, A. Bosoy, J. F. Stoddart and J. I. Zink, *Chem. Soc. Rev.*, 2012, **41**, 2590–2605.
188 W. Cheng, C. Liang, L. Xu, G. Liu, N. Gao, W. Tao, L. Luo, Y. Zuo, X. Wang, X. Zhang, X. Zeng and L. Mei, *Small*, 2017, **13**, 1700623.
189 H. S. Jung, K. J. Cho, Y. Seol, Y. Takagi, A. Dittmore, P. A. Roche and K. C. Neuman, *Adv. Funct. Mater.*, 2018, **28**, 1801252.
190 Z. Zhang, J. Zhang, B. Zhang and J. Tang, *Nanoscale*, 2013, **5**, 118–123.
191 Q. Wu, M. Niu, X. Chen, L. Tan, C. Fu, X. Ren, J. Ren, L. Li, K. Xu, H. Zhong and X. Meng, *Biomaterials*, 2018, **162**, 132–143.
192 H. Wang, W. Zhu, Y. Ping, C. Wang, N. Gao, X. Yin, C. Gu, D. Ding, C. J. Brinker and G. Li, *ACS Appl. Mater. Interfaces*, 2017, **9**, 14258–14264.
193 S. Yang, L. Peng, D. T. Sun, M. Asgari, E. Oveisi, O. Trukhina, S. Bulut, A. Jamali and W. L. Queen, *Chem. Sci.*, 2019, **10**, 4542–4549.
194 A. A. Sara, F. Meng, B. K. Kim, H. Hyun and Y. Yeo, *ACS Biomater. Sci. Eng.*, 2016, **2**, 2294–2303.
195 F. Ding, X. Gao, X. Huang, H. Ge, M. Xie, J. Qian, J. Song, Y. Li, X. Zhu and C. Zhang, *Biomaterials*, 2020, **245**, 119976.
196 J. Guo, B. L. Tardy, A. J. Christofferson, Y. Dai, J. J. Richardson, W. Zhu, M. Hu, Y. Ju, J. Cui, R. R. Dagastine, I. Yarovsky and F. Caruso, *Nat. Nanotechnol.*, 2016, **11**, 1105–1111.
197 H. Xu, X. Liu and D. Wang, *Chem. Mater.*, 2011, **23**, 5105–5110.
198 B. Yu, D. A. Wang, Q. Ye, F. Zhou and W. Liu, *Chem. Commun.*, 2009, 6789–6791.
199 X. Chen, Y. Yan, M. Müllner, M. P. Van Koeverden, K. F. Noi, W. Zhu and F. Caruso, *Langmuir*, 2014, **30**, 2921–2925.
200 X. Wang, D. Miao, X. Liang, J. Liang, C. Zhang, J. Yang, D. Kong, C. Wang and H. Sun, *Biomater. Sci.*, 2017, **5**, 658–662.
201 Y. Ping, J. Guo, H. Ejima, X. Chen, J. J. Richardson, H. Sun and F. Caruso, *Small*, 2015, **11**, 2032–2036.
202 Z. Dong, Y. Hao, Q. Li, Z. Yang, Y. Zhu, Z. Liu and L. Feng, *Nano Res.*, 2020, **13**, 3057–3067.
203 J. Duan, Z. Chen, X. Liang, Y. Chen and J. Yang, *Biomaterials*, 2020, **255**, 120199.
204 M. Hu, Y. Ju, K. Liang, T. Suma, J. Cui and F. Caruso, *Adv. Funct. Mater.*, 2016, **26**, 5827–5834.
205 J. Shi, C. Yang, S. Zhang, X. Wang, Z. Jiang, W. Zhang, X. Song, Q. Ai and C. Tian, *ACS Appl. Mater. Interfaces*, 2013, **5**, 9991–9997.
206 H. Li, Y. Jia, X. Feng and J. Li, *J. Colloid Interface Sci.*, 2017, **487**, 12–19.
207 Y. Z. Ni, W. F. Jiang, G. S. Tong, J. X. Chen, J. Wang, H. M. Li, C. Y. Yu, X. H. Huang and Y. F. Zhou, *Org. Biomol. Chem.*, 2014, **13**, 686–690.
208 H. Zhuang, H. Su, X. Bi, Y. Bai, L. Chen, D. Ge, W. Shi and Y. Sun, *ACS Biomater. Sci. Eng.*, 2017, **3**, 1799–1808.
209 Z. Ye, S. Wu, C. Zheng, L. Yang, P. Zhang and Z. Zhang, *Langmuir*, 2017, **33**, 12952–12959.
210 L. Lybaert, E. D. Vlieghere, R. D. Rycke, N. Vanparijs and B. G. D. Geest, *Adv. Funct. Mater.*, 2014, **24**, 7139–7150.
211 D. Pham-Hua, L. E. Padgett, B. Xue, B. Anderson, M. Zeiger, J. M. Barra, M. Bethea, C. S. Hunter, V. Kozlovskaya, E. Kharlampieva and H. M. Tse, *Biomaterials*, 2017, **128**, 19–32.
212 A. Aaron, R. Megan, K. Veronika, C. Jun, S. Jennifer, B. Mark, W. Jason, B. Yuping and K. Eugenia, *Adv. Ther.*, 2018, **1**, 1800051.
213 A. Alford, V. Kozlovskaya, B. Xue, N. Gupta, W. Higgins, D. Pham-Hua, L. He, S. V. Urban, M. H. Tse and E. Kharlampieva, *Chem. Mater.*, 2018, **30**, 344–357.
214 J. Sun, C. Su and X. Zhang, *J. Colloid Interface Sci.*, 2017, **513**, 470–479.
215 Y. Han, Z. Lin, J. Zhou, G. Yun, R. Guo, J. J. Richardson and F. Caruso, *Angew. Chem., Int. Ed.*, 2020, **59**, 15618–15625.
216 D. R. Amin, C. J. Higginson, A. B. Korpusik, A. R. Gonthier and P. B. Messersmith, *ACS Appl. Mater. Interfaces*, 2018, **10**, 34792–34801.
217 J. Fei, J. Zhao, C. Du, A. Wang, H. Zhang, L. Dai and J. Li, *ACS Nano*, 2014, **8**, 8529–8536.
218 J. Zhou, Y. Jiang, S. Hou, P. K. Upputuri, D. Wu, J. Li, P. Wang, X. Zhen, M. Pramanik, K. Pu and H. Duan, *ACS Nano*, 2018, **12**, 2643–2651.
219 X. Zhang, C. Zheng, Y. Zhang, H. Yang, X. Liu and J. Liu, *J. Nanopart. Res.*, 2016, **18**, 174.
220 J. V. Jokerst, T. Lobovkina, R. N. Zare and S. S. Gambhir, *Nanomedicine*, 2011, **6**, 715–728.
221 W. Zeng, H. Zhang, Y. Deng, A. Jiang and L. Mei, *Chem. Eng. J.*, 2020, **389**, 124494.
222 A. Priyam, P. Nagar, A. K. Sharma and P. Kumar, *Colloids Surf., B*, 2017, **161**, 403–412.
223 P. Zhang, Q. Xu, J. Du and Y. Wang, *RSC Adv.*, 2018, **8**, 34596–34602.

224 P. Zhang, Q. Xu, X. Li and Y. Wang, *Mater. Sci. Eng., C*, 2019, **108**, 110396.
225 K. S. Kim, J. H. Han, J. H. Park, H. K. Kim, S. H. Choi, G. R. Kim, H. Song, H. J. An, D. K. Han, W. Park and K. S. Park, *Biomaterials*, 2019, **221**, 119418.
226 S. Yu, G. Li, R. Liu, D. Ma and W. Xue, *Adv. Funct. Mater.*, 2018, **28**, 1707440.
227 S. Sotoma and Y. Harada, *Langmuir*, 2019, **35**, 8357–8362.
228 W. Sheng, B. Li, X. Wang, B. Dai, B. Yu, X. Jia and F. Zhou, *Chem. Sci.*, 2015, **6**, 2068–2073.
229 Z. Zeng, M. Wen, G. Ye, X. Huo, F. Wu, Z. Wang, J. Yan, Y. Lu, J. Chen, K. Matyjaszewski and J. Chen, *Chem. Mater.*, 2017, **29**, 10212–10219.
230 Q. Huang, M. Liu, Q. Wan, R. Jiang, L. Mao, G. Zeng, H. Huang, F. Deng, X. Zhang and Y. Wei, *Mater. Chem. Phys.*, 2017, **193**, 501–511.
231 N. Li, T. Li, X. Y. Qiao, R. Li, Y. Yao and Y. K. Gong, *ACS Appl. Mater. Interfaces*, 2020, **12**, 12337–12344.
232 Y. Ju, Q. Dai, J. Cui, Y. Dai and F. Caruso, *ACS Appl. Mater. Interfaces*, 2016, **8**, 22914–22922.
233 B. L. Tardy, J. J. Richardson, V. Nithipipat, K. Kempe, J. Guo, K. L. Cho, M. A. Rahim, H. Ejima and F. Caruso, *Biomacromolecules*, 2019, **20**, 1421–1428.
234 W. Zhang, Q. A. Besford, A. J. Christofferson, P. Charchar, J. J. Richardson, A. Elbourne, K. Kempe, C. E. Hagemeyer, M. R. Field, C. F. McConville, I. Yarovsky and F. Caruso, *Nano Lett.*, 2020, **20**, 2660–2666.
235 Y. Wu, H. Wang, F. Gao, Z. Xu, F. Dai and W. Liu, *Adv. Funct. Mater.*, 2018, **28**, 1801000.
236 Q. Zhan, X. Shi, J. Zhou, L. Zhou and S. Wei, *Small*, 2019, **15**, 1803926.
237 J. Song, X. Yang, Z. Yang, L. Lin, Y. Liu, Z. Zhou, Z. Shen, G. Yu, Y. Dai and O. Jacobson, *ACS Nano*, 2017, **11**, 6102–6113.
238 A. Kumar, S. Kumar, W. K. Rhim, G. H. Kim and J.-M. Nam, *J. Am. Chem. Soc.*, 2014, **136**, 16317–16325.
239 Y. Zhang, D. Pan, Q. Zhou, J. Zhao, N. Pan, Y. Zhang, L. X. Wang and Y. Shen, *J. Mater. Chem. B*, 2018, **6**, 8180–8187.
240 K. C. L. Black, T. S. Sileika, J. Yi, R. Zhang, J. G. Rivera and P. B. Messersmith, *Small*, 2014, **10**, 169–178.
241 X. Wang, J. Zeng, M. Zhang, X. Zeng and X. Xuan, *Adv. Funct. Mater.*, 2018, **28**, 1801783.
242 R. Lv, P. Yang, B. Hu, J. Xu, W. Shang and J. Tian, *ACS Nano*, 2017, **11**, 1064–1072.
243 S. Kumar, A. Kumar, G. H. Kim, W. K. Rhim, K. L. Hartman and J. M. Nam, *Small*, 2017, **13**, 1701584.
244 X. Ding, J. Liu, D. Liu, J. Li, F. Wang, L. Li, Y. Wang, S. Song and H. Zhang, *Nano Res.*, 2017, **10**, 3434–3446.
245 N. G. Khlebtsov, L. Lin, B. N. Khlebtsov and J. Ye, *Theranostics*, 2019, **10**, 2067–2094.
246 J. Zhou, Q. Xiong, J. Ma, J. Ren, P. B. Messersmith, P. Chen and H. Duan, *ACS Nano*, 2016, **10**, 11066–11075.
247 C. K. K. Choi, X. Zhuo, Y. T. E. Chiu, H. Yang, J. Wang and C. H. J. Choi, *Nanoscale*, 2017, **9**, 16968–16980.
248 H. Wen, P. Jiang, Y. Hu and G. Li, *Microchim. Acta*, 2018, **185**, 353.
249 J. Wang, Y. Ni, W. Jiang, H. Li, Y. Liu, S. Lin, Y. Zhou and D. Yan, *Small*, 2015, **11**, 4485–4490.
250 D. Wang, H. Wu, J. Zhou, P. Xu, C. Wang, R. Shi, H. Wang, H. Wang, Z. Guo and Q. Chen, *Adv. Sci.*, 2018, **5**, 1800287.
251 D. T. Sun, L. Peng, W. S. Reeder, S. M. Moosavi, D. Tiana, D. K. Britt, E. Oveisi and W. L. Queen, *ACS Cent. Sci.*, 2018, **4**, 349–356.
252 Q. Dai, H. Geng, Q. Yu, J. Hao and J. Cui, *Theranostics*, 2019, **9**, 3170–3190.
253 H. Ando, Y. Niki, M. Ito, K. Akiyama, M. S. Matsui, D. B. Yarosh and M. Ichihashi, *J. Invest. Dermatol.*, 2012, **132**, 1222–1229.
254 J. Hong, H. Lu, X. Meng, J. H. Ryu, Y. Hara and C. S. Yang, *Cancer Res.*, 2003, **62**, 7241–7246.
255 Y. Huang, Y. Li, Z. Hu, X. Yue, M. T. Proetto, Y. Jones and N. C. Gianneschi, *ACS Cent. Sci.*, 2017, **3**, 564–569.
256 C. Sun, Y. Ding, L. Zhou, D. Shi, L. Sun, T. J. Webster and Y. Shen, *Nanomedicine*, 2017, **13**, 2605–2621.
257 A. O. Elzoghby, M. M. Abd-Elwakil, K. Abd-Elsalam, M. T. Elsayed, Y. Hashem and O. Mohamed, *Curr. Pharm. Des.*, 2016, **22**, 3305–3323.
258 S. Mayor and R. E. Pagano, *Nat. Rev. Mol. Cell Biol.*, 2007, **8**, 603–612.
259 S. D. Conner and S. L. Schmid, *Nature*, 2003, **422**, 37–44.
260 K. H. S. Sy, L. W. C. Ho, W. C. Y. Lau, H. Ko and C. H. J. Choi, *Langmuir*, 2018, **34**, 14033–14045.
261 B. Poinard, S. Kamaluddin, A. Q. Q. Tan, K. G. Neoh and J. C. Y. Kah, *ACS Appl. Mater. Interfaces*, 2019, **11**, 4777–4789.
262 L. Ding, X. Zhu, Y. Wang, B. Shi, X. Ling, H. Chen, W. Nan, A. Barrett, Z. Guo, W. Tao, J. Wu and X. Shi, *Nano Lett.*, 2017, **17**, 6790–6801.
263 Y. Lu, P. Luo, C. Huang, Y. Leu, T. Wang, K. Wei, H. Wang and Y. Ma, *Nanoscale*, 2014, **6**, 10297–10306.
264 S. Behzadi, V. Serpooshan, W. Tao, M. A. Hamaly, M. Y. Alkawareek, E. C. Dreaden, D. Brown, A. M. Alkilany, O. C. Farokhzad and M. Mahmoudi, *Chem. Soc. Rev.*, 2017, **46**, 4218–4244.
265 A. Gutjahr, C. Phelip, A.-L. Coolen, C. Monge, A.-S. Boisgard, S. Paul and B. Verrier, *Vaccines*, 2016, **4**, 34.
266 J. Chen, J. Li, J. Zhou, Z. Lin, F. Cavalieri, E. Czuba-Wojnilowicz, Y. Hu, A. Glab, Y. Ju, J. J. Richardson and F. Caruso, *ACS Nano*, 2019, **13**, 11653–11664.
267 A. Akinc, M. Thomas, A. M. Klibanov and R. Langer, *J. Gene Med.*, 2005, **7**, 657–663.
268 H. Xiong, Z. Wang, C. Wang and J. Yao, *Nano Lett.*, 2020, **20**, 1781–1790.
269 G. Yang, S. Z. F. Phua, A. K. Bindra and Y. Zhao, *Adv. Mater.*, 2019, **31**, 1805730.
270 Y. Wei, L. Quan, C. Zhou and Q. Zhan, *Nanomedicine*, 2018, **13**, 1495–1512.
271 H. S. Choi, W. Liu, P. Misra, E. Tanaka, J. P. Zimmer, B. I. Ipe, M. G. Bawendi and J. V. Frangioni, *Nat. Biotechnol.*, 2007, **25**, 1165–1170.
272 S. D. Li and L. Huang, *Mol. Pharmaceutics*, 2008, **5**, 496.
273 J. Zhou, C. Wang, P. Wang, P. B. Messersmith and H. Duan, *Chem. Mater.*, 2015, **27**, 3071–3076.

274 X. Zhang, G. Zeng, J. Tian, Q. Wan, Q. Huang, K. Wang, Q. Zhang, M. Liu, F. Deng and Y. Wei, *Appl. Surf. Sci.*, 2015, **351**, 425–432.
275 U. Termsarasab, I. S. Yoon, J. H. Park, H. T. Moon, H. J. Cho and D.-D. Kim, *Int. J. Pharm.*, 2014, **464**, 127–134.
276 S. Sunoqrot, J. Bugno, D. Lantvit, J. E. Burdette and S. Hong, *J. Controlled Release*, 2014, **191**, 115–122.
277 B. Xiao, X. Zhou, H. Xu, B. Wu, D. Hu, H. Hu, K. Pu, Z. Zhou, X. Liu and J. Tang, *ACS Nano*, 2018, **12**, 12682–12691.
278 H. Lee, J. H. Bae and S. R. Lee, *J. Neurosci. Res.*, 2004, **77**, 892–900.
279 I. Figueira, G. Garcia, R. Pimpão, A. Terrasso, I. Costa, A. Almeida, L. Tavares, T. Pais, P. Pinto, M. R. Ventura, A. Filipe, G. J. McDougall, D. Stewart, K. S. Kim, I. Palmela, D. Brites, M. A. Brito, C. Brito and C. N. Santos, *Sci. Rep.*, 2017, **7**, 1–16.
280 P. Lockman, R. Mumper, M. Khan and D. Allen, *Drug Dev. Ind. Pharm.*, 2002, **28**, 1–13.
281 J. Hu, X. Zhang, Z. Wen, Y. Tan, N. Huang, S. Cheng, H. Zheng and Y. Cheng, *Oncotarget*, 2016, **7**, 73681–73696.
282 T. Shoji, Y. Akazome, T. Kanda and M. Ikeda, *Food Chem. Toxicol.*, 2004, **42**, 959–967.
283 J. Cao, J. Han, H. Xiao, J. Qiao and M. Han, *Nutrients*, 2016, **8**, 762.
284 J. Li, T. Wang, A. R. Kirtane, Y. Shi, A. Jones, Z. Moussa, A. Lopes, J. Collins, S. M. Tamang and K. Hess, *Sci. Transl. Med.*, 2020, **12**, eabc0441.
285 A. Woźniak, M. Walawender, D. Tempka, E. Coy, K. Załęski, B. F. Grześkowiak and R. Mrówczyński, *Toxicol. In Vitro*, 2017, **44**, 256–265.
286 J. S. Pappalardo, J. R. Macairan, A. Macina, A. Poulhazan, V. Quattrocchi, I. Marcotte and R. Naccache, *Phys. Chem. Chem. Phys.*, 2020, **22**, 16595–16605.
287 J. Hu, Q. Wang, Y. Wang, G. You, P. Li, L. Zhao and H. Zhou, *J. Colloid Interface Sci.*, 2020, **571**, 326–336.
288 H. Liu, Y. Yang, Y. Liu, J. Pan, J. Wang, F. Man, W. Zhang and G. Liu, *Adv. Sci.*, 2020, **7**, 1903129.
289 B. Yang, S. Zhou, J. Zeng, L. Zhang, R. Zhang, K. Liang, L. Xie, B. Shao, S. Song, G. Huang, D. Zhao, P. Chen and B. Kong, *Nano Res.*, 2020, **13**, 1013–1019.
290 B. Li, T. Gong, N. Xu, F. Cui, B. Yuan, Q. Yuan, H. Sun, L. Wang and J. Liu, *Small*, 2020, **16**, 2003969.
291 J. Liu, Y. Hu, L. Li, C. Wang, J. Wang, Y. Li, D. Chen, X. Ding, C. Shen and F. Xu, *Adv. Sci.*, 2020, **7**, 2002243.
292 K. Li, Y. Dai, W. Chen, K. Yu, G. Xiao, J. J. Richardson, W. Huang, J. Guo, X. Liao and B. Shi, *Adv. Biosyst.*, 2019, **3**, 1800241.
293 J. Li, X. Li, S. Gong, C. Zhang, C. Qian, H. Qiao and M. Sun, *Nano Lett.*, 2020, **20**, 4842–4849.
294 J. S. Suk, Q. Xu, N. Kim, J. Hanes and L. M. Ensign, *Adv. Drug Delivery Rev.*, 2016, **99**, 28–51.
295 E. Amstad, T. Gillich, I. Bilecka, M. Textor and E. Reimhult, *Nano Lett.*, 2009, **9**, 4042–4048.
296 B. Malisova, S. Tosatti, M. Textor, K. Gademann and S. Zürcher, *Langmuir*, 2010, **26**, 4018–4026.
297 M. Amiri, E. Amali, A. Nematollahzadeh and H. Salehniya, *Sens. Actuators, B*, 2016, **228**, 53–58.
298 J. Zhang, L. Mou and X. Jiang, *Anal. Chem.*, 2018, **90**, 11423–11430.
299 S. Ma, Y. Qi, X. Jiang, J. Chen, Q. Zhou, G. Shi and M. Zhang, *Anal. Chem.*, 2016, **88**, 11647–11653.
300 L. Ma, Z. Lei, F. Liu and Z. Wang, *Sens. Bio-Sens. Res.*, 2015, **3**, 92–97.
301 W. Qiang, H. Hu, L. Sun, H. Li and D. Xu, *Anal. Chem.*, 2015, **87**, 12190–12196.
302 Y. Yao, D. Zhao, N. Li, F. Z. Shen, J. O. Machuki, D. Z. Yang, J. J. Li, D. Q. Tang, Y. Y. Yu, J. W. Tian, H. F. Dong and F. L. Gao, *Anal. Chem.*, 2019, **91**, 7850–7857.
303 D. Chen, X. Zhu, J. Huang, G. Wang, Y. Zhao, F. Chen, J. Wei, Z. Song and Y. Zhao, *Anal. Chem.*, 2018, **90**, 9048–9054.
304 J. Zhai, M. Zhao, X. Cao, M. Li and M. Zhao, *J. Am. Chem. Soc.*, 2018, **140**, 16925–16928.
305 W. Zhou, C. Lu, X. Guo, F. Chen, H. Yang and X. Wang, *J. Mater. Chem.*, 2010, **20**, 880–883.
306 A. Turco, S. Corvaglia, E. Mazzotta, P. P. Pomba and C. Malitesta, *Sens. Actuators, B*, 2018, **255**, 3374–3383.
307 S. Hou, Y. Chen, D. Lu, Q. Xiong, Y. Lim and H. Duan, *Adv. Mater.*, 2020, **32**, 1906475.
308 M. Zandieh and J. W. Liu, *Langmuir*, 2020, **36**, 3260–3267.
309 H. Xiang, Y. Wang, M. Wang, Y. Shao, Y. Jiao and Y. Zhu, *Nanoscale*, 2018, **10**, 13572–13580.
310 R. Ren, G. Cai, Z. Yu, Y. Zeng and D. Tang, *Anal. Chem.*, 2018, **90**, 11099–11105.
311 J. Li, M. A. Baird, M. A. Davis, W. Tai, L. S. Zweifel, K. M. A. Waldorf, M. Gale Jr, L. Rajagopal, R. H. Pierce and X. Gao, *Nat. Biomed. Eng.*, 2017, **1**, 0082.
312 J. Huang, J. Meng, S. Chen, S. Zhang, T. Liu, C. Li and F. Wang, *Biosens. Bioelectron.*, 2020, **164**, 112310.
313 G. Wang, J. Qin, X. Zhou, Y. Deng, H. Wang, Y. Zhao and J. Wei, *Adv. Funct. Mater.*, 2018, **28**, 1806144.
314 G. Yang, X. Li, Y. He, X. Xiong, P. Wang and S. Zhou, *ACS Biomater. Sci. Eng.*, 2018, **4**, 2081–2088.
315 D. Fan, C. Wu, K. Wang, X. Gu, Y. Liu and E. Wang, *Chem. Commun.*, 2016, **52**, 406–409.
316 J. J. Zhou, Q. R. Xiong, J. L. Ma, J. H. Ren, P. B. Messersmith, P. Chen and H. W. Duan, *ACS Nano*, 2016, **10**, 11066–11075.
317 Q. Xiong, C. Y. Lim, J. Ren, J. Zhou, K. Pu, M. B. Chan-Park, H. Mao, Y. C. Lam and H. Duan, *Nat. Commun.*, 2018, **9**, 1743.
318 B. Yang, H. Gong, C. Y. Chen, X. M. Chen and C. Q. Cai, *Biosens. Bioelectron.*, 2017, **87**, 679–685.
319 J. Rao, A. Dragulescu-Andrasi and H. Yao, *Curr. Opin. Biotechnol.*, 2007, **18**, 17–25.
320 R. Wombacher and V. W. Cornish, *J. Biophotonics*, 2011, **4**, 391–402.
321 D. Shcherbo, C. S. Murphy, G. V. Ermakova, E. A. Solovieva, T. V. Chepurnykh, A. S. Shcheglov, V. V. Verkhusha, V. Z. Pletnev, K. L. Hazelwood and P. M. Roche, *Biochem. J.*, 2009, **418**, 567–574.

322 P. Yang, S. Zhang, X. Chen, X. Liu, Z. Wang and Y. Li, *Mater. Horiz.*, 2020, **7**, 746–761.
323 W. Qiang, W. Li, X. Li, X. Chen and D. Xu, *Chem. Sci.*, 2014, **5**, 3018–3024.
324 N. Li, T. Li, C. Hu, X. Lei, Y. Zuo and H. Han, *ACS Appl. Mater. Interfaces*, 2016, **8**, 15013–15023.
325 X. Song, S. Li, J. Dai, L. Song, G. Huang, R. Lin, J. Li, G. Liu and H. Yang, *Small*, 2017, **13**, 1603997.
326 X. Zhang, S. Wang, L. Xu, L. Feng, Y. Ji, L. Tao, S. Li and Y. Wei, *Nanoscale*, 2012, **4**, 5581–5584.
327 J. Lin, C. Yu, Y. Yang and W. Tseng, *Phys. Chem. Chem. Phys.*, 2015, **17**, 15124–15130.
328 M. Liu, J. Ji, X. Zhang, X. Zhang, B. Yang, F. Deng, Z. Li, K. Wang, Y. Yang and Y. Wei, *J. Mater. Chem. B*, 2015, **3**, 3476–3482.
329 M. Zhang, Y. Zou, Y. Zhong, G. Liao, C. Yu and Z. Xu, *ACS Appl. Bio Mater.*, 2019, **2**, 630–637.
330 Y. Dai, C. Wu, S. Wang, Q. Li, M. Zhang, J. Li and K. Xu, *Nanomedicine*, 2018, **14**, 547–555.
331 J. E. Lemaster, Z. Wang, A. Hariri, F. Chen, Z. Hu, Y. Huang, C. V. Barback, R. Cochran, N. C. Gianneschi and J. V. Jokerst, *Chem. Mater.*, 2018, **31**, 251–259.
332 S. Wang, J. Lin, Z. Wang, Z. Zhou, R. Bai, N. Lu, Y. Liu, X. Fu, O. Jacobson and W. Fan, *Adv. Mater.*, 2017, **29**, 1701013.
333 X. Meng, B. Zhang, Y. Yi, H. Cheng, B. Wang, Y. Liu, T. Gong, W. Yang, Y. Yao and H. Wang, *Nano Lett.*, 2020, **20**, 2522–2529.
334 Y. Yang, J. Liu, C. Liang, L. Feng, T. Fu, Z. Dong, Y. Chao, Y. Li, G. Lu and M. Chen, *ACS Nano*, 2016, **10**, 2774–2781.
335 G. Zhao, H. Wu, R. Feng, D. Wang, P. Xu, P. Jiang, K. Yang, H. Wang, Z. Guo and Q. Chen, *ACS Appl. Mater. Interfaces*, 2018, **10**, 3295–3304.
336 Y. Wang, S. Song, T. Lu, Y. Cheng, Y. Song, S. Wang, F. Tan, J. Li and N. Li, *Biomaterials*, 2019, **220**, 119405.
337 M. Xu and L. V. Wang, *Rev. Sci. Instrum.*, 2006, **77**, 041101.
338 Q. Fu, R. Zhu, J. Song, H. Yang and X. Chen, *Adv. Mater.*, 2019, **31**, 1805875.
339 J. Weber, P. C. Beard and S. E. Bohndiek, *Nat. Methods*, 2016, **13**, 639–650.
340 T. Repenko, S. Fokong, L. De Laporte, D. Go, F. Kiessling, T. Lammers and A. J. Kuehne, *Chem. Commun.*, 2015, **51**, 6084–6087.
341 Y. Li, C. Jiang, D. Zhang, Y. Wang, X. Ren, K. Ai, X. Chen and L. Lu, *Acta Biomater.*, 2017, **47**, 124–134.
342 Z. Zhou, Y. Yan, L. Wang, Q. Zhang and Y. Cheng, *Biomaterials*, 2019, **203**, 63–72.
343 L. Zhang, P. Yang, R. Guo, J. Sun, R. Xie and W. Yang, *Int. J. Nanomed.*, 2019, **14**, 8647–8663.
344 Y. Wang, F. Liu, N. Yan, S. Sheng, C. Xu, H. Tian and X. Chen, *ACS Biomater. Sci. Eng.*, 2019, **5**, 4700–4707.
345 X. Li, K. Luo, X. Lin and C. Zhu, *ChemNanoMat*, 2019, **5**, 1115–1122.
346 T. Guo, Y. Lin, G. Jin, R. Weng, J. Song, X. Liu, G. Huang, L. Hou and H. Yang, *Chem. Commun.*, 2019, **55**, 850–853.
347 W. Guo, F. Wang, D. Ding, C. Song, C. Guo and S. Liu, *Chem. Mater.*, 2017, **29**, 9262–9274.
348 L. Zhang, H. Su, J. Cai, D. Cheng, Y. Ma, J. Zhang, C. Zhou, S. Liu, H. Shi and Y. Zhang, *ACS Nano*, 2016, **10**, 10404–10417.
349 X. Han, Y. Xu, Y. Li, X. Zhao, Y. Zhang, H. Min, Y. Qi, G. J. Anderson, L. You and Y. Zhao, *ACS Nano*, 2019, **13**, 4379–4391.
350 J. Xu, X. Cheng, F. Chen, W. Li, X. Xiao, P. Lai, G. Xu, L. Xu and Y. Pan, *J. Mater. Sci. Technol.*, 2021, **63**, 97–105.
351 K. Huang, Y. Zhang, J. Lin and P. Huang, *Biomater. Sci.*, 2019, **7**, 472–479.
352 Y. Mantri and J. V. Jokerst, *ACS Nano*, 2020, **14**, 9408–9422.
353 Q. Lin, Y. Yang, Y. Ma, R. Zhang, J. Wang, X. Chen and Z. Shao, *Nano Lett.*, 2018, **18**, 7485–7493.
354 H. Wang, Q. Chen and S. Zhou, *Chem. Soc. Rev.*, 2018, **47**, 4198–4232.
355 J. Wang, W. Sang, Z. Yang, Z. Shen, Z. Wang, O. Jacobson, Y. Chen, Y. Wang, M. Shao and G. Niu, *J. Mater. Chem. B*, 2019, **7**, 5688–5694.
356 X. Wang, J. Yan, D. Pan, R. Yang, L. Wang, Y. Xu, J. Sheng, Y. Yue, Q. Huang and Y. Wang, *Adv. Healthcare Mater.*, 2018, **7**, 1701505.
357 D. Li, Y. Zhang, S. Wen, Y. Song, Y. Tang, X. Zhu, M. Shen, S. Mignani, J.-P. Majoral and Q. Zhao, *J. Mater. Chem. B*, 2016, **4**, 4216–4226.
358 Y. Dai, D. Yang, D. Yu, C. Cao, Q. Wang, S. Xie, L. Shen, W. Feng and F. Li, *ACS Appl. Mater. Interfaces*, 2017, **9**, 26674–26683.
359 N. Deshpande, A. Needles and J. K. Willmann, *Clin. Radiol.*, 2010, **65**, 567–581.
360 Y. Xie, J. Wang, Z. Wang, K. A. Krug and J. D. Rinehart, *Nanoscale*, 2018, **10**, 12813–12819.
361 Y. Xie, J. Wang, J. Wang, Z. Hu, A. Hariri, N. Tu, K. A. Krug, M. D. Burkart, N. C. Gianneschi and J. V. Jokerst, *J. Mater. Chem. B*, 2019, **7**, 4833–4842.
362 C. Jiang, Y. Wang, J. Wang, W. Song and L. Lu, *Biomaterials*, 2017, **114**, 54–61.
363 X. Zhong, K. Yang, Z. Dong, X. Yi, Y. Wang, C. Ge, Y. Zhao and Z. Liu, *Adv. Funct. Mater.*, 2015, **25**, 7327–7336.
364 L. Tsai, H. Hsieh, K. Lu, S. Wang and F. Mi, *Nanomedicine*, 2016, **11**, 9–30.
365 Y. Ju, J. Cui, H. Sun, M. Müllner, Y. Dai, J. Guo, N. Bertleff-Zieschang, T. Suma, J. J. Richardson and F. Caruso, *Biomacromolecules*, 2016, **17**, 2268–2276.
366 H. Zhang, Z. Yi, Z. Sun, X. Ma and X. Li, *J. Mater. Chem. B*, 2017, **5**, 7622–7631.
367 M. Manzano and M. Vallet-Regí, *Adv. Funct. Mater.*, 2020, **30**, 1902634.
368 S. Wang, X. Zhao, S. Wang, J. Qian and S. He, *ACS Appl. Mater. Interfaces*, 2016, **8**, 24368–24384.
369 L. Sun, Q. Li, L. Zhang, Z. Xu, Y. Kang and P. Xue, *ACS Appl. Nano Mater.*, 2017, **1**, 325–336.
370 M. Liu, Y. Peng, Y. Nie, P. Liu, S. Hu, J. Ding and W. Zhou, *Acta Biomater.*, 2020, **110**, 242–253.
371 F. Hu, B. Liu, H. Chu, C. Liu, Z. Li, D. Chen and L. Li, *Nanoscale*, 2019, **11**, 9201–9206.
372 Y. Zhang, X. Wu, C. Hou, K. Shang, K. Yang, Z. Tian, Z. Pei, Y. Qu and Y. Pei, *Int. J. Nanomed.*, 2018, **13**, 2161.

373 C. Chen, T. Ma, W. Tang, X. Wang, Y. Wang, J. Zhuang, Y. Zhu and P. Wang, *Nanoscale Horiz.*, 2020, **5**, 986–998.
374 Y. Dai, Z. Yang, S. Cheng, Z. Wang, R. Zhang, G. Zhu, Z. Wang, B. C. Yung, R. Tian, O. Jacobson, C. Xu, Q. Ni, J. Song, X. Sun, G. Niu and X. Chen, *Adv. Mater.*, 2018, **30**, 1704877.
375 Q. V. Le, J. Suh, J. J. Choi, G. T. Park, J. W. Lee, G. Shim and Y. K. Oh, *ACS Nano*, 2019, **13**, 7442–7462.
376 D. Zhu, W. Tao, H. Zhang, G. Liu, T. Wang, L. Zhang, X. Zeng and L. Mei, *Acta Biomater.*, 2016, **30**, 144–154.
377 L. Cheng, L. Yang, F. Meng and Z. Zhong, *Adv. Healthcare Mater.*, 2018, **7**, 1800685.
378 N. Nayerossadat, T. Maedeh and P. A. Ali, *Adv. Biomed. Res.*, 2012, **1**, 27.
379 S. Taranejoo, J. Liu, P. Verma and K. Hourigan, *J. Appl. Polym. Sci.*, 2015, **132**, 42096.
380 J. Feng, W. Yu, Z. Xu, J. Hu, J. Liu and F. Wang, *ACS Appl. Mater. Interfaces*, 2020, **12**, 22613–22623.
381 D. Wu, J. Zhou, X. Chen, Y. Chen, S. Hou, H. Qian, L. Zhang, G. Tang, Z. Chen, Y. Ping, W. Fang and H. Duan, *Biomaterials*, 2020, **238**, 119847.
382 Y. Han, J. Zhou, Y. Hu, Z. Lin, Y. Ma, J. J. Richardson and F. Caruso, *ACS Nano*, 2020, **14**, 12972–12981.
383 Y. Liu, P. Bhattarai, Z. Dai and X. Chen, *Chem. Soc. Rev.*, 2019, **48**, 2053–2108.
384 X. Huang and M. A. El-Sayed, *Alexandria J. Med.*, 2011, **47**, 1–9.
385 W. Yin, L. Yan, J. Yu, G. Tian, L. Zhou, X. Zheng, X. Zhang, Y. Yong, J. Li and Z. Gu, *ACS Nano*, 2014, **8**, 6922–6933.
386 T. Liu, M. Zhang, W. Liu, X. Zeng, X. Song, X. Yang, X. Zhang and J. Feng, *ACS Nano*, 2018, **12**, 3917–3927.
387 X. Chen, Z. Yi, G. Chen, X. Ma, W. Su, X. Cui and X. Li, *J. Mater. Chem. B*, 2019, **7**, 4066–4078.
388 Z. Yu, W. K. Chan, Y. Zhang and T. T. Y. Tan, *Biomaterials*, 2020, 120459.
389 D. Wu, X. Chen, J. Zhou, Y. Chen, T. Wan, Y. Wang, A. Lin, Y. Ruan, Z. Chen, X. Song, W. Fang, H. Duan and Y. Ping, *Mater. Horiz.*, 2020, **7**, 2929–2935.
390 Y. Wang, G. Wei, X. Zhang, X. Huang, J. Zhao, X. Guo and S. Zhou, *Small*, 2018, **14**, 1702994.
391 J. Nam, S. Son, L. J. Ochyl, R. Kuai, A. Schwendeman and J. J. Moon, *Nat. Commun.*, 2018, **9**, 1074.
392 L. Shao, R. Zhang, J. Lu, C. Zhao, X. Deng and Y. Wu, *ACS Appl. Mater. Interfaces*, 2017, **9**, 1226–1236.
393 F. Wang, Q. Sun, B. Feng, Z. Xu, J. Zhang, J. Xu, L. Lu, H. Yu, M. Wang and Y. Li, *Adv. Healthcare Mater.*, 2016, **5**, 2227–2236.
394 X. Li, S. Lee and J. Yoon, *Chem. Soc. Rev.*, 2018, **47**, 1174–1188.
395 W. Fan, P. Huang and X. Chen, *Chem. Soc. Rev.*, 2016, **45**, 6488–6519.
396 Y. Wei, Z. Wei, P. Luo, W. Wei and S. Liu, *Artif. Cells, Nanomed., Biotechnol.*, 2018, **46**, 1552–1561.
397 J. Liang, Y. Zheng, X. Wu, C. Tan, L. Ji and Z. Mao, *Adv. Sci.*, 2020, **7**, 1901992.
398 D. Wang, H. Wu, W. Q. Lim, S. Z. F. Phua, P. Xu, Q. Chen, Z. Guo and Y. Zhao, *Adv. Mater.*, 2019, **31**, 1901893.
399 J. Feng, W. Yu, Z. Xu and F. Wang, *Chem. Sci.*, 2020, **11**, 1649–1656.
400 X. Yang, D. Wang, J. Zhu, L. Xue, C. Ou, W. Wang, M. Lu, X. Song and X. Dong, *Chem. Sci.*, 2019, **10**, 3779–3785.
401 H. Chen, J. Yang, L. Sun, H. Zhang, Y. Guo, J. Qu, W. Jiang, W. Chen, J. Ji, Y. Yang and B. Wang, *Small*, 2019, **15**, 1903880.
402 A. Curcio, A. K. Silva, S. Cabana, A. Espinosa, B. Baptiste, N. Menguy, C. Wilhelm and A. Abou-Hassan, *Theranostics*, 2019, **9**, 1288–1302.
403 W. Li, J. Peng, L. Tan, J. Wu, K. Shi, Y. Qu, X. Wei and Z. Qian, *Biomaterials*, 2016, **106**, 119–133.
404 Y. Wang, N. Gong, Y. Li, Q. Lu, X. Wang and J. Li, *J. Am. Chem. Soc.*, 2019, **142**, 1735–1739.
405 M. S. Goldberg and Nat Rev, *Cancer*, 2019, **19**, 587–602.
406 N. Wang, Y. Yang, X. Wang, X. Tian, W. Qin, X. Wang, J. Liang, H. Zhang and X. Leng, *ACS Biomater. Sci. Eng.*, 2019, **5**, 2330–2342.
407 X. Wang, N. Wang, Y. Yang, X. Wang, J. Liang, X. Tian, H. Zhang and X. Leng, *Biomater. Sci.*, 2019, **7**, 3062–3075.
408 X. Wang, Z. Chen, C. Zhang, C. Zhang, G. Ma, J. Yang, X. Wei and H. Sun, *Adv. Healthcare Mater.*, 2019, **8**, 1900474.
409 L. Wang, Y. He, T. He, G. Liu, C. Lin, K. Li, L. Lu and K. Cai, *Biomaterials*, 2020, **255**, 120208.
410 M. S. Taha, G. M. Cresswell, J. Park, W. Lee, T. L. Ratliff and Y. Yeo, *Nano Lett.*, 2019, **19**, 8333–8341.
411 A. Seth, H. Gholami Derami, P. Gupta, Z. Wang, P. Rathi, R. Gupta, T. Cao, J. J. Morrissey and S. Singamaneni, *ACS Appl. Mater. Interfaces*, 2020, **12**, 42499–42510.
412 F. Zhang, G. Lu, X. Wen, F. Li, X. Ji, Q. Li, M. Wu, Q. Cheng, Y. Yu and J. Tang, *J. Controlled Release*, 2020, **326**, 131–139.
413 R. Chen, C. Zhu, Y. Fan, W. Feng, J. Wang, E. Shang, Q. Zhou and Z. Chen, *ACS Appl. Bio Mater.*, 2019, **2**, 874–883.
414 F. Shahidi and P. Ambigaipalan, *J. Funct. Foods*, 2015, **18**, 820–897.
415 H. Xie, C. Xiang, Y. Li, L. Wang, Y. Zhang, Z. Song, X. Ma, X. Lu, Q. Lei and W. Fang, *Food Hydrocolloids*, 2018, **89**, 111–121.
416 C. Nathan and A. Cunningham-Bussel, *Nat. Rev. Immunol.*, 2013, **13**, 349–361.
417 K. Y. Ju, Y. Lee, S. Lee, S. B. Park and J. K. Lee, *Biomacromolecules*, 2011, **12**, 625–632.
418 H. Zhao, Z. Zeng, L. Liu, J. Chen, H. Zhou, L. Huang, J. Huang, H. Xu, Y. Xu and Z. Chen, *Nanoscale*, 2018, **10**, 6981–6991.
419 X. Bao, J. Zhao, J. Sun, M. Hu and X. Yang, *ACS Nano*, 2018, **12**, 8882–8892.
420 Y. Liu, K. Ai, X. Ji, D. Askhatova, R. Du, L. Lu and J. Shi, *J. Am. Chem. Soc.*, 2017, **139**, 856–862.
421 J. Yeo, J. Lee, S. Yoon and W. J. Kim, *Biomater. Sci.*, 2020, **8**, 1148–1159.
422 S. Lin, Y. Cheng, H. Zhang, X. Wang, Y. Zhang, Y. Zhang, L. Miao, X. Zhao and H. Wei, *Small*, 2019, **16**, 1902123.
423 D. Liu, L. Ma, L. Liu, L. Wang, Y. Liu, Q. Jia, Q. Guo, G. Zhang and J. Zhou, *ACS Appl. Mater. Interfaces*, 2016, **8**, 24455–24462.

424 L. Tan, W. Tang, T. Liu, X. Ren, C. Fu, B. Liu, J. Ren and X. Meng, *ACS Appl. Mater. Interfaces*, 2016, **8**, 11237–11245.
425 W. Tang, B. Liu, S. Wang, T. Liu, C. Fu, X. Ren, L. Tan, W. Duan and X. Meng, *RSC Adv.*, 2016, **6**, 32434–32440.
426 C. Liu, W. Yao, M. Tian, J. Wei, Q. Song and W. Qiao, *Biomaterials*, 2018, **179**, 83–95.
427 M. Battaglini, A. Marino, A. Carmignani, C. Tapeinos, V. Cauda, A. Ancona, N. Garino, V. Vighetto, G. La Rosa, E. Sinibaldi and G. Ciofani, *ACS Appl. Mater. Interfaces*, 2020, **12**, 35782–35798.

